

ISRDC-79/002

AD AO 67122

DDC FILE COPY

AERODYNAMIC C
LOW-TO-MODERA

LEVEL

2

**DAVID W. TAYLOR NAVAL SHIP
RESEARCH AND DEVELOPMENT CENTER**



Bethesda, Md. 20084

**AERODYNAMIC CHARACTERISTICS OF THE CLOSE-COUPLED CANARD
AS APPLIED TO LOW-TO-MODERATE SWEEP WINGS
VOLUME 2: SUBSONIC SPEED REGIME**

by

David W. Lacey

DDC
RECEIVED
APR 10 1979
C

APPROVED FOR PUBLIC RELEASE: DISTRIBUTION UNLIMITED

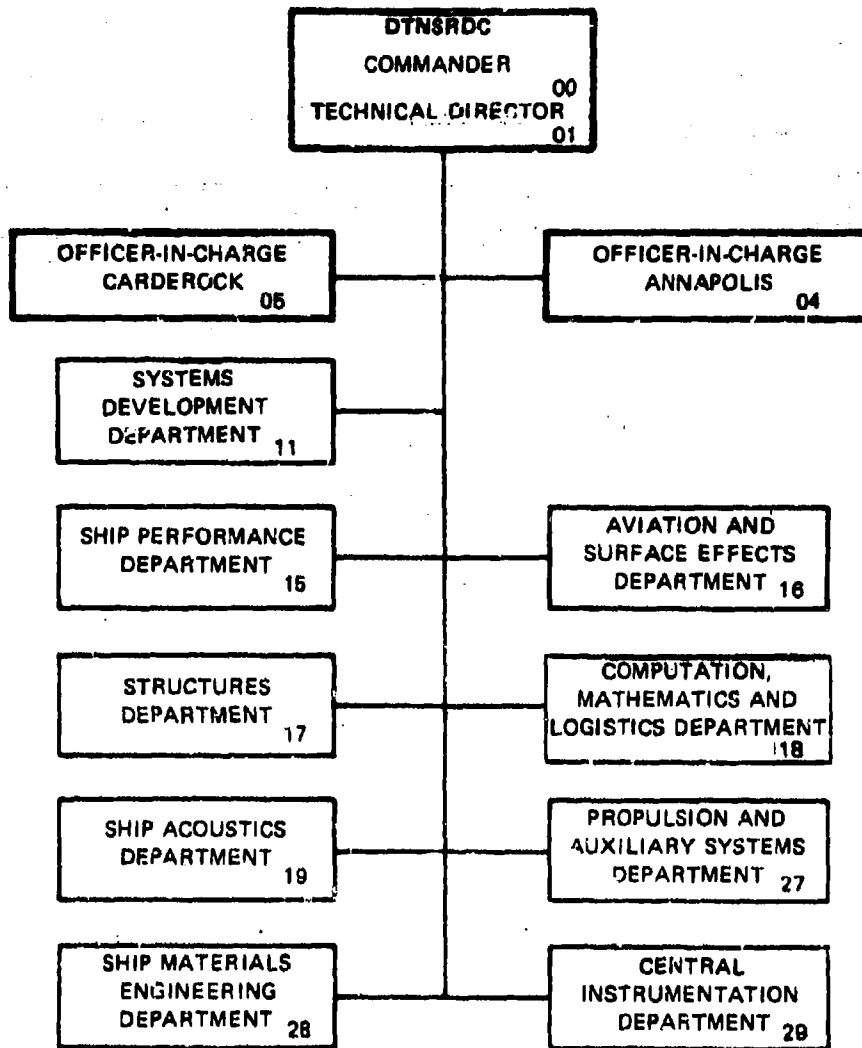
AVIATION AND SURFACE EFFECTS DEPARTMENT
RESEARCH AND DEVELOPMENT REPORT

January 1979

DTN3RDC-79/002

PAGES _____
ARE
MISSING
IN
ORIGINAL
DOCUMENT

MAJOR DTNSRDC ORGANIZATIONAL COMPONENTS



UNCLASSIFIED

SECURITY CLASSIFICATION OF THIS PAGE (When Data Entered)

REPORT DOCUMENTATION PAGE		READ INSTRUCTIONS BEFORE COMPLETING FORM
1. REPORT NUMBER DTNSRDC 79/002	2. GOVT ACCESSION NO.	3. RECIPIENT'S CATALOG NUMBER
4. TITLE (and Subtitle) AERODYNAMIC CHARACTERISTICS OF THE CLOSE- COUPLED CANARD AS APPLIED TO LOW-TO- MODERATE SWEEP WINGS, VOLUME 2. SUBSONIC SPEED REGIME.	5. TYPE OF REPORT & PERIOD COVERED Final	6. PERFORMING ORG. REPORT NUMBER Aero Report 1257
7. AUTHOR(s) David W./Lacey	8. CONTRACT OR GRANT NUMBER(s)	
9. PERFORMING ORGANIZATION NAME AND ADDRESS David W. Taylor Naval Ship Research and Development Center Bethesda, Maryland 20884	10. PROGRAM ELEMENT, PROJECT, TASK AREA & WORK UNIT NUMBERS Program Element 62241N Task Area WP 1 41421-09 Work Unit 1600-079	
11. CONTROLLING OFFICE NAME AND ADDRESS NAVPAC	12. REPORT DATE January 1979	13. NUMBER OF PAGES 114
14. MONITORING AGENCY NAME & ADDRESS (if different from Controlling Office) Naval Air Systems Command AIR 320 Washington, D.C. 20361	15. SECURITY CLASS. (of this report) UNCLASSIFIED	15a. DECLASSIFICATION/DOWNGRADING SCHEDULE
16. DISTRIBUTION STATEMENT (of this Report) APPROVED FOR PUBLIC RELEASE: DISTRIBUTION UNLIMITED		
17. DISTRIBUTION STATEMENT (of the abstract entered in Block 20, if different from Report) UNCLASSIFIED		
18. SUPPLEMENTARY NOTES		
19. KEY WORDS (Continue on reverse side if necessary and identify by block number) Canards, subsonic, lift, drag, pitching moment, research models		
20. ABSTRACT (Continue on reverse side if necessary and identify by block number) An analysis of the effects of canard size, shape, position and deflection on the aerodynamic characteristics of two general research models having leading edge sweep angles of 25 and 50 degrees is presented. The analysis summarizes the findings of four experimental subsonic wind-tunnel programs conducted at the David W. Taylor Naval Ship Research and Development Center between 1970 and 1974. The analysis is based on four canard geometries varying in planform from a 60-degree delta to a 25-degree swept wing (Continued on reverse side)		

DD FORM 1473
1 JAN 73EDITION OF 1 NOV 65 IS OBSOLETE
S/N 0102-014-6001

UNCLASSIFIED

SECURITY CLASSIFICATION OF THIS PAGE (When Data Entered)

UNCLASSIFIED

SECURITY CLASSIFICATION OF THIS PAGE(When Data Entered)

(Block 20 continued)

high aspect ratio canard. The canards were located at seven different positions and deflected from -10 to 25 degrees.

Significant findings include: the excellent correlation between canard exposed area ratio and changes in lift, drag, and pitching moment; the detrimental effect of positive canard deflection; and the optimum longitudinal position for each canard shape for maximum improvements in lift and drag. It is further concluded that the favorable aerodynamic changes caused by interference of the close-coupled canard are not significantly dependent on wing leading edge sweep or wing leading edge modifications.

ACCESSION for White Section
 Buff Section

NTIS
DOC
UNCLASSIFIED
EXEMPT FROM GDS

BY
PROJECT NUMBER: 100-107-1000
DATE: 10/1/70

A

UNCLASSIFIED

SECURITY CLASSIFICATION OF THIS PAGE(When Data Entered)

FOREWORD

This report summarizes the findings of close-coupled canard research performed by the Aviation and Surface Effects Department of the David W. Taylor Naval Ship Research and Development Center. The work was performed between 1970 and 1974 and was funded by the Naval Air Systems Command (AIR 320). The purpose of the report is to provide a summary of the aerodynamic findings obtained from a series of wind tunnel evaluations involving three general research models and the F-4 aircraft. The report is presented in four volumes--Volume 1: General Trends; Volume 2: Subsonic Speed Regime; Volume 3: Transonic-Supersonic Speed Regime; and Volume 4: F-4 Phantom II Aircraft.

TABLE OF CONTENTS

	Page
LIST OF FIGURES	vi
LIST OF TABLES	ix
NOTATION	x
ABSTRACT	1
ADMINISTRATIVE INFORMATION	1
INTRODUCTION	1
LIFT	4
SIZE	5
SHAPE	6
POSITION	9
DEFLECTION	16
WING LEADING EDGE CHANGES	25
PITCHING MOMENT	28
SIZE	30
SHAPE	35
POSITION	35
DEFLECTION	43
WING LEADING EDGE CHANGES	50
DRAG	51
SIZE	55
SHAPE	58
POSITION	60
DEFLECTION	70
WING LEADING EDGE CHANGES	79
FLOW VISUALIZATION	84
SUMMARY	89
SIZE	90
SHAPE	90

	Page
POSITION.	90
DEFLECTION.	91
WING LEADING EDGE CHANGES	91
ACKNOWLEDGMENTS.	92
APPENDIX - MODEL GEOMETRY.	93
REFERENCES	101

LIST OF FIGURES

1 - Sketch of Models.	2
2 - Canards	2
3 - Geometrically Similar Canards	3
4 - Canard Positions.	3
5 - Typical Lift Characteristics.	4
6 - $C_{L_{20}}$ versus Canard Exposed Area Ratio	5
7 - Incremental Lift Characteristics of the Various Canard Shapes	7
8 - Lift Characteristics of 25- and 50-Degree Wing Models.	8
9 - Position Effects of Incremental Lift.	10
10 - Maximum Incremental Lift Variation with Canard Position.	13
11 - Incremental Lift at 32-Degree Angle of Attack	15
12 - Variation in Lift Coefficient at $\sigma = 20$ Degrees versus Canard Deflection Angle δ_c	17
13 - Incremental Lift Variation with Canard Deflection	19
14 - Variation of a $\Delta C_{L_{32}}$ with Canard Deflection	22
15 - Variation of a $\Delta C_{L_{32}}$ with Canard-Wing Vertical Gap.	23

	Page
16 - Variation of a $\Delta C_M / \Delta C_L$ with Canard-Wing Vertical Gap.	24
17 - Geometry of Wing Leading Edge Droops and Radii.	25
18 - Effect of Wing Leading Edge Droop and Radius on Lift Characteristics	26
19 - Lift Characteristics of 25-Degree Model Modified with -9-Degree Wing Leading Edge Droop.	27
20 - Incremental Lift due to Canard for Basic and -9-Degree Droop, 25-Degree Wing Model	28
21 - Typical Pitching Moment Characteristics	29
22 - Variation of Pitching Moment Coefficient at Zero Lift C_{M_0} with Canard Deflection Angle δ	31
23 - Zero Lift Pitching Moment versus Projected Area Ratio.	33
24 - Zero Lift Pitching Moment versus Exposed Area Ratio.	33
25 - Zero Lift Pitching Moment Variation with Canard Exposed Volume Coefficient	34
26 - Neutral Point Shift Variation with Canard Exposed Volume Coefficient.	34
27 - Incremental Moment Variation with Canard Shape	36
28 - Incremental Moment Variation with Canard Position.	37
29 - Variation of a $\Delta C_{M_{32}}$ with Canard Position	40
30 - Incremental Moment Slope Variation with Canard Position	42
31 - Correlation of Neutral Point Change with Canard Exposed Volume Coefficient	43

	Page
32 - Incremental Moment Change due to Canard Deflection.	44
33 - Variations of a $AC_{M_{32}}$ with Canard Deflection.	48
34 - Canard Control Power.	49
35 - Moment Characteristics of Basic 25-Degree Wing and 25-Degree Wing with -9-Degree Droop	51
36 - Incremental Moments due to Canard on Basic and Modified 25-Degree Wing	52
37 - Typical Drag Characteristics.	53
38 - Typical Lift-to-Drag Ratio Characteristics.	54
39 - Effect of Deflection on Zero Lift Drag C_{D_0}	56
40 - Variation of Canard Drag Coefficient with Canard Lift	57
41 - Variation of (L/D) with Canard Exposed Area Ratio	57
42 - Lift-to-Drag Ratio Variation with Canard Shape	59
43 - Induced Drag Factor	61
44 - Lift-to-Drag Ratio Variation with Canard Position.	62
45 - Effect of Canard Position on Minimum Drag Coefficient	66
46 - Induced Drag Factor Variation with Canard Position for the 50-Degree Wing	67
47 - Induced Drag Factor Variation with Canard Position for the 25-Degree Wing	69
48 - Locus of Minimum Induced Drag Factor.	71
49 - Lift-to-Drag Ratio Variation with Canard Deflection.	72
50 - Minimum Drag Variation with Canard Deflection	75

	Page
51 - Effect of Canard Deflection on Induced Drag Factor.	76
52 - Effect of -9-Degree Droop on Lift-to-Drag Ratio.	80
53 - Incremental Change in Lift-to-Drag Ratio due to -9-Degree Droop	83
54 - Tuft Patterns of the 50-Degree Wing.	85
55 - Effect of Canard on Unseparated Flow Region.	86
56 - Effect of Canard Shape	88
57 - Effect of Position	88
58 - Research Aircraft Fuselage	96
59 - Planform View of the Wings	97
60 - Planform View of the Canards	98
61 - Canard Pivot Locations	99
62 - Wind Tunnel Model Components	100

LIST OF TABLES

1 - Geometric Characteristics of the Wings	94
2 - Geometric Characteristics of the Canards	95

NOTATION

AR	Aspect ratio
B	Body
B_C	Canard projected span
C_D	Drag coefficient, D/qS_w
C_{D_C}	Drag coefficient of canard referenced to total canard exposed area
C_{D_0}	Minimum drag coefficient
C_i	Canard
C_L	Lift coefficient, L/qS_w
C_{L_B}	Lift coefficient of body alone
$C_{L_{B+C}}$	Lift coefficient of body and canard
$C_{L_{max}}$	Maximum lift coefficient
$C_{L_{WB}}$	Lift coefficient of wing and body
C_{L_0}	Lift coefficient evaluated at minimum drag value
$C_{L_{20}}$	Lift coefficient evaluated at $\alpha = 20$ degrees
$C_{L_{32}}$	Lift coefficient evaluated at $\alpha = 32$ degrees
C_{L_α}	$\partial C_L / \partial \alpha$
$C_{L_{\alpha_c}}$	$\left(\frac{\partial C_L}{\partial \alpha} \right)$ lift curve slope of canard, referenced to canard exposed area

$C_{L\delta_c}$	$\left(\frac{\partial C_L}{\partial \delta_c}\right)$ lift curve slope of canard due to deflection referred to canard exposed area
C_M	Pitching moment coefficient, pitching moment/ qS_w
C_{M_B}	Pitching moment coefficient of body alone
$C_{M_{B+C}}$	Pitching moment coefficient of body and canard
$C_{M_{WB}}$	Pitching moment coefficient of body and wing
C_{M_0}	Zero lift pitching moment
$C_{M_{32}}$	Pitching moment coefficient evaluated at $\alpha = 32$ degrees
C_{M_δ}	$\partial C_M / \partial \delta$
C_{M_α}	$\partial C_M / \partial \alpha$
\bar{c}	Mean aerodynamic chord, inches
D	Drag, pounds
i	Canard shape
j	Canard position
L	Lift, pounds
L/D	Lift-to-drag ratio
$(L/D)_{\max}$	Maximum lift-to-drag ratio
l_c	Distance between center of gravity of wing and canard pivot location, inches
P_j	Canard position
q	Dynamic pressure, pounds per square foot

S_C	Canard Projected area, square feet
S_{C_e}	Canard exposed area, square feet
S_W	Wing reference area, square feet
W	Wing
\bar{x}	Longitudinal distance, inches
\bar{z}	Vertical distance, inches
z_t	Vertical gap measured from canard trailing edge to wing upper surface, inches
α	Angle of attack, degrees
ΔC_L	$C_L - C_{L_W}$
ΔC_{L_C}	$C_{L_{B+C}} - C_{L_B}$
$\Delta C_{L_{max}}$	Maximum value of incremental lift
$\Delta C_{L_{32}}$	Incremental lift evaluated at $\alpha = 32$ degrees
ΔC_M	$C_M - C_{M_{WB}}$
ΔC_{M_C}	$C_{M_{B+C}} - C_{M_B}$
$\Delta C_{M_{32}}$	ΔC_M evaluated at $\alpha = 32$ degrees
δ_c	Canard deflection angle, degrees
λ	Wing leading edge sweep angle, degrees
λ_{25}	Quarter chord sweep angle of canard, degrees

ABSTRACT

An analysis of the effects of canard size, shape, position and deflection on the aerodynamic characteristics of two general research models having leading edge sweep angles of 25 and 50 degrees is presented. The analysis summarizes the findings of four experimental subsonic wind-tunnel programs conducted at the David W. Taylor Ship Research and Development Center between 1970 and 1974. The analysis is based on four canard geometries varying in planform from a 60-degree delta to a 25-degree swept wing high aspect ratio canard. The canards were located at seven different positions and deflected from -10 to 25 degrees.

Significant findings include: the excellent correlation between canard exposed area ratio and changes in lift, drag, and pitching moment; the detrimental effect of positive canard deflection; and the optimum longitudinal position for each canard shape for maximum improvements in lift and drag. It is further concluded that the favorable aerodynamic changes caused by interference of the close-coupled canard are not significantly dependent on wing leading edge sweep or wing leading edge modifications.

ADMINISTRATIVE INFORMATION

This work was undertaken by the Aircraft Division of the Aviation and Surface Effects Department of the David W. Taylor Naval Ship Research and Development Center. The program was sponsored by the Naval Air Systems Command (AIR 320) and was funded under WF 41432-09, Work Unit 1600-078.

INTRODUCTION

This is the second volume of a four-volume report summarizing the close-coupled canard work accomplished at the David W. Taylor Naval Ship Research and Development Center between 1970 and 1974. This volume summarizes the findings of a series of wind-tunnel programs conducted at subsonic speeds.

Volume 1 of this report presented the general trends of close-coupled canards on aircraft of low to moderate wing sweep. It was shown that close-coupled canards can significantly improve stall angle of attack, increase

the maximum lift coefficient, and reduce drag. The extent to which these improvements occur is a function of canard size, shape, position, and deflection. These variables, as well as the influence of wing leading edge modifications, are discussed in detail in this volume.

The discussion is based on four wind-tunnel programs conducted in the DTNSRDC 8 × 10 foot subsonic wind tunnel. Two general research models were utilized in this program. The models had leading edge sweep angles of 25 and 50 degrees. Sketches of the models are shown in Figure 1. Four canards

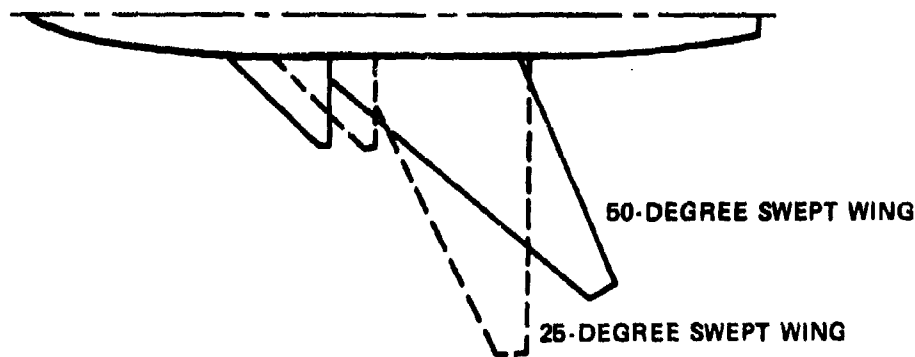


Figure 1 - Sketch of Models

of different planform were evaluated. The shapes were a 45-degree clipped delta designated C_0 , a 60-degree pure delta C_1 , a 45-degree high aspect ratio canard C_2 , and a 25-degree canard C_3 , as shown in Figure 2. In addition,

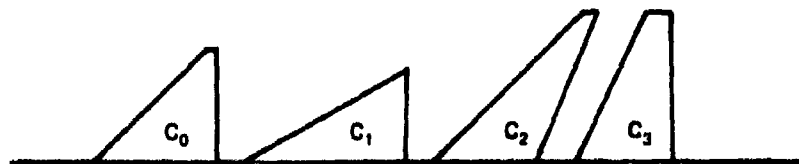
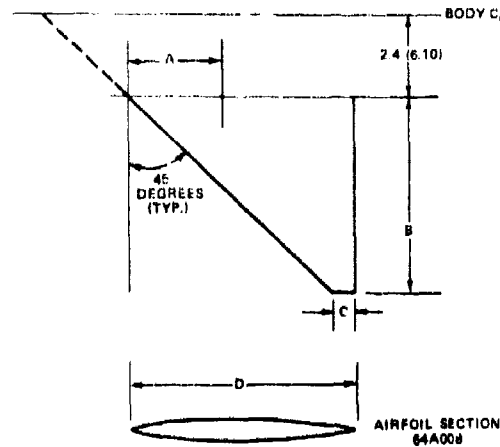


Figure 2 - Canards

tion, four geometrically similar versions of canard C_0 were evaluated with projected area ratios of 0.10, 0.15, 0.20, and 0.25. Relative sizes of the four canards are shown in Figure 3.



S _c /S _w	PIVOT DISTANCE A		SPAN B		TIP CHORD C		ROOT CHORD D		CANARD AREAS	
	IN.	CM.	IN.	CM.	IN.	CM.	IN.	CM.	IN. ²	CM. ²
0.10	1.38	3.51	2.74	6.96	0.38	0.97	3.12	7.92	30.5	198.8
0.15	1.75	4.44	3.91	9.93	0.44	1.12	4.35	11.05	45.7	294.8
0.20	2.25	5.72	4.84	12.29	0.55	1.42	5.40	13.72	61.0	393.5
0.25	2.82	6.85	5.74	14.58	0.59	1.50	6.33	16.08	75.8	489.0

Figure 3 - Geometrically Similar Canards

The models have seven positions at which the canards can be located (see Figure 4). Positions are numbered from fore to aft and top to bottom. Position 1 is the highest, most forward and position 7 is the lowest position. Deflection range varied from -10 to 25 degrees. Detailed dimensions of the models, canards, and positions are given in the Appendix.

NOTE: ALL DIMENSIONS ARE IN INCHES (CENTIMETERS)

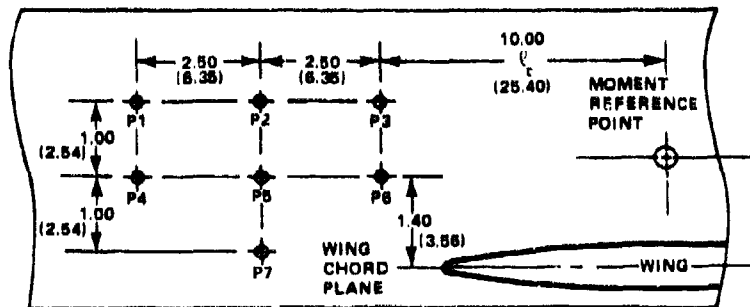


Figure 4 - Canard Positions

The discussion is organized into major topics of lift, pitching moment, and drag. Subtopics include the effect of canard size, shape, position, deflection, and wing leading edge changes. The data are primarily presented as incremental changes in lift and pitching moment due to the above parameters. Drag is presented primarily as lift-to-drag ratio at constant lift coefficient. Data for both 25- and 50-degree wings are presented to indicate that the favorable effects of close-coupled canards are applicable to aircraft of relatively arbitrary wing planforms.

LIFT

Typical variation of lift coefficient with angle of attack for the 25- and 50-degree wing are presented in Figure 5. Data are shown for three

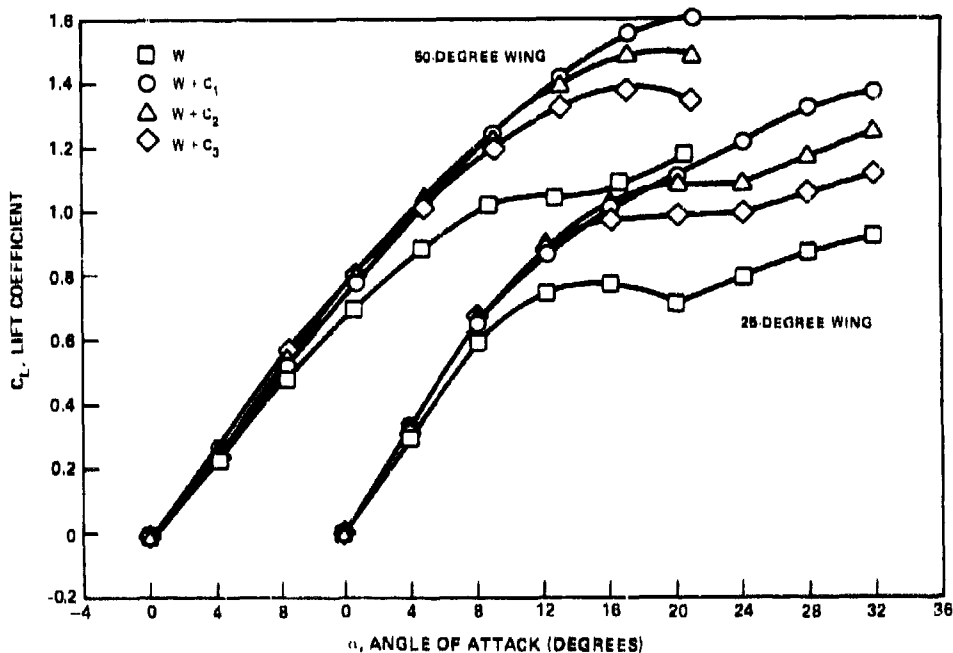


Figure 5 - Typical Lift Characteristics

canard shapes: a 60-degree delta, a 45-degree high aspect ratio canard, and a 25-degree high aspect ratio canard. For all configurations there is a sizeable increase in lift when the canard is installed to the basic

wing-body. The increase in lift varies somewhat with the particular canard size, shape, position, and deflection. These differences in lift are discussed in the following sections.

SIZE

One of the prime variables of the first canard wind tunnel program^{1*} conducted at DTNSRDC was the effect of canard size on the aerodynamic characteristics of the 50-degree research model. Four geometrically similar canards having projected area ratios of 0.10, 0.15, 0.20, and 0.25 were evaluated. Relative sizes of each canard are shown in Figure 3. Data from this wind tunnel evaluation were limited to an angle of attack of 20 degrees. The variation of lift coefficient at 20 degrees is presented in Figure 6 for seven canard positions.

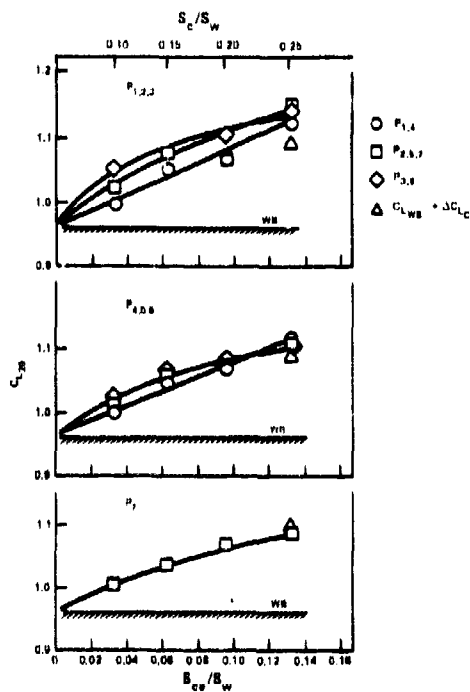


Figure 6 - C_{L20} versus Canard Exposed Area Ratio

* A complete listing of references is given on page 101.

The effect on canard size varied somewhat with canard position. At those positions where the canard is fairly close to the wing, P_2 , P_3 , P_5 , P_6 , there is a distinct curvature to the data, however, as the canard is moved further forward the variation of $C_{l,20}$ with size becomes linear.

Little favorable effect would be expected because the interference is minimized. Included in the figure is the value of the lift coefficient for the 0.25 canard and wing body if no interference were present.

Comparison between this value and the data shows favorable interference for the high canard locations (P_1 , P_2 , P_3), and unfavorable interference when the canard is in the plane of the wing (P_7).

SHAPE

Incremental lift is presented in Figure 7 for the various canard shapes. The canard location is position P_3 for all four canard shapes. As stated in Volume 1, P_3 was near optimum for all canard shapes. The figure is for both 25- and 50-degree research models and contains isolated data for each canard shape.

The most significant conclusion which can be drawn from the figure is that the large difference in incremental lift between 25- and 50-degree wing configurations is in the angle of attack range between 12 and 28 degrees. This difference is attributable to the poor stall characteristics at the 25-degree wing.

A comparison between the canard-off characteristics of the two configurations is given in Figure 8. The 25-degree wing configuration exhibits as expected a higher lift curve slope than the 50-degree configuration but the stall angle of attack is only 10 degrees for the 25-degree wing versus 20 degrees for the 50-degree wing.

The favorable interference between canard and wing, therefore, delays stall at a lower angle of attack for the 25-degree wing.

This reduction in angle of attack due to favorable interference is clearly seen in the low cross-over point between the isolated canard data

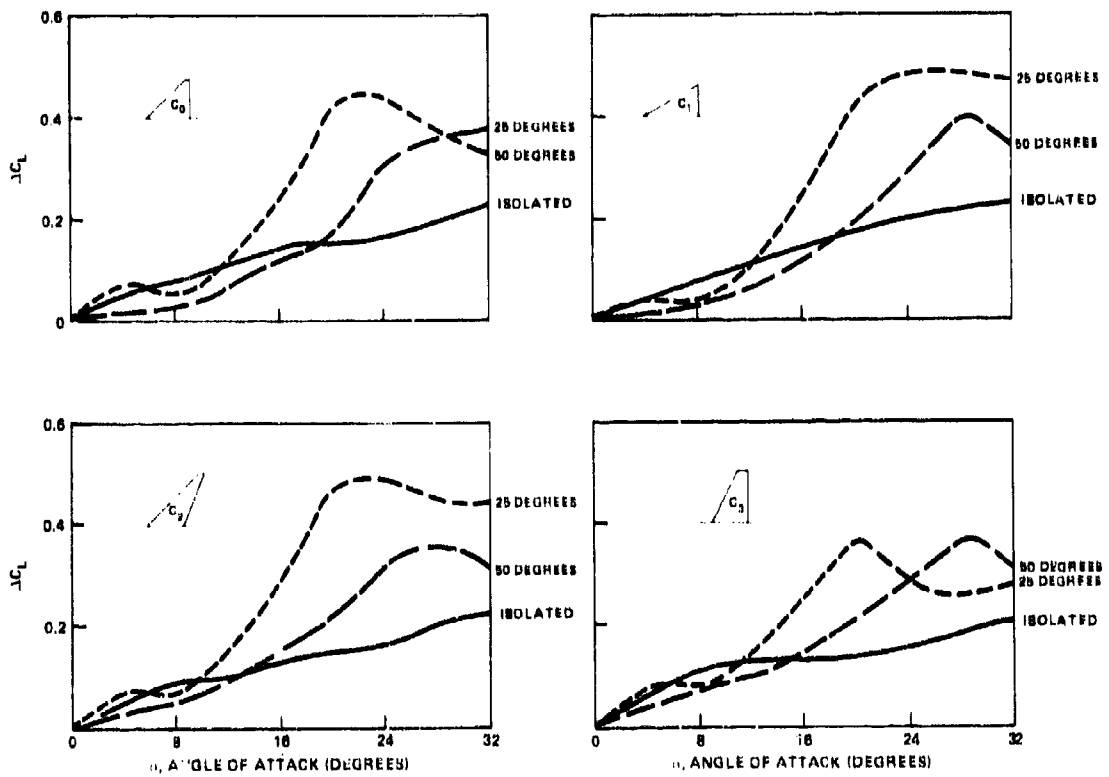


Figure 7 - Incremental Lift Characteristics of the Various Canard Shapes

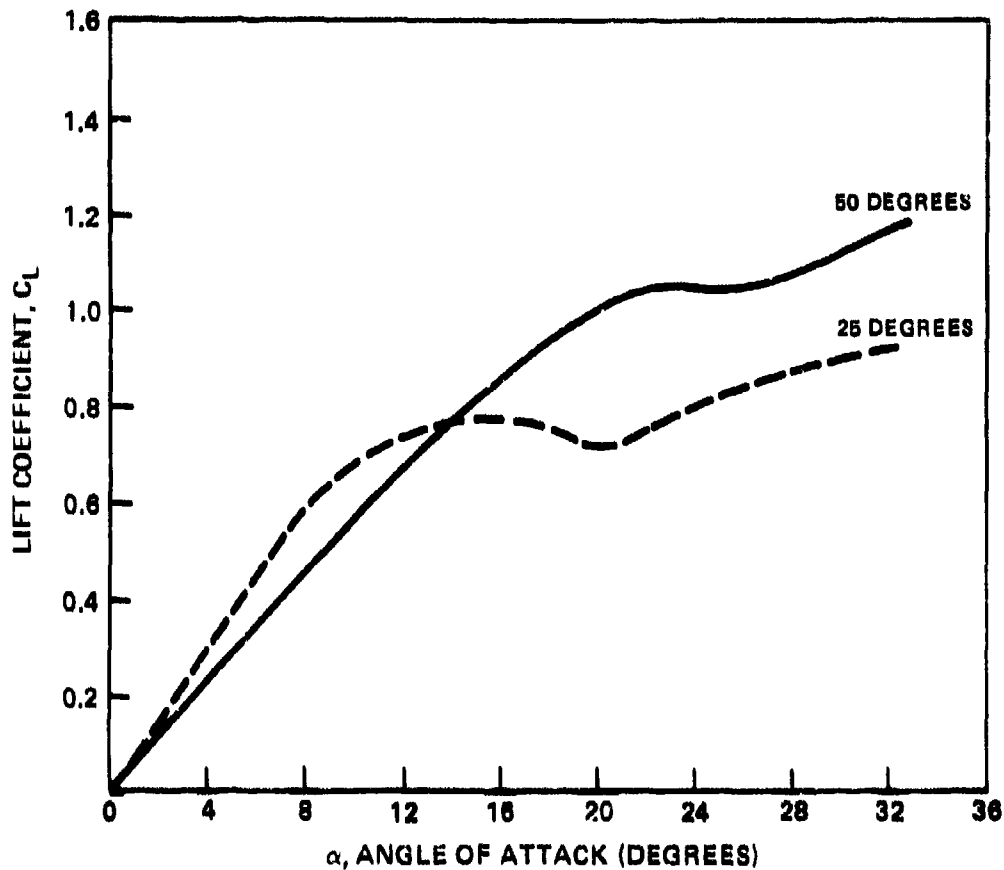


Figure 8 - Lift Characteristics of 25- and 50- Degree Wing Models

and the complete configuration. Favorable interference occurs at approximately 12 degrees for the 25-degree wing, whereas favorable interference does not occur until the angle of attack reaches approximately 16 to 20 degrees for the 50-degree wing. It can be said that the poorer the wing design, the more the canard can help.

Examination of the data with regard to the individual canard shape indicates that the 60-degree delta canard C_1 maximizes the increase in lift for both wings. The 60-degree canard is closely followed by the 45-degree high aspect ratio canard C_2 and the 45-degree clipped delta C_0 .

The low sweep canard C_3 exhibited the lowest incremental lift for the 25-degree sweep model, and, in fact, the canard appears to have stalled at approximately 20-degree angle of attack.

Incremental lift for the low sweep canard is approximately the same as the other canards for the 50-degree wing model. It thus appears that while low sweep canards are inadequate for the low sweep wing, the low sweep canard does delay separation sufficiently for the wing of higher sweep if located at the proper position. The effect of position change on incremental lift for the various canard shapes and the two wing sweeps is discussed in the next section.

POSITION

Incremental lift versus angle of attack is presented in Figure 9 for both 25- and 50-degree sweep research models. Data² are presented for seven positions for the 50-degree model and three positions for the 25-degree model. The data are for the four canard configurations at zero degrees canard deflection.

Incremental lift was, in general, maximized at 28-degrees angle of attack for the canards on the 50-degree model and between 20- and 24-degrees angle of attack for the 25-degree model.

The variation of maximum incremental lift with canard position is shown in Figure 10. The interference free value of canard lift at the corresponding angle of attack for each position are also shown in the figure.

For all configurations, as the canard was moved to the most forward position, $l_c/\bar{c} \sim 1.5$ for the 50-degree wing, $l_c/\bar{c} \sim 1.30$ for the 25-degree wing, the maximum incremental lift dropped off. Similarly, lowering the canard reduced maximum incremental lift. The only exceptions to the latter statement were the low sweep 25-degree canard C_3 , and the high aspect ratio 45-degree canard C_2 . Canard C_3 had an increase in maximum lift at the lowest, most aft position for both 25- and 50-degree wing models. Similarly, lift was maximized at P_6 for the 45-degree high aspect ratio canard C_2 .

Figure 9 - Position Effects of Incremental Lift

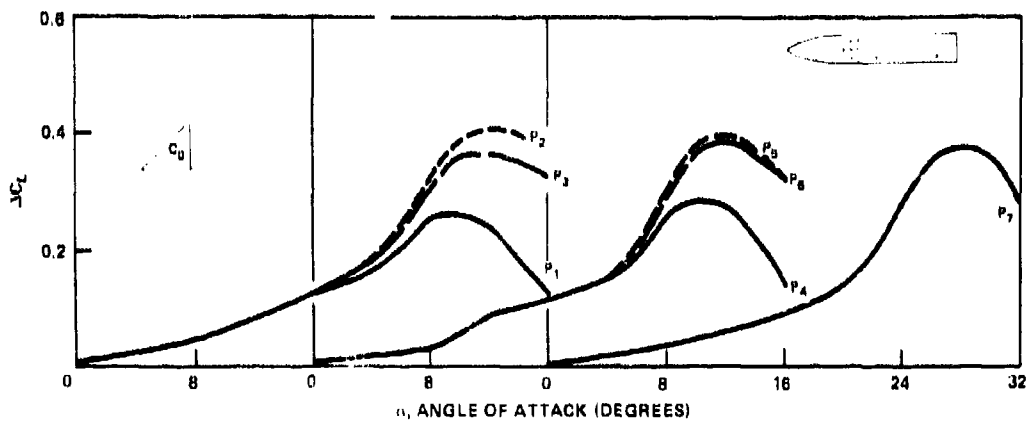


Figure 9a - Canard C_0 on 50-Degree Wing

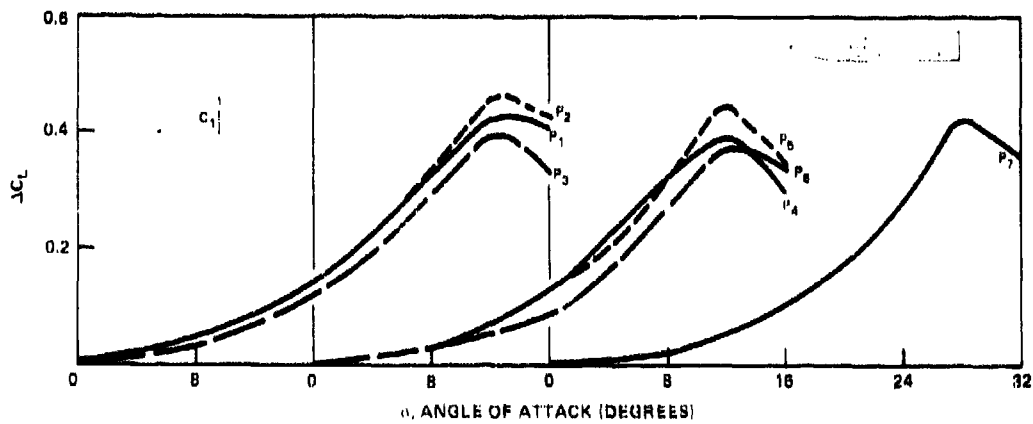


Figure 9b - Canard C_1 on 50-Degree Wing

Figure 9 (Continued)

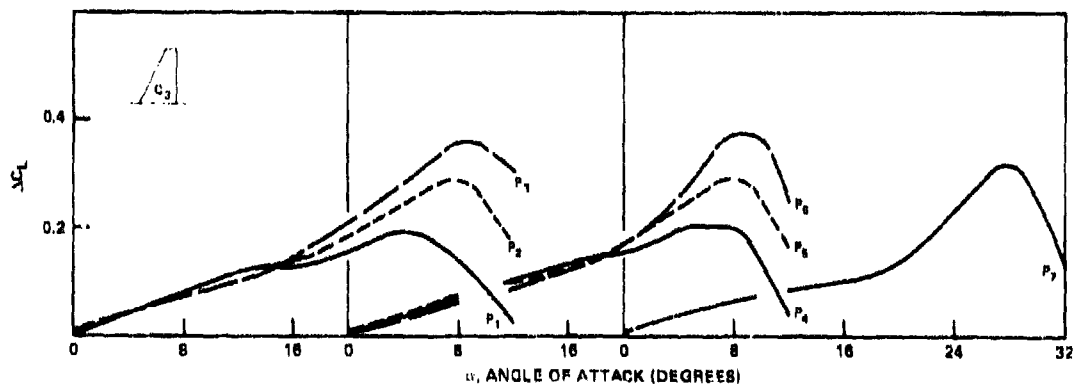
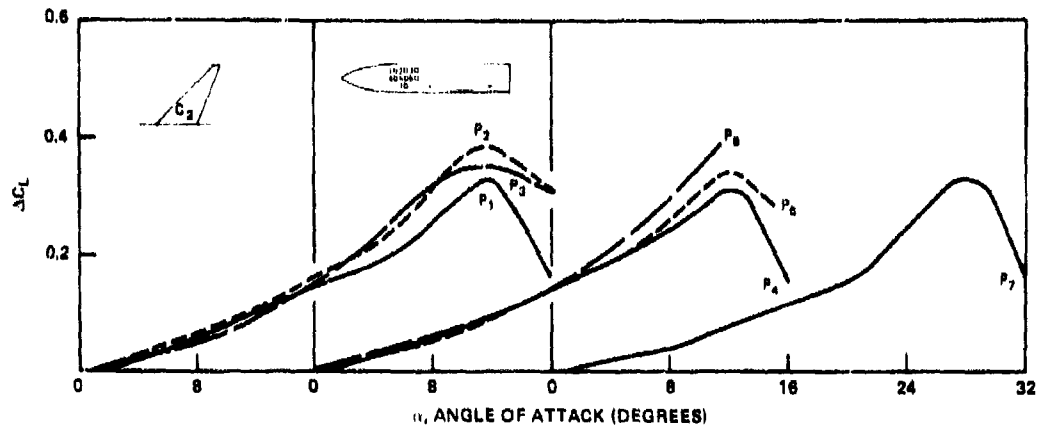


Figure 9 (Continued)

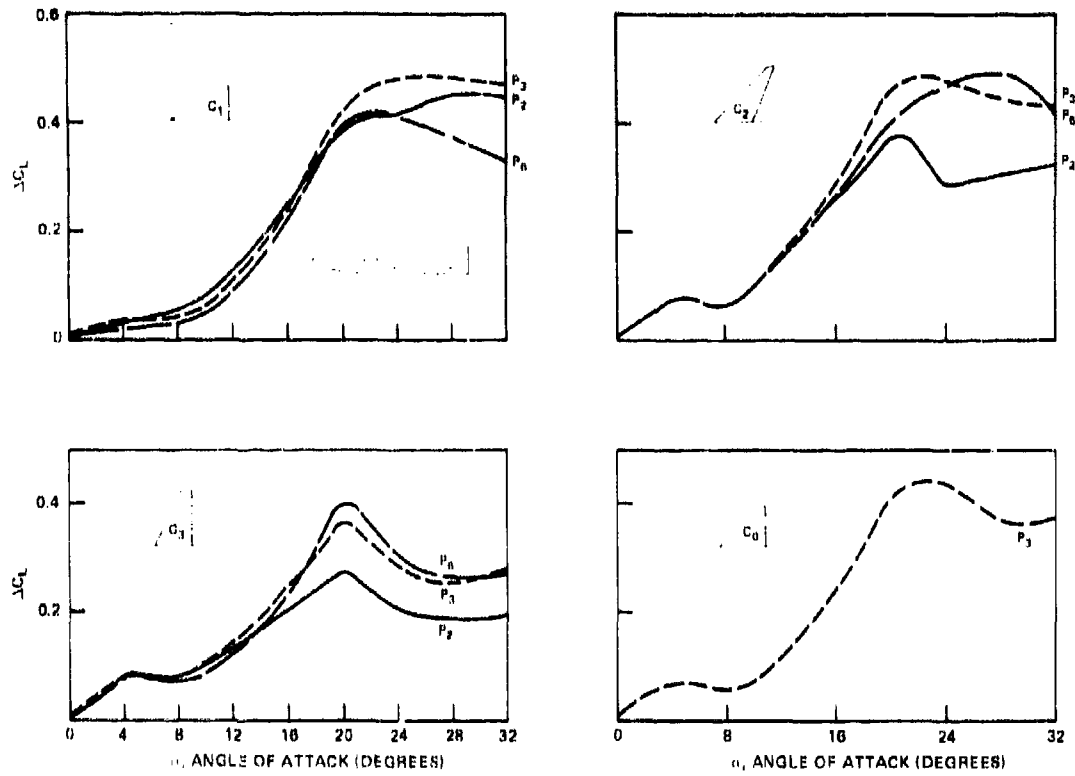


Figure 9e - Canards on 25-Degree Wing

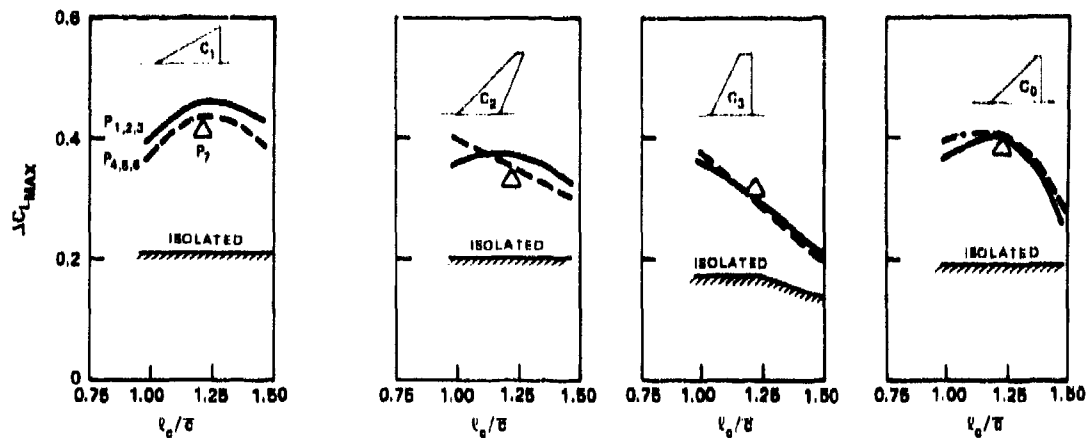


Figure 10a - Lift on 50-Degree Wing

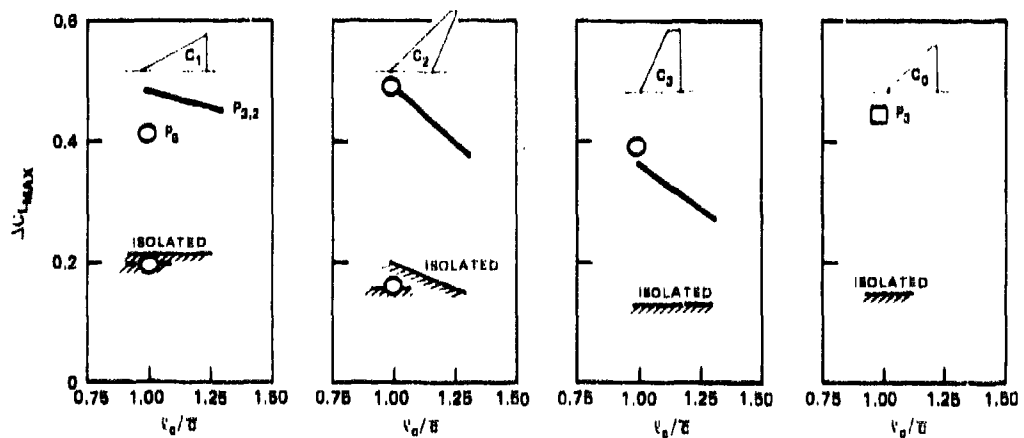


Figure 10b - Lift on 25-Degree Wing

Figure 10 - Maximum Incremental Lift Variation with Canard Position

Examination of the data relative to the interference free value indicates that the incremental lift is approximately double that of the interference free lift, if the canard is properly located. Improper location, i.e., too far forward or too low, reduces the value of the incremental lift to approximately 1 1/2 times the interference free value.

The value of incremental lift obtained is approximately the same for both 25- and 50-degree research models for properly located canards. The only exception is the 45-degree high aspect ratio canard which had significantly higher values of incremental lift when mounted on the 25-degree research model.

The data presented in Figure 10 are not at a constant angle of attack, hence, they do not represent the maximum lift coefficient obtained by the complete configuration. The angle of attack where maximum lift for the complete configurations occurred was generally at 32 degrees. Figure 11 presents the canard incremental lift at 32 degrees versus canard position, thus also showing the influence of canard placement on the maximum lift coefficient. Included in each figure is the interference free lift for each canard shape. In Figure 10, the incremental lift was always greater than the interference free lift. This is not the case at 32 degrees, particularly for the 50-degree research model. For all but the 60-degree delta canard C_1 , there are canard locations where the incremental lift is less than what would be obtained from the interference free value, thus indicating unfavorable interference. The onset of this unfavorable interference occurs at l_c/\bar{c} of approximately 1.4 for canards C_0 and C_2 and approximately l_c/\bar{c} of 1.2 for canard C_3 . Lowering the canard further moved the intersection point aft and reduced the lift.

The trends for the 25-degree research model are similar to those of the 50-degree model, although the only intersection point noted is for the 25-degree canard C_2 . This intersection point occurs at approximately the same l_c/\bar{c} value as that of the 50-degree wing model.

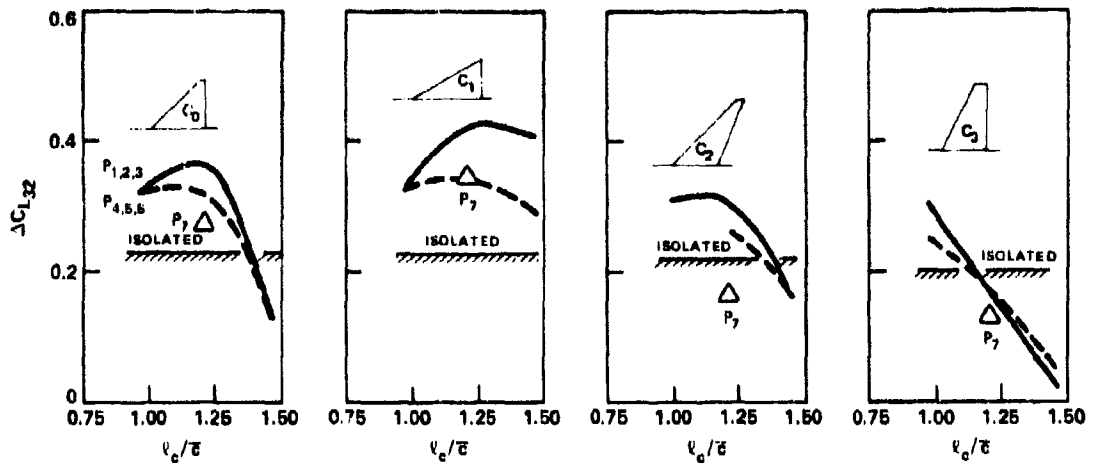


Figure 11a - Lift on 50-Degree Wing

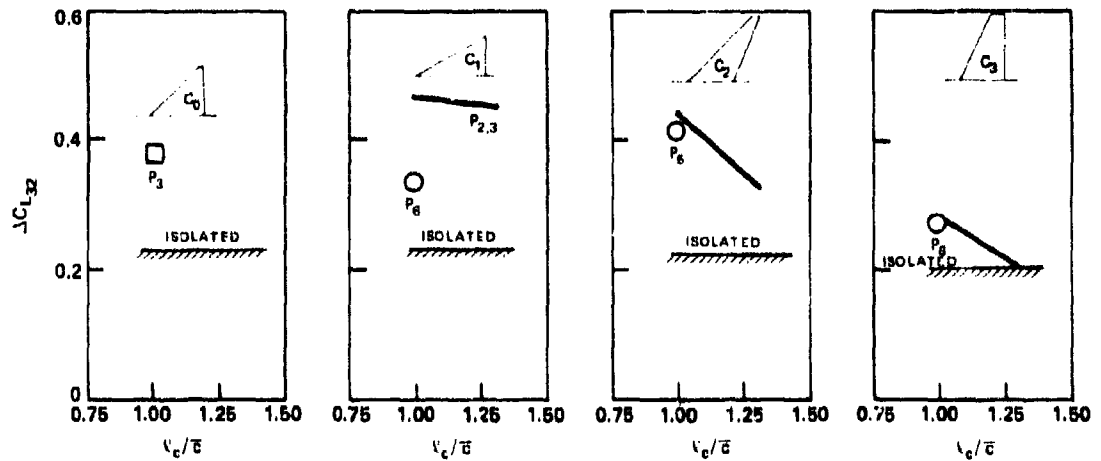


Figure 11b - Lift on 25-Degree Wing

Figure 11 - Incremental Lift at 32-Degree Angle of Attack

DEFLECTION

Canard deflection has direct influence on the maximum lift generated. This influence, either favorable or unfavorable, is dependent on canard position and size.

The variation of lift coefficient at 20-degree angle of attack are presented in Figure 12 for the four sizes of the 45-degree truncated delta canard C_0 . In general at low deflection angles, $\delta_c \leq 10$ degrees, there is little change in the lift coefficient for all positions and sizes. As deflection is increased different trends occur. The smaller canards $S_c/S_w = 0.10$, and 0.15 located in the high positions P_1, P_2, P_3 exhibit little change in lift coefficient with increasing deflection angle. As the canard size is increased or moved closer to the wing, there is a decrease in lift coefficient with increasing deflection angle. This reduction in lift occurs primarily at P_6 and P_7 for the smallest canard $S_c/S_w = 0.10$, and Positions 3, 6 and 7 for larger sizes. Thus, for canards which might be used for control purposes, i.e., removed from the wing, there is little lift loss due to the canard. Canards which are located close to the wing, however, exhibit lift losses with increasing deflection angle. The previous discussion is based on data at 20-degree angle of attack. At higher angles of attack it should be remembered that when the canard is moved longitudinally away from the wing the likelihood of canard stall increases and, thus, the above discussion is not likely to hold.

The effect of canard deflection on the incremental lift characteristics of the four different canard shapes is presented in Figure 13 for both 25- and 50-degree research models. Data are presented for canard deflection angles of $\pm 10, \pm 5$, and 0 degrees for the 50-degree wing and 0 and -10 degrees for the 25-degree wing model. Canard positions represented are Positions 3 and 6 ($l_c/\bar{c} \sim 1.0$).

Canard deflection has little effect on the incremental lift characteristics at low angle of attack and, as reported in Volume 1, $C_{L\delta}$ is approximately $1/2 C_{L\alpha}$ of the isolated canard. At higher angles of attack distinct differences in incremental lift appear as shown in Figure 14 for the case of 32-degree angle of attack. Examination of the figure reveals the large

Figure 12 - Variation in Lift Coefficient at $\alpha = 20$ Degrees versus Canard Deflection Angle δ_c

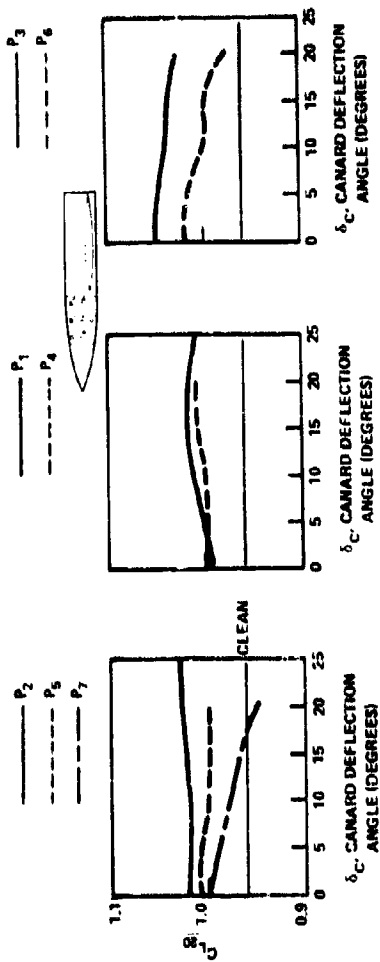


Figure 12a - Canard 0.10

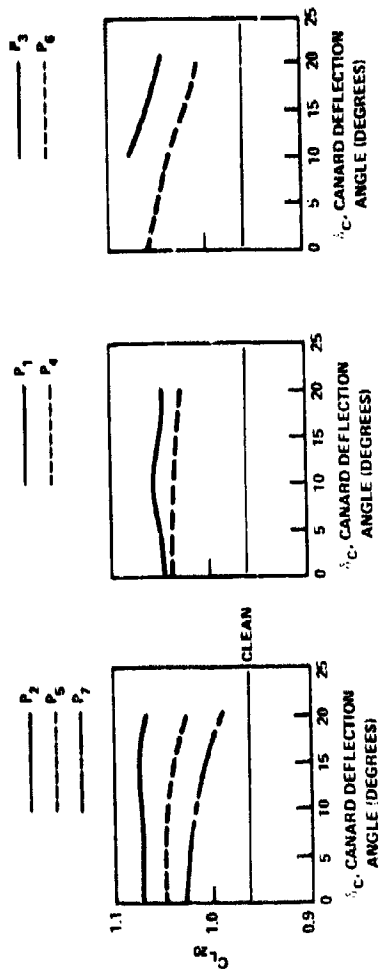


Figure 12b - Canard 0.15

Figure 12 (Continued)

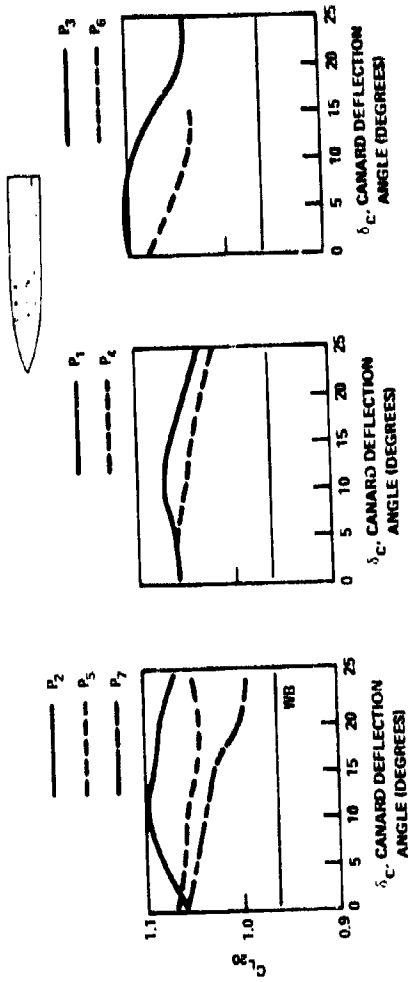


Figure 12c - Canard 0.20

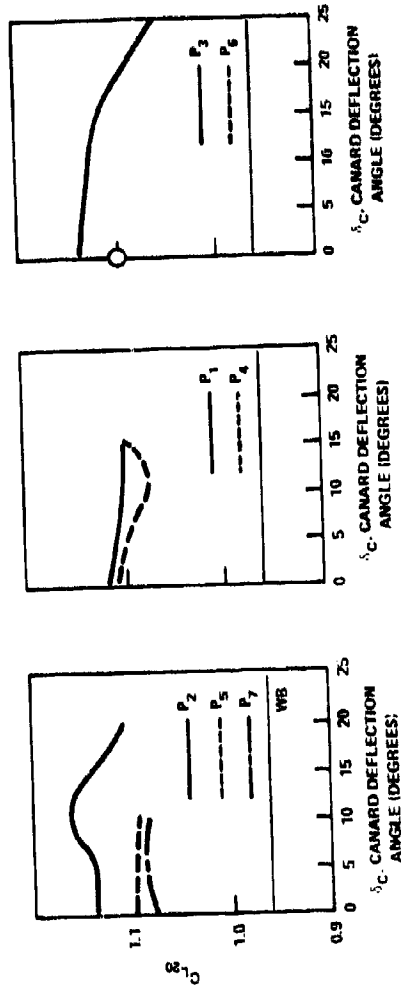


Figure 12d - Canard 0.25

Figure 13 - Incremental Lift Variation with Canard Deflection

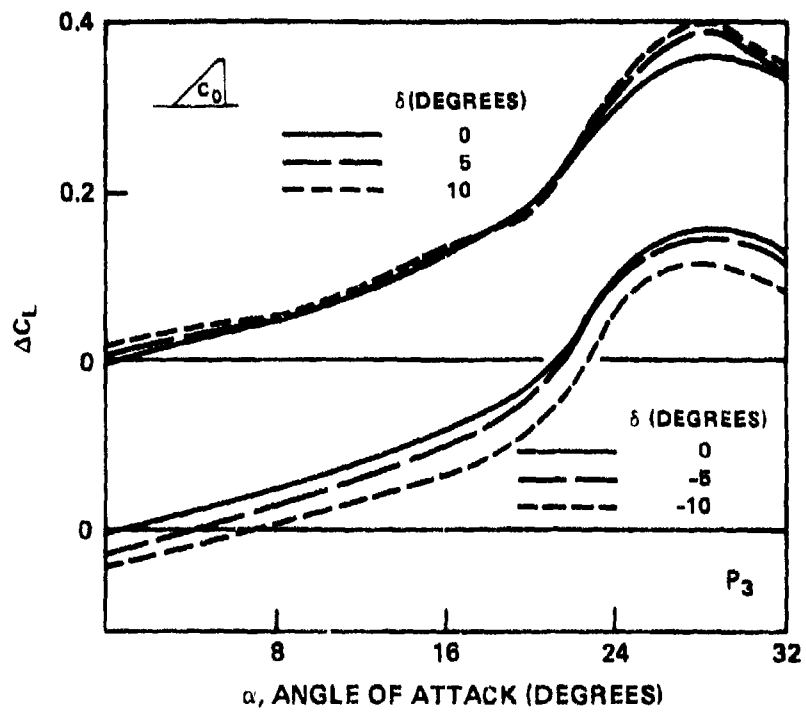


Figure 13a - Canard C_0 on 50-Degree Wing

Figure 13 (Continued)

δ_c (DEGREES)

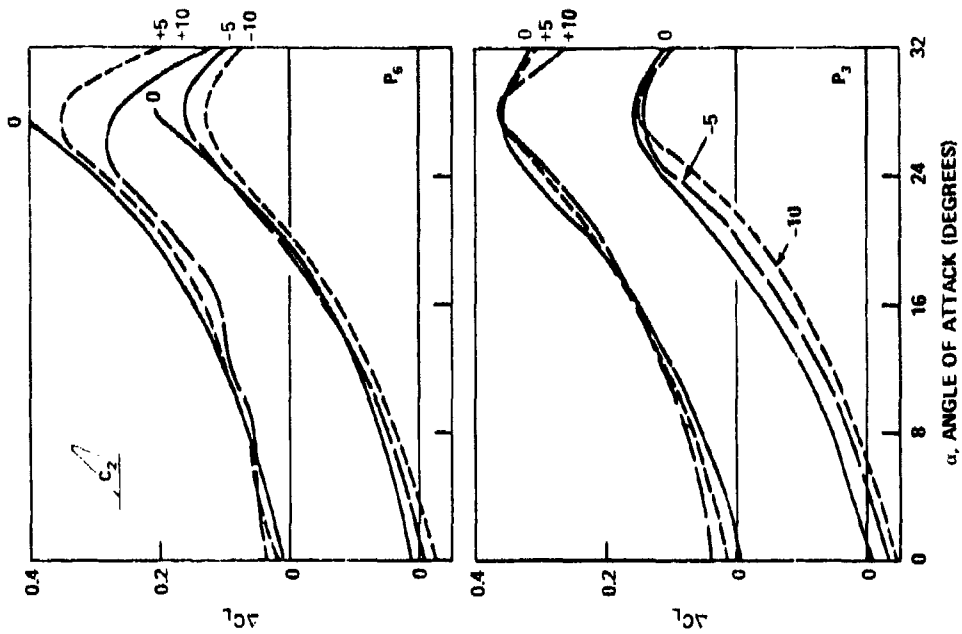


Figure 13c - Canard C_2 on 50-Degree Wing

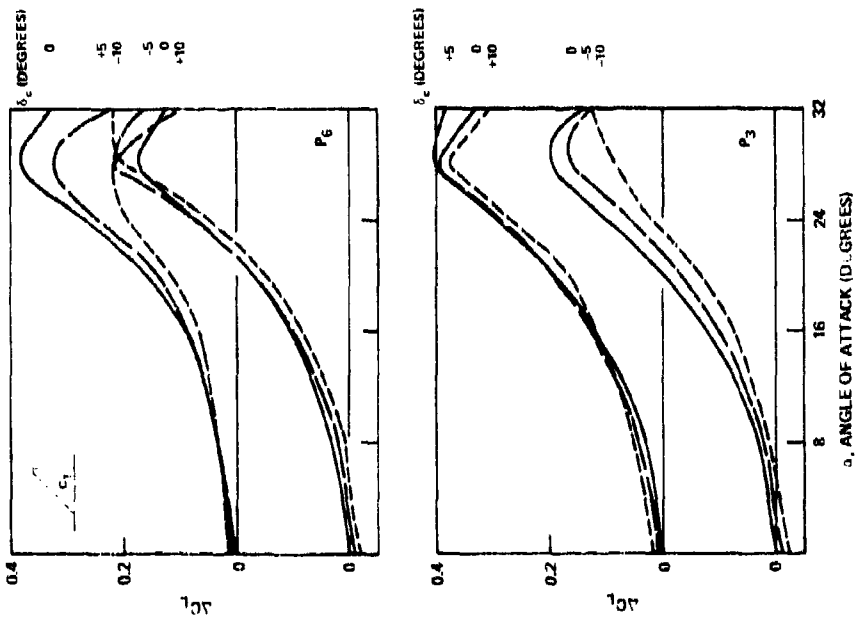


Figure 13b - Canard C_1 on 50-Degree Wing

Figure 13 (Continued)

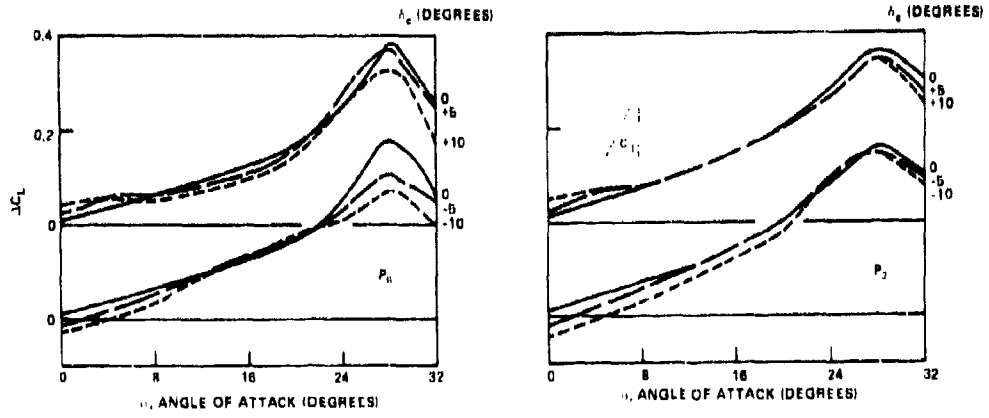


Figure 13d - Canard C_3 on 50-Degree Wing

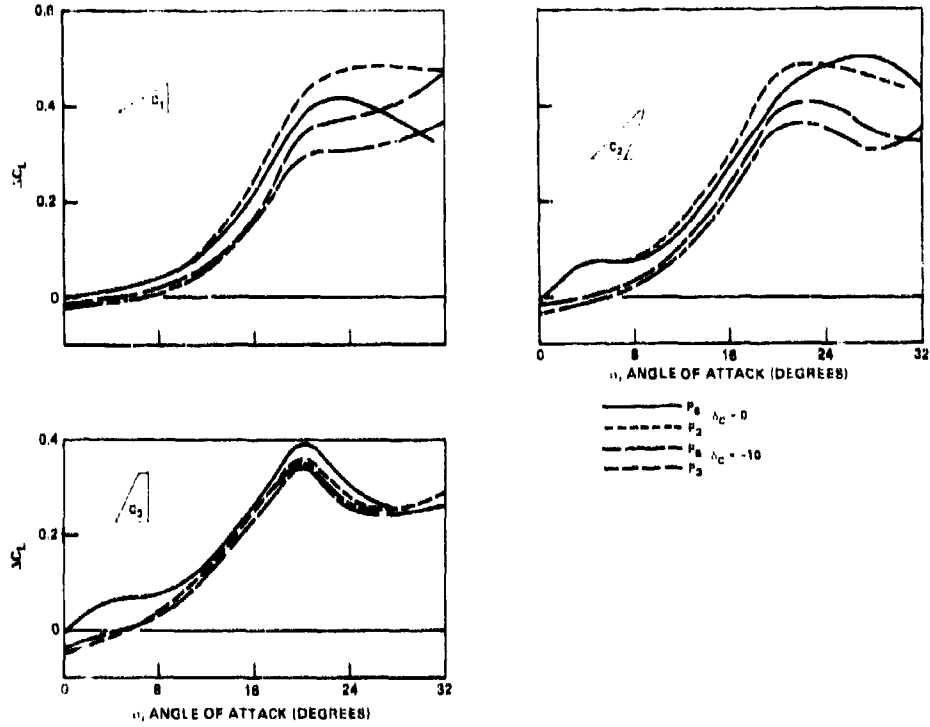


Figure 13e - Canards on 25-Degree Wing

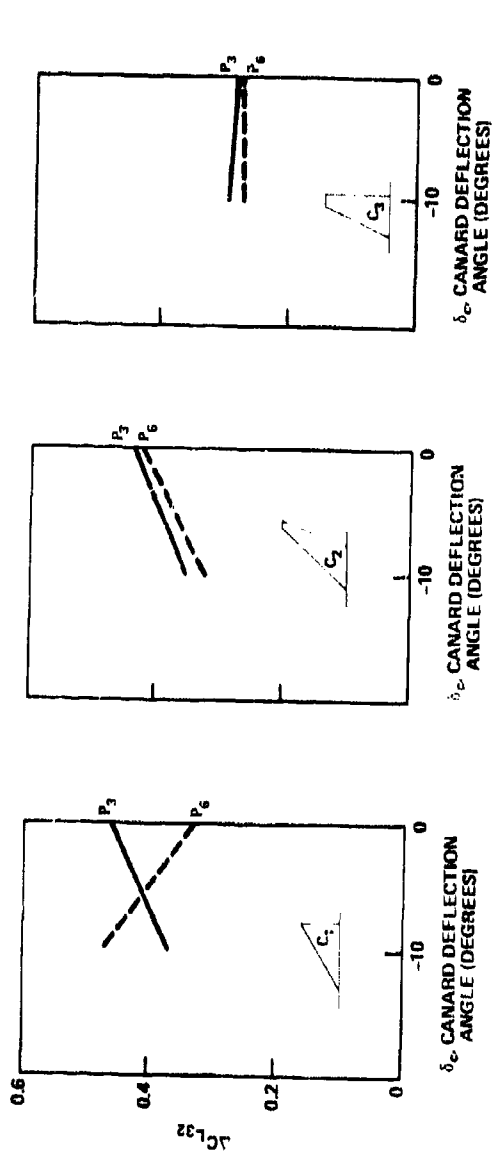


Figure 14a - Lift on a 25-Degree Wing

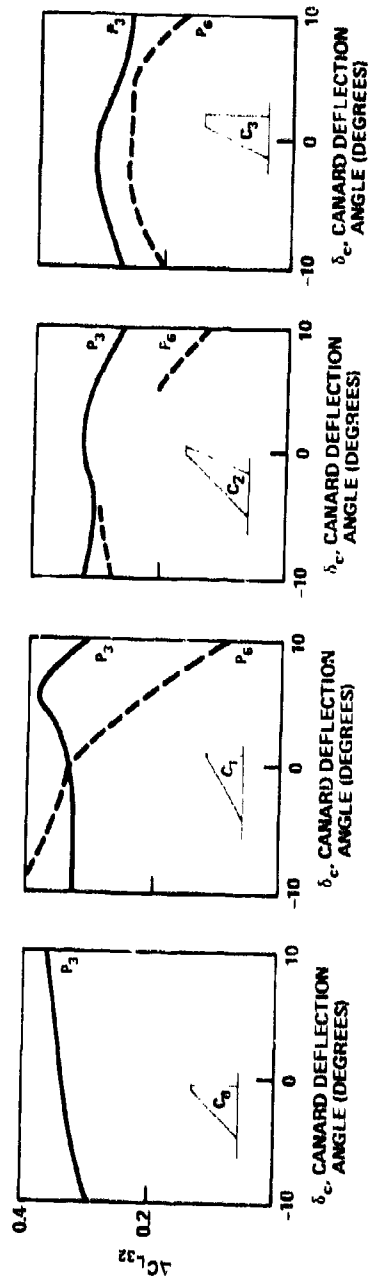


Figure 14b - Variation of $\Delta C_{L_{32}}$ with Canard Deflection

dependence of position on lift at equal canard deflection angles. This is seen most clearly for the 60-degree delta canard C_1 and for both 25- and 50-degree models. When the canard is at the low position P_6 , positive deflections cause a severe lift loss and negative deflections cause a lift gain. Similar trends occur for both the high aspect ratio canards C_2 and C_3 on the 50-degree wing model.

Figure 15 utilizing the data from Figure 14 presents incremental lift versus the canard trailing edge gap measured between the wing upper surface and the canard trailing edge. The gap was made nondimensional with respect to projected canard span.

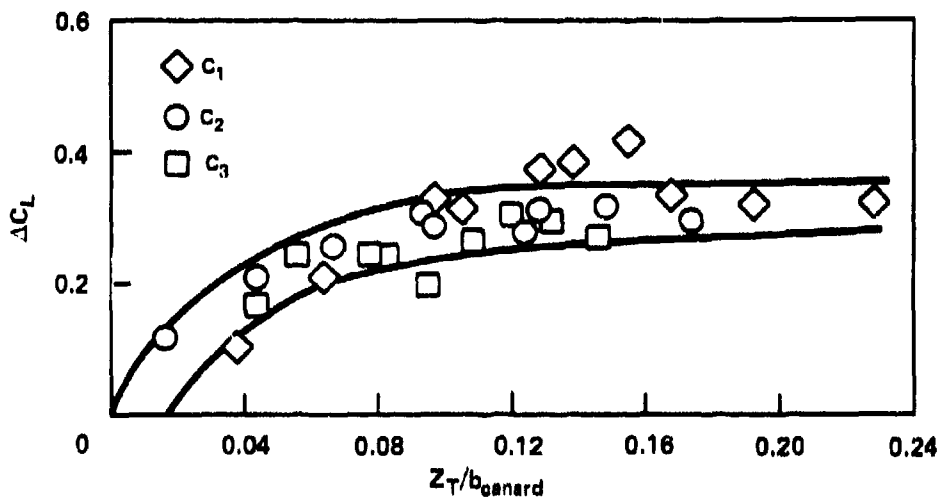


Figure 15 - Variation of $\Delta C_{L_{32}}$ with Canard-Wing Vertical Gap

Without taking into account differences in canard lift curve slope, a pattern of incremental lift versus gap height can be seen which is somewhat similar to a ground effect plot albeit in an inverted sense. In true ground effect, C_L increases with respect to proximity to the ground. In the case of the canard, close proximity of the canard to the wing causes a lift loss.

By taking the incremental moment data presented in a later section at the same angle of attack and dividing by the corresponding incremental lift, Figure 16 has been developed.

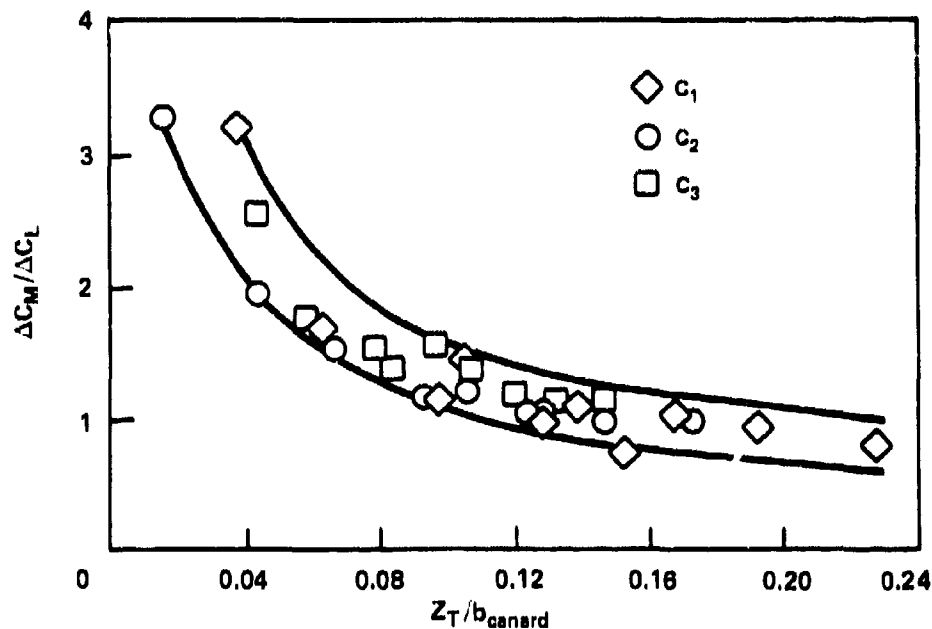


Figure 16 - Variation of $\Delta C_M/\Delta C_L$ with Canard-Wing Vertical Gap

It is seen that at gap ratios greater than 0.1 the ratio $\Delta C_M/\Delta C_L$ is approximately 1 which is where the canards are located, i.e., $z/\bar{c} = 1$. However, as gap height is decreased $\Delta C_M/\Delta C_L$ moves rapidly forward indicating that the canard is very highly loaded (typical of ground effect) and the wing is unloading. This behavior of the wing is perhaps due to the canard downwash having an unfavorable effect on the lift. It thus appears that for good high angle of attack characteristics the canard should be at least 0.10 canard spans above the wing plane.

WING LEADING EDGE CHANGES

The research models utilized in the previous discussions had symmetrical leading edges and the normal leading edge radius associated with the 65A008 airfoil. It is well known that increases in performance can be obtained by suitable changes in wing leading edge radius or droop. In order to examine the effect of such changes on the aerodynamic characteristics, three radius changes and four leading edge droops were evaluated on the 50-degree model. Details of the radius changes and droops are given in Figure 17.

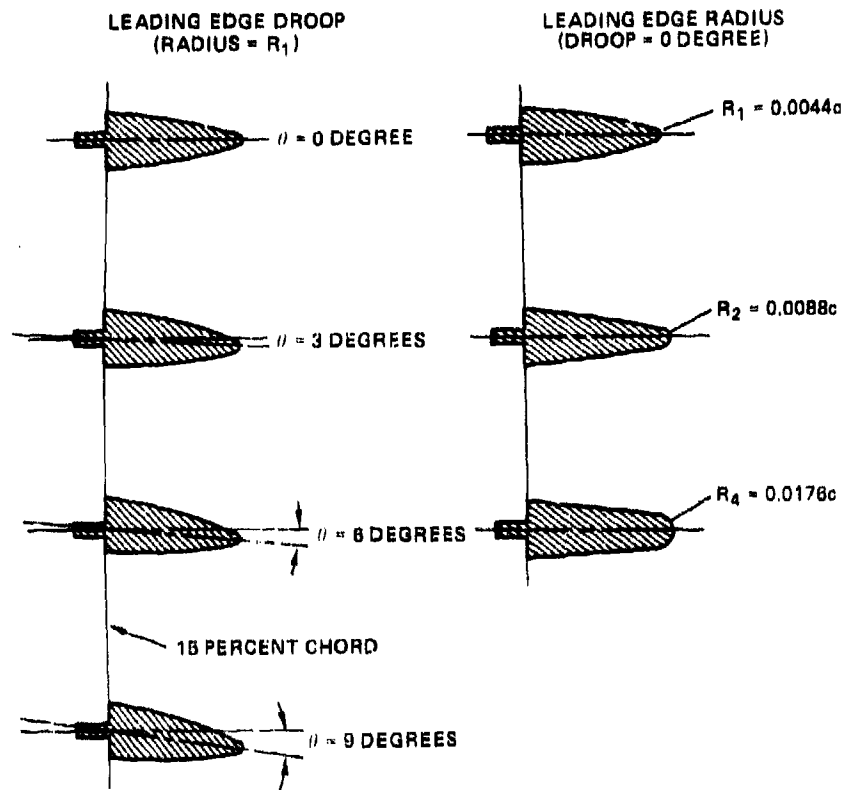


Figure 17 - Geometry of Wing Leading Edge Droops and Radii

Lift versus angle of attack is presented in Figure 18 for the 50-degree wing both with and without the canard for the varying radius and droops. The canard is the 45-degree truncated delta C_0 located at position P_3 and 0 degree deflection. As can be seen in the figure, neither radius change nor droop causes any appreciable change in lift for either canard-on or -off configurations.

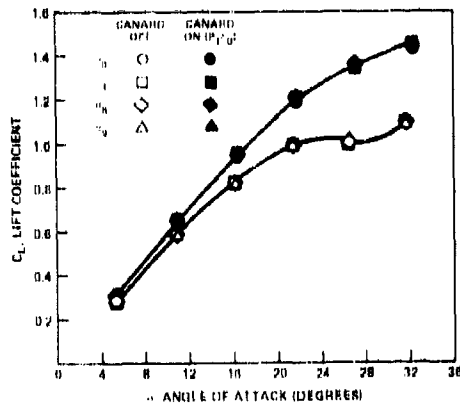


Figure 18a - Droops

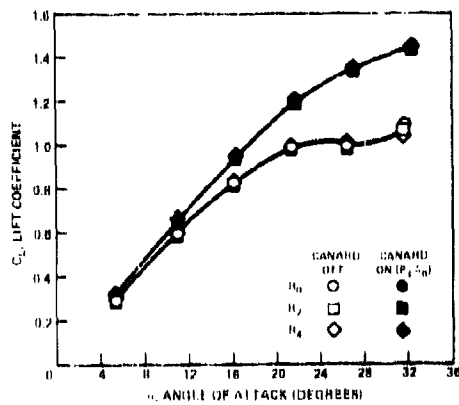


Figure 18b - Radius

Figure 18 - Effect of Wing Leading Edge Droop and Radius on Lift Characteristics

This lack of change was not the case for the 25-degree research model as shown in Figure 19. In the case of the 25-degree model, the -9-degree

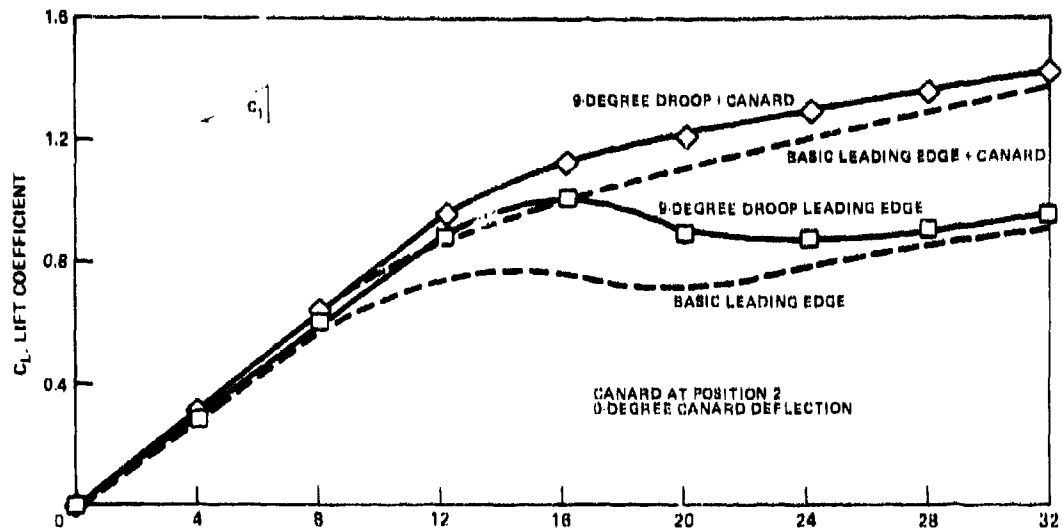


Figure 19 - Lift Characteristics of 25-Degree Model Modified with -9-Degree Wing Leading Edge Droop

droop delays stall by approximately 4-degree angle of attack and improves the maximum lift coefficient by 0.24. The effect of adding the canard to the modified model is presented in Figure 19. Data are presented for the 60-degree delta canard C_L located at P_3 and 0 degree deflection. Incremental lift versus angle of attack for the baseline and -9-degree droop models is presented in Figure 20 for the 60-degree canard at Positions 3 and 6 for deflections of 0 and -10 degrees.

Better stall characteristics of the wing, modified with the -9-degree droop, delays the effect of the canard by approximately 4-degree angle of attack. As angle of attack is increased beyond stall angle of attack; the value of incremental lift is approximately the same or slightly higher for the modified wing. It is thus seen that as the basic wing characteristics are improved the influence of the canard is delayed to higher angles of attack.

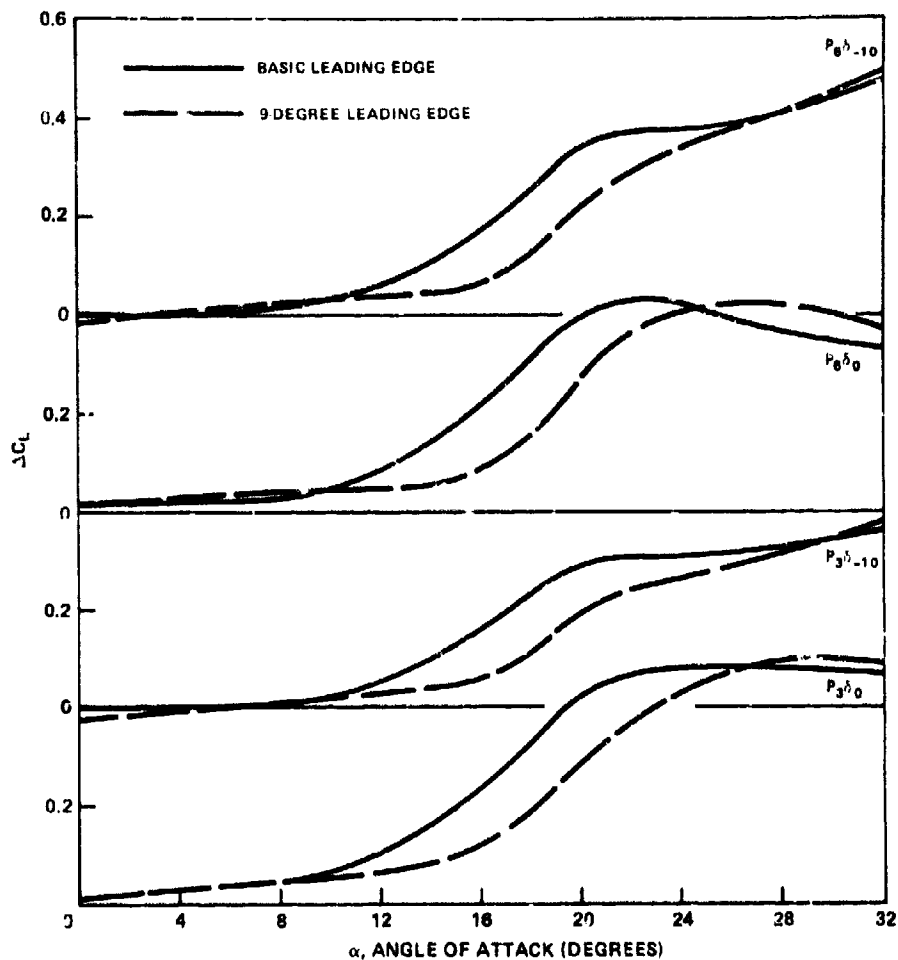


Figure 20 - Incremental Lift due to Canard for Basic and -9-Degree Droop, 25-Degree Wing Model

PITCHING MOMENT

The variation of pitching moment with angle of attack is presented in Figure 21. The data are for the same three canard geometries and positions as those presented in Figure 5 of the section of lift, mainly, the 60-degree delta, and the 45-degree and 25-degree sweep high aspect ratio on

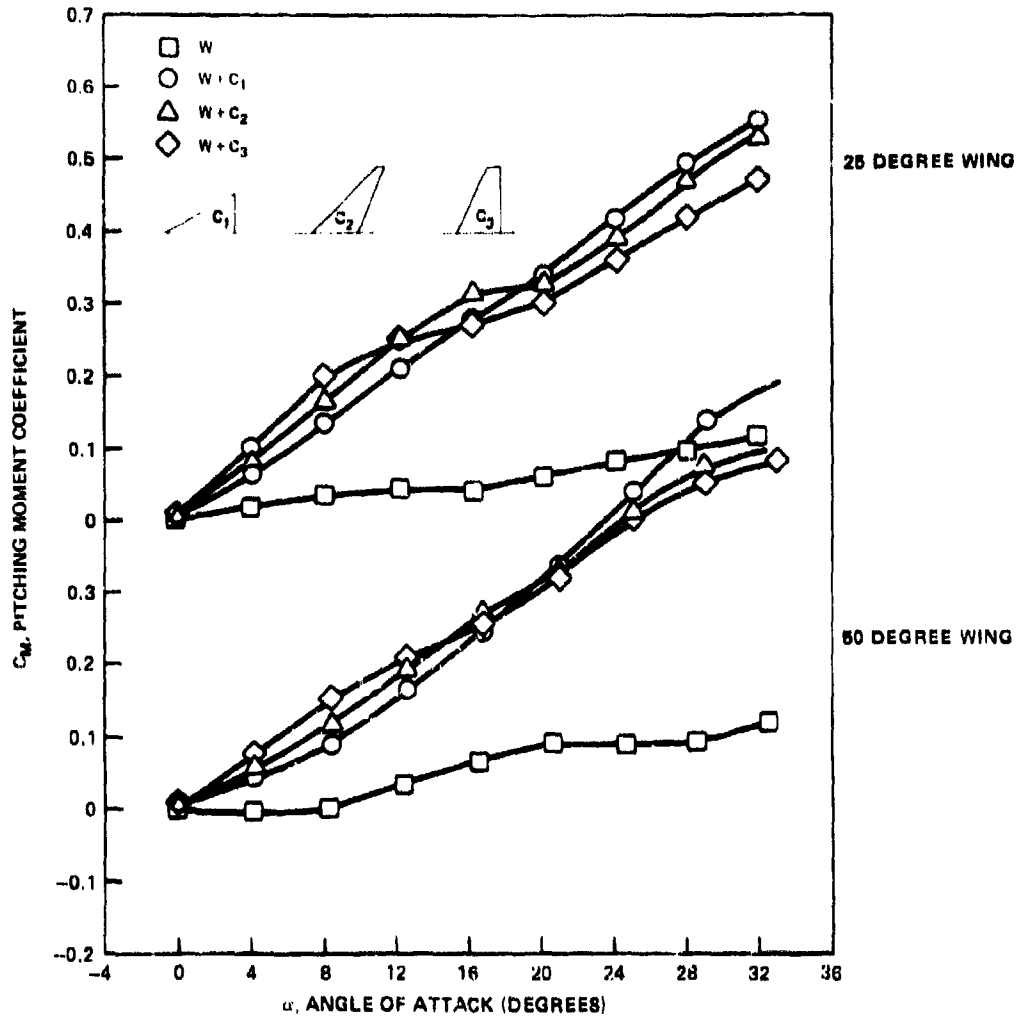


Figure 21 - Typical Pitching Moment Characteristics

canards. As with lift, differences occur due to canard shape. The data, however, indicate a fairly linear variation of pitching moment over the angle of attack range when the canards are installed. The influence of size, shape, and position on pitching moment are discussed in this section.

Examination of the data presented in Figure 21 indicates that the pitching moment behavior of the basic wing-body is not linear. This

nonlinear behavior is most pronounced for the 50-degree sweep wing model. To determine the effect of the canard, incremental pitching moments ΔC_M will be used almost exclusively in the following discussion. The basic data from which these incremental moments have been obtained can be found in the references.

SIZE

The influence of canard size on pitching moment at zero lift C_{M_0} is presented in Figure 22. Shown is C_{M_0} versus deflection for canard projected area ratios S_c/S_w from 0.10 to 0.25. As indicated, the increase in moment with deflection is reasonably linear for each canard position and size.

Figure 23 presents zero lift pitching moment at 10-degree deflection versus canard area ratio at Positions 1 and 3. As shown, the data do not intercept the zero value at zero canard size, therefore, indicating that the canard projected area ratio is too large a parameter for good agreement. The data, when plotted versus canard exposed area ratio, converge to zero at zero canard size as indicated in Figure 24. Data are presented for each of the seven canard positions evaluated and, as shown, linear fits of the data are obtained at each position. As expected, moving the canard forward increases the pitching moment; not so expected is the fact that lowering the canard reduces the magnitude of the pitching moment change.

The data from Positions 1, 2, and 3 have been plotted versus canard exposed volume coefficient and are presented in Figure 25. Canard volume coefficient is defined as $l_c/\bar{c} \times S_{c_e}/S_w$, where l_c is measured from the 0.27 \bar{c} position of the wing to the 40 percent exposed root chord of the canard. The variation in C_{M_0} with exposed volume coefficient is linear as shown.

The forward shift in neutral point due to canard size is presented in Figure 26. The parameters chosen are incremental moment slope evaluated at zero lift versus canard exposed volume coefficient. Data are presented

Figure 22 - Variation of Pitching Moment Coefficient at Zero Lift C_{M_0} with Canard Deflection Angle δ_c

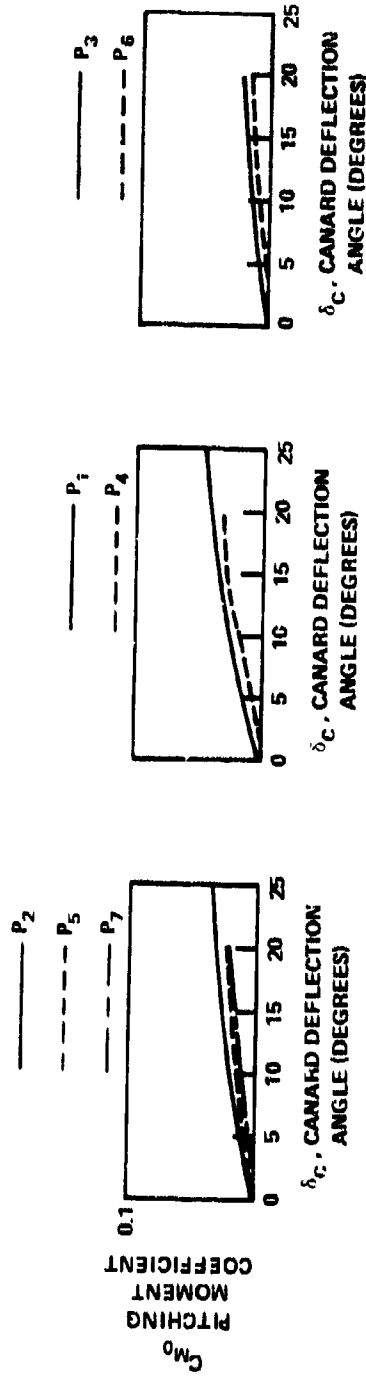


Figure 22a - Canard 0.10

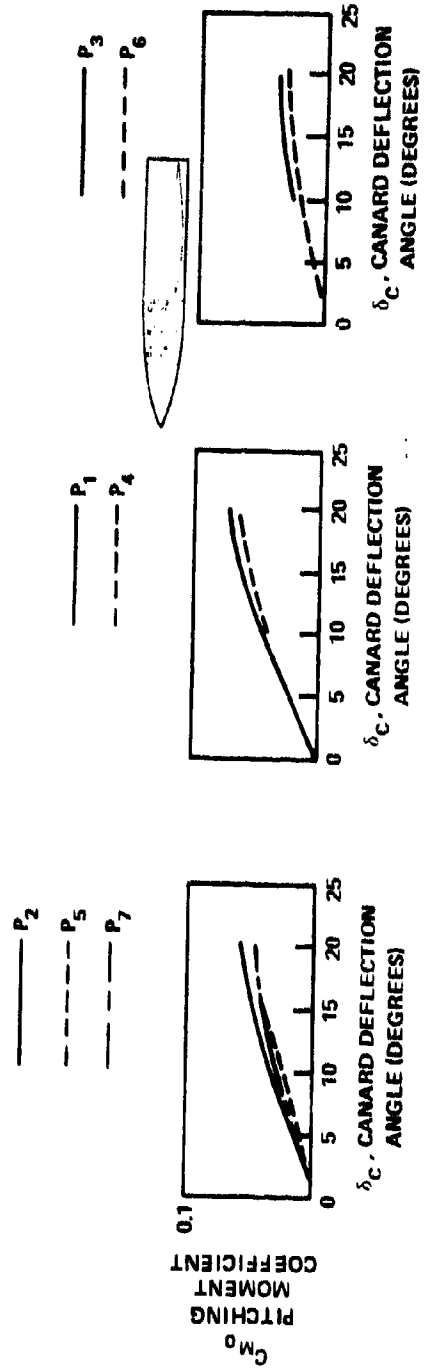


Figure 22b - Canard 0.15

Figure 22 (Continued)

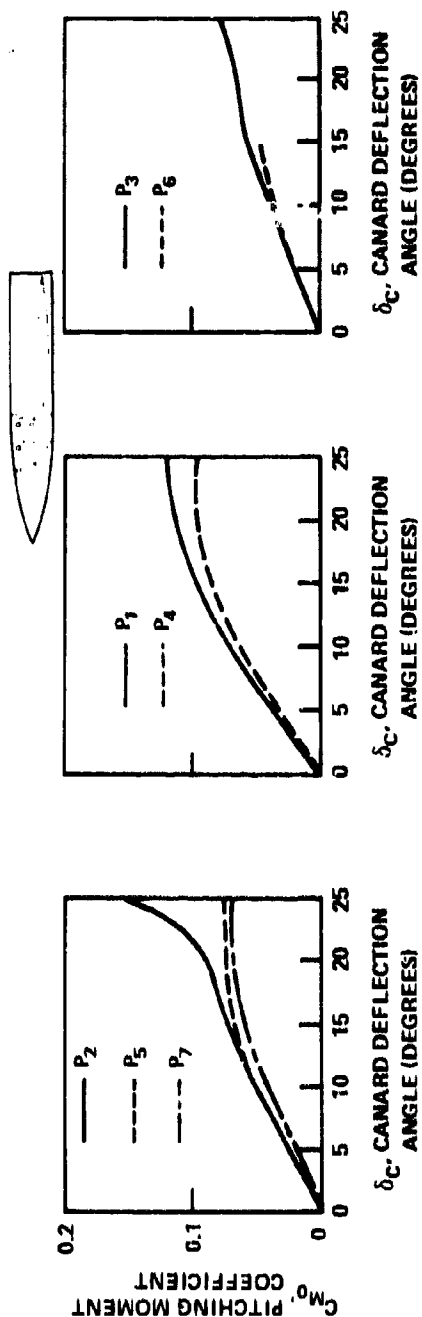


Figure 22c - Canard 0.20

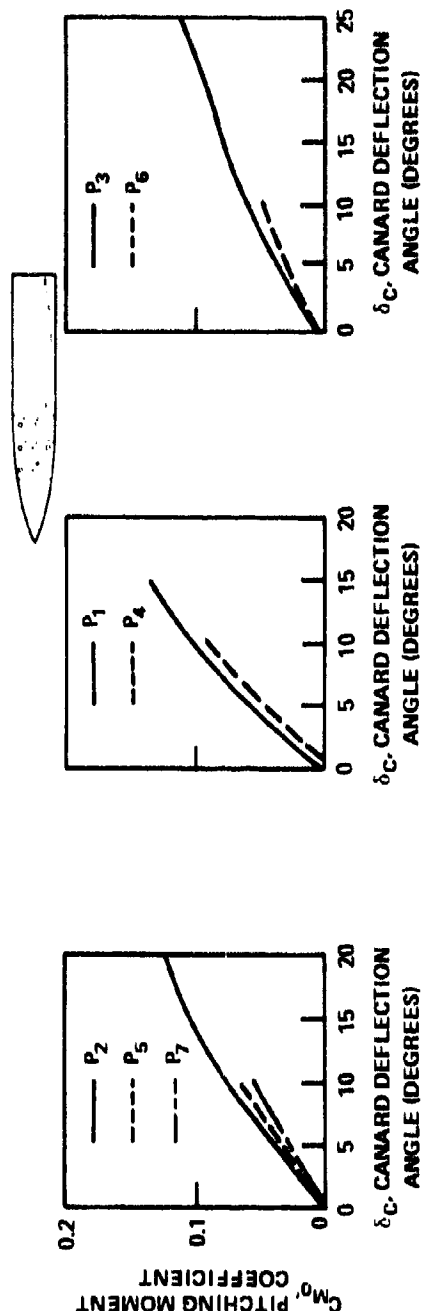


Figure 22d - Canard 0.25

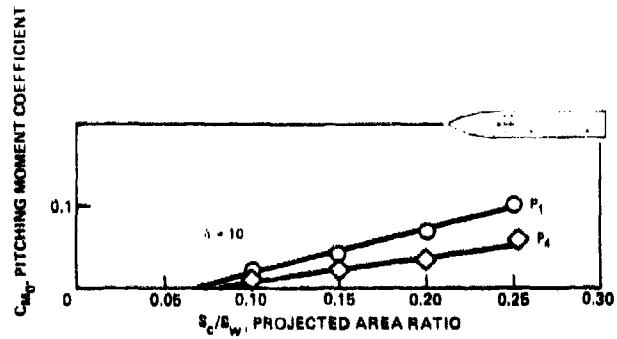


Figure 23 - Zero Lift Pitching Moment versus Projected Area Ratio

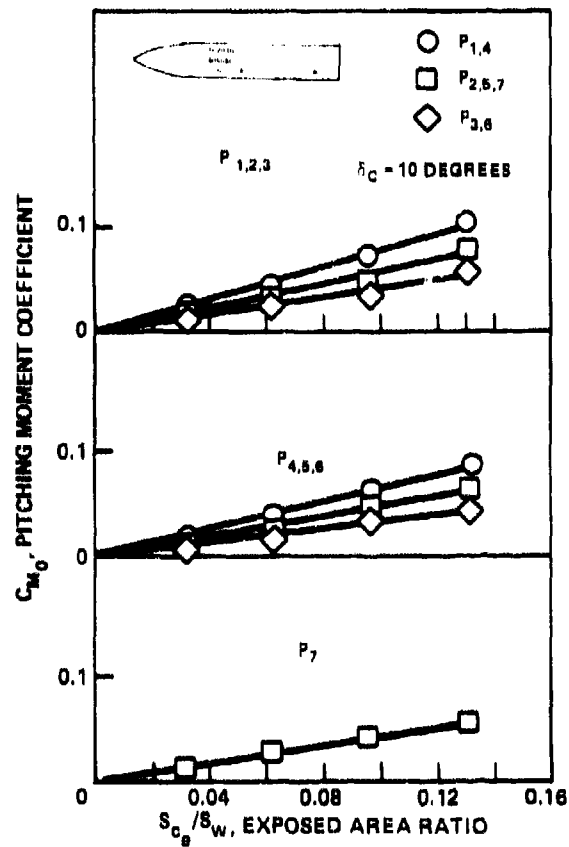


Figure 24 - Zero Lift Pitching Moment versus Exposed Area Ratio

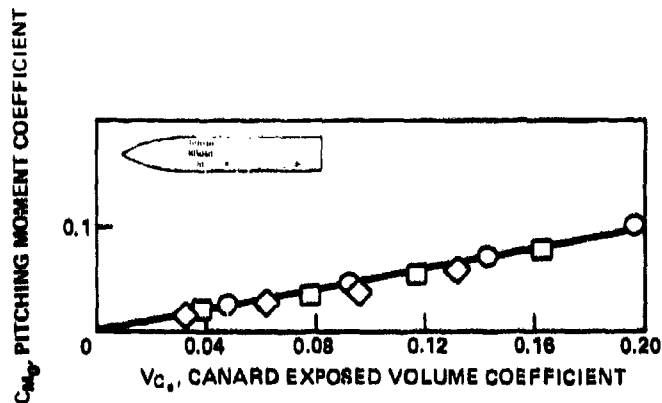


Figure 25 - Zero Lift Pitching Moment Variation with Canard Exposed Volume Coefficient

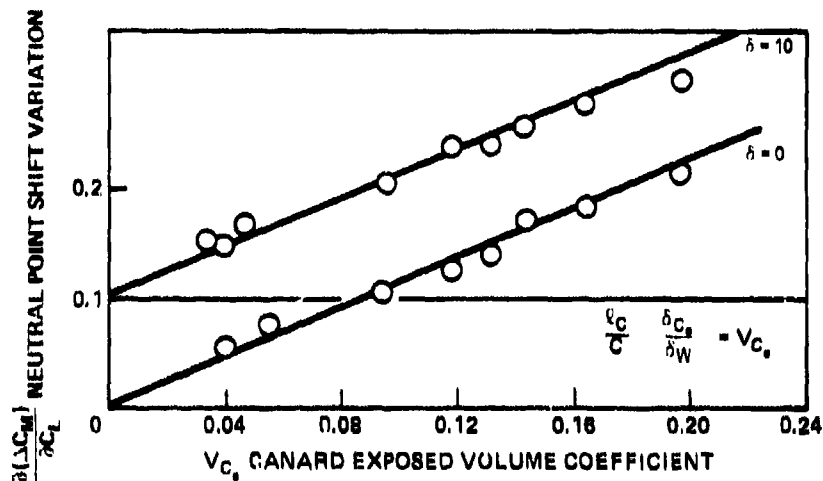


Figure 26 - Neutral Point Shift Variation with Canard Exposed Volume Coefficient

at 0- and 10-degree canard deflection. The variation of $\frac{\partial(\Delta C_M)}{\partial C_L}$ is linear for both deflection angles and ranges from a forward shift of $0.04 \bar{c}$ for the smallest canard tested at the aft position ($l_c/\bar{c} \sim 1$, $S_c/S_w = 0.1$) to a shift of $0.20 \bar{c}$ for the largest canard at the most forward position ($l_c/\bar{c} \sim 1.5$, $S_c/S_w = 0.25$).

SHAPE

The variation of incremental moment with canard shape is shown in Figure 27. Data are presented for the four canard shapes located at P_3 for both 25- and 50-degree sweep models. Included on each figure are the values for each isolated canard shape at P_3 .

As with incremental lift, the most significant changes noted are the early differences between the 25-degree data and the isolated data. This is undoubtedly due to the early stall of the 25-degree wing.

At low angles of attack the incremental moment has the same value and slope as that of the isolated canard data for the four canard shapes and both wings, thus indicating little if any upwash effects due to the wing. As angle of attack is increased, significant differences occur primarily in magnitude. This is due to the fact that the canard is delaying stall over the root position of both wings. Thus, the center of pressure has moved inboard and forward for each wing thereby generating increased, nose-up moments.

Comparison between the incremental and isolated canard data indicates reasonable agreement between the slopes and general shape of the curves for each canard shape--most notably for the 25-degree sweep model. For example, the isolated 25-degree high aspect ratio canard C_3 has a stall at angles of attack between 12 and 16 degrees; similarly, the incremental data indicate a reduction in slope in this angle of attack region. Reductions in slope are also evident for both the 45-degree high aspect ratio canard C_2 and the 45-degree truncated delta canard C_0 and these reductions occur for both isolated and incremental data. No reduction in slope is evident for the 60-degree canard isolated data and no reduction is seen for the incremental data.

It is thus apparent that the general shape of the incremental moment curve is the same as that of the isolated surface.

POSITION

Incremental moment versus angle of attack is presented in Figure 28 for seven positions for the 50-degree wing model and three positions for

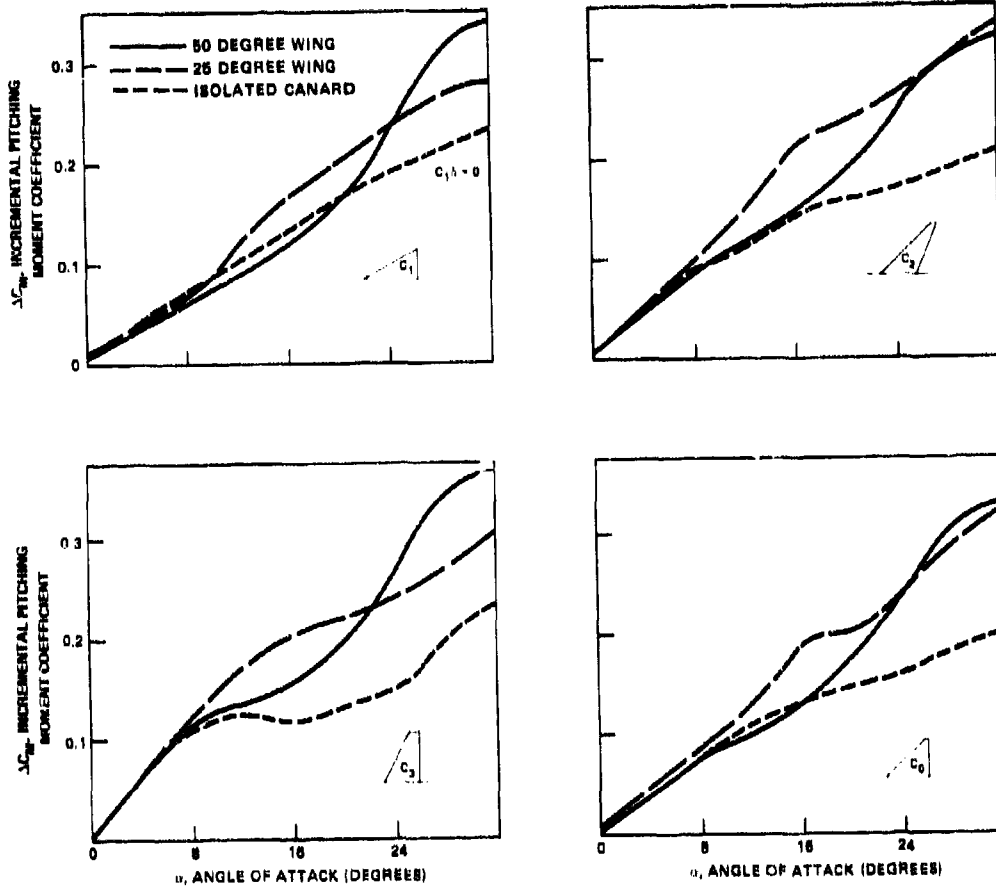


Figure 27 - Incremental Moment Variation with Canard Shape

Figure 28 - Incremental Moment Variation with Canard Position

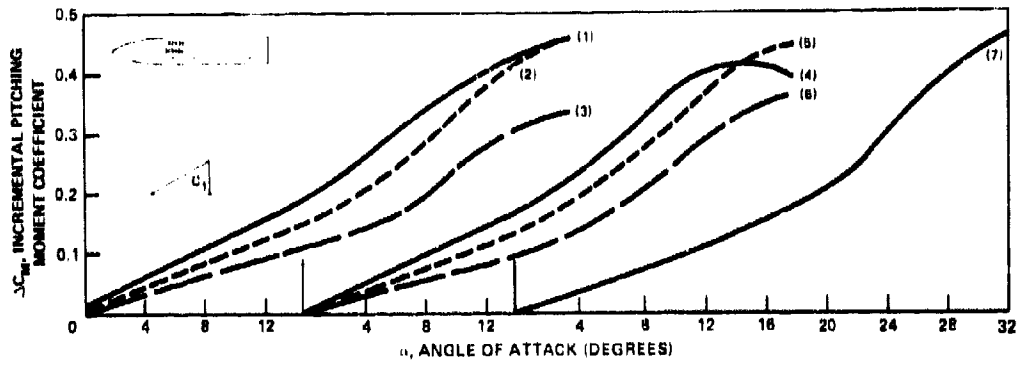


Figure 28a - Canard C_1 on 50-Degree Wing

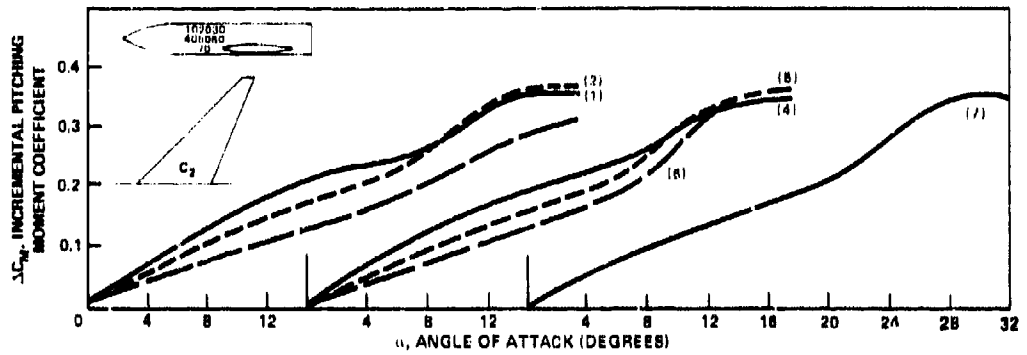


Figure 28b - Canard C_2 on 50-Degree Wing

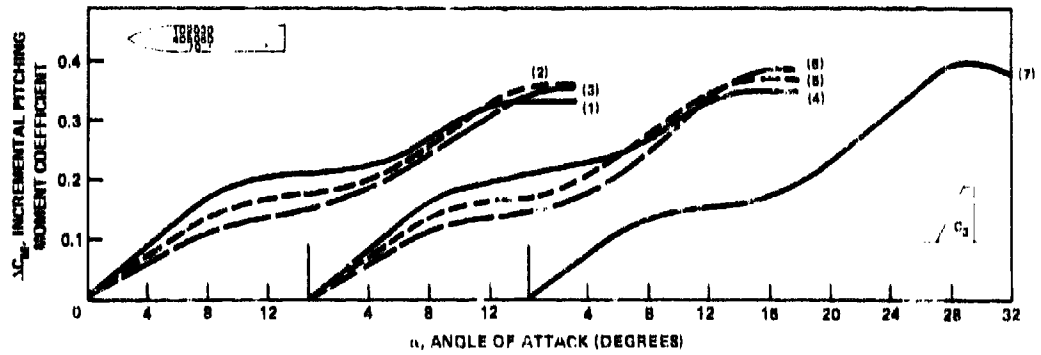


Figure 28c - Canard C_3 on 50-Degree Wing

Figure 28 (Continued)

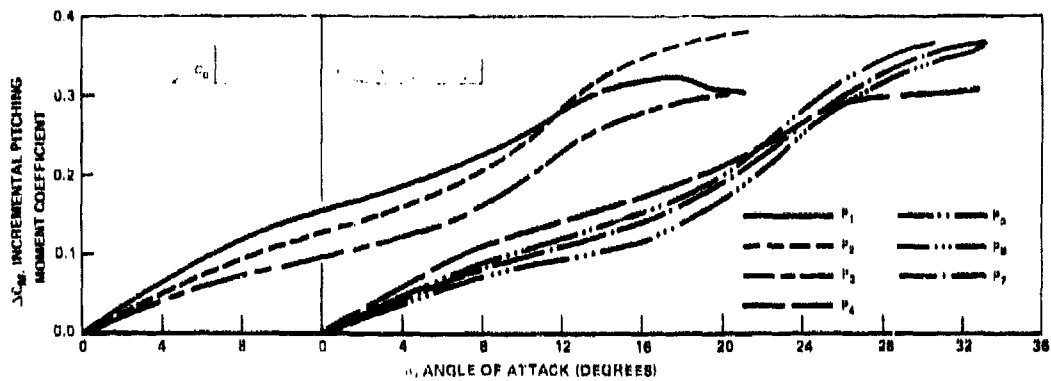


Figure 28d - Canard C_0 on 50-Degree Wing

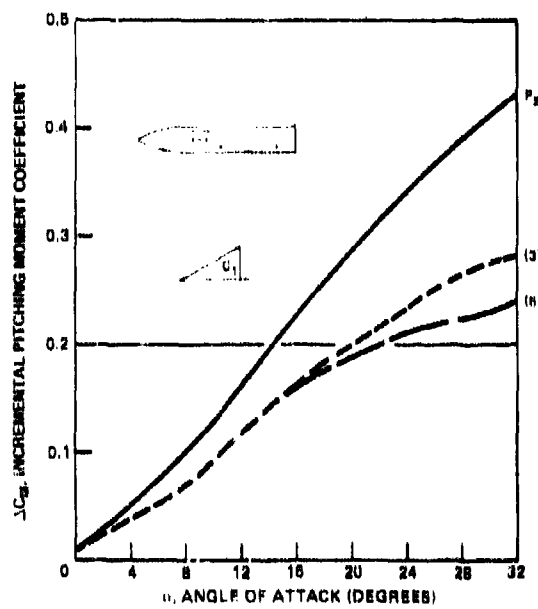


Figure 28e - Canard C_1 on 25-Degree Wing

Figure 28 (Continued)

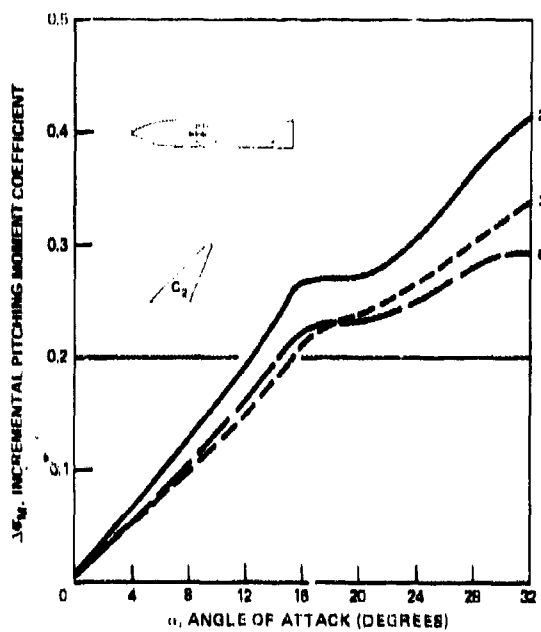


Figure 28f - Canard C_2 on 25-Degree Wing

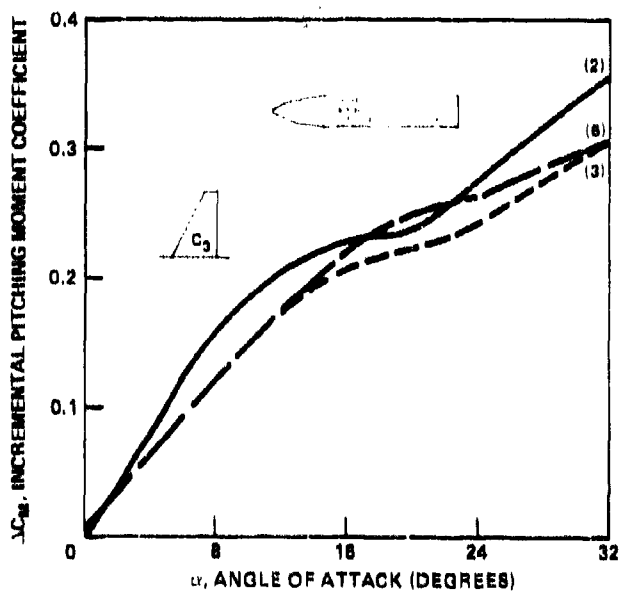


Figure 28g - Canard C_2 on 25-Degree Wing

the 25-degree wing configuration. The data are for the four canards at 0-degree canard deflection. In general, the incremental moments behave as expected at low angles of attack, that is, moving the canard forward increases the incremental moment for all configurations. At higher angles of attack, the effectiveness of the forward position drops off and the incremental moment is often less than that generated by the canards at further aft positions. This is shown in Figure 29 where incremental pitching

Figure 29 - Variation of $\Delta C_{M_{32}}$ with Canard Position

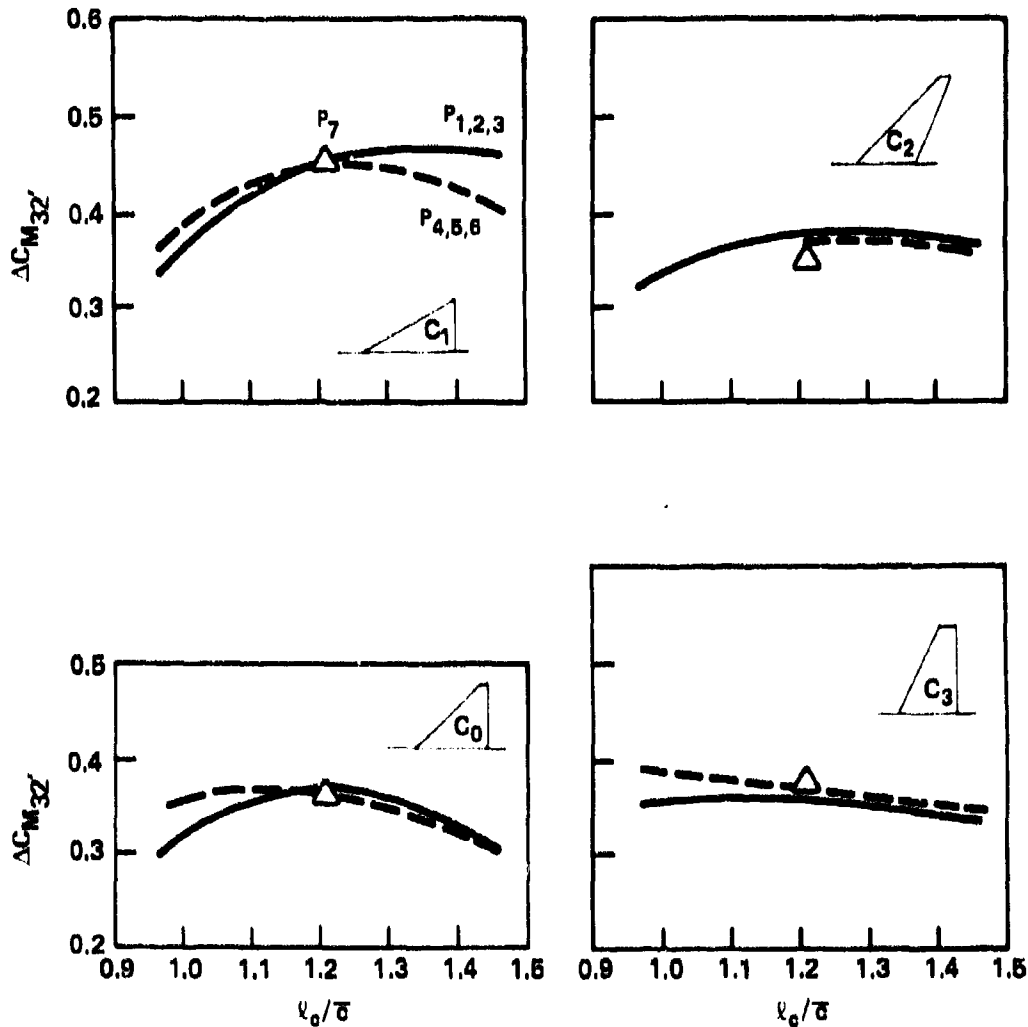


Figure 29a - Moment on a 50-Degree Wing

Figure 29 (Continued)

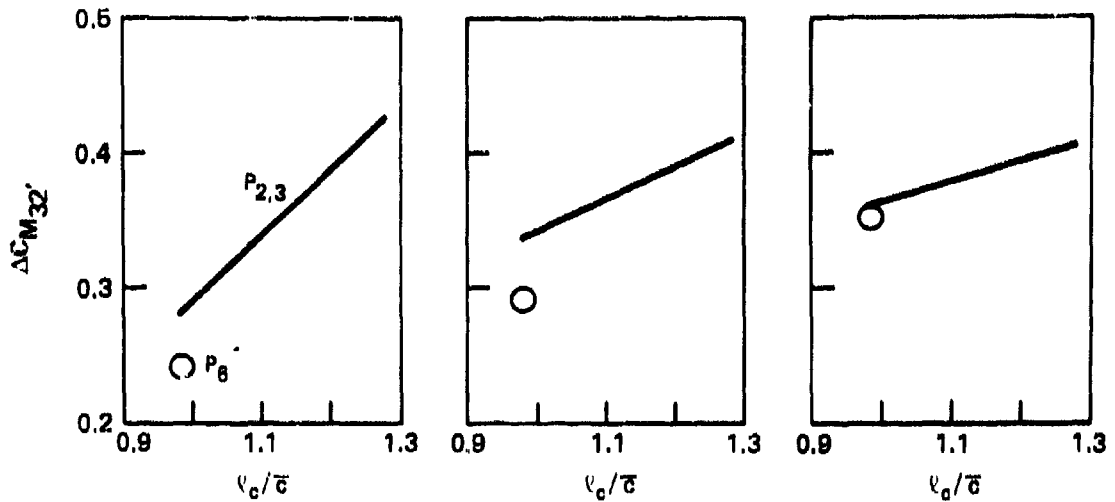


Figure 29b - Moment on a 25-Degree Wing

moment at 32-degree angle of attack is presented. As can be seen, maximum incremental moment occurs at the most forward position in only one case, that case being the 60-degree delta canard C_1 located in the highest most forward position P_1 . Maximum moment in general occurred at P_2 for most configurations. One exception to the rule was the 25-degree high aspect ratio canard C_3 where maximum moment occurred in the lowest most aft position. It is interesting to compare the shape of the variation of maximum lift coefficient with canard position shown in Figure 10 and the above variation of incremental moment. In both instances the shapes of the curves for each canard are extremely similar. Thus it appears that it is the lift being generated by the canard rather than the absolute canard position which is the primary determining factor of the moment generated.

Returning to Figure 28 it is seen that the incremental pitching moment slope is reasonably linear with angle of attack up to angles of attack of approximately 8 degrees. This variation of incremental pitching moment slope is presented in Figure 30 for both 25- and 50-degree models. In contrast with the moment data at 32-degree angle of attack, the variation of

$\Delta C_{M\alpha}$ behaves in a linear manner, in that increasing moment arm increases incremental pitching moment slope. As noted, lowering the canard reduces the slope slightly. The data from Figure 30 show a varying degree of slope change with canard shape as expected, due to the differences in canard lift curve slope and canard exposed area. The data from Figure 30 have been divided by the isolated canard lift curve slope and plotted in Figure 31 against canard exposed volume coefficient.

The plotted data fit a straight line reasonably well, thus indicating very little upwash with canard position and that the linear approximation

$$\frac{\partial(\Delta C_{M\alpha})}{\partial \alpha} \approx C_{L\alpha_T} \times V_{C_e} \text{ is reasonable at low angles of attack.}$$

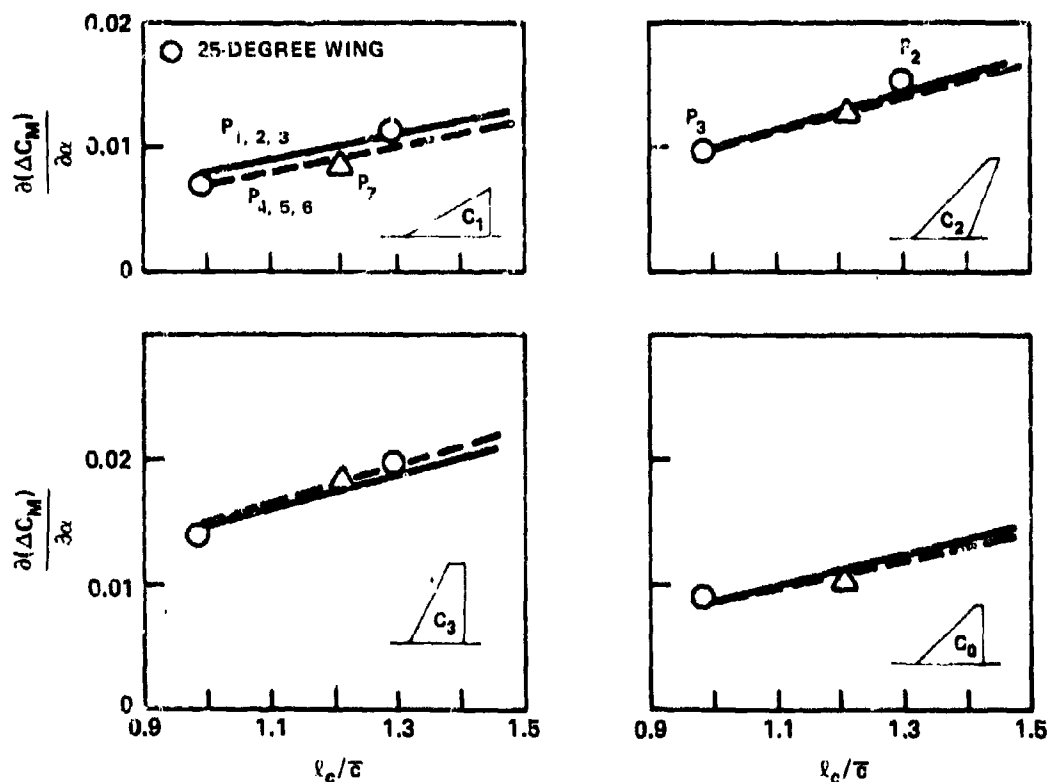


Figure 30 - Incremental Moment Slope Variation with Canard Position

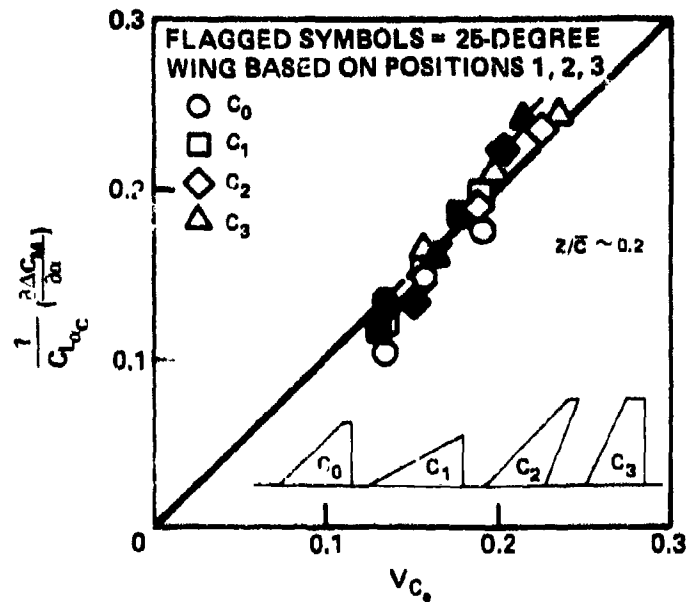


Figure 31 - Correlation of Neutral Point Change with Canard Exposed Volume Coefficient

DEFLECTION

The variation of incremental moment with canard deflection is presented in Figure 32. Data are presented for both 25- and 50-degree sweep models and the four canard shapes. The canards are located at Positions 3 and 6 and the deflection range is from -10 to +10 degrees for the 50-degree model and -10 to 0 degrees for the 25-degree model. When the canards are located in the high position P_3 , there is little change in incremental slope throughout the deflection range. An exception to this is the 25-degree high aspect ratio canard C_3 at low angles of attack. This canard has a varying incremental slope which is progressively reduced with increasing canard deflection. This reduction in slope is due to stall of the canard.

Figure 32 - Incremental Moment Change due to Canard Deflection

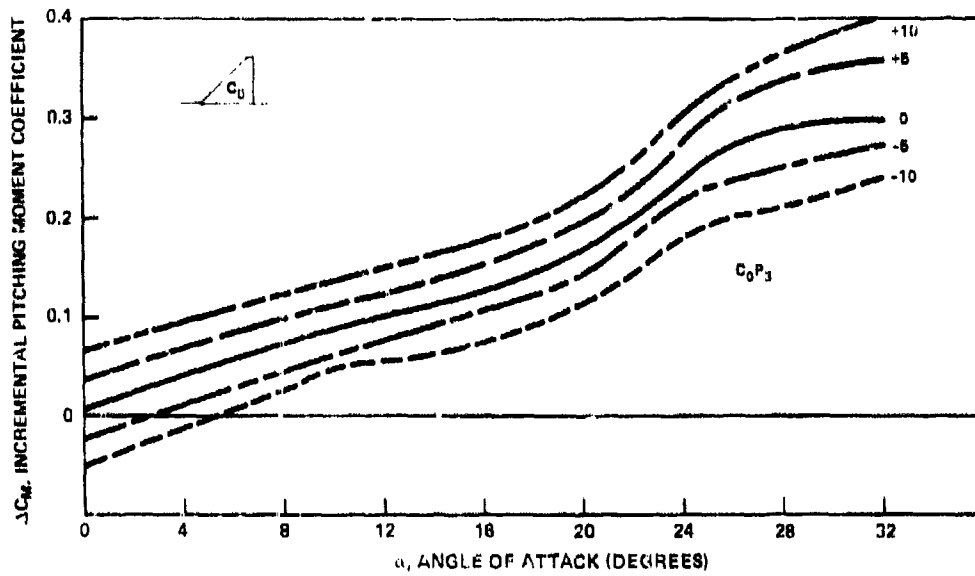


Figure 32a - Canard C_0 on 50-Degree Wing

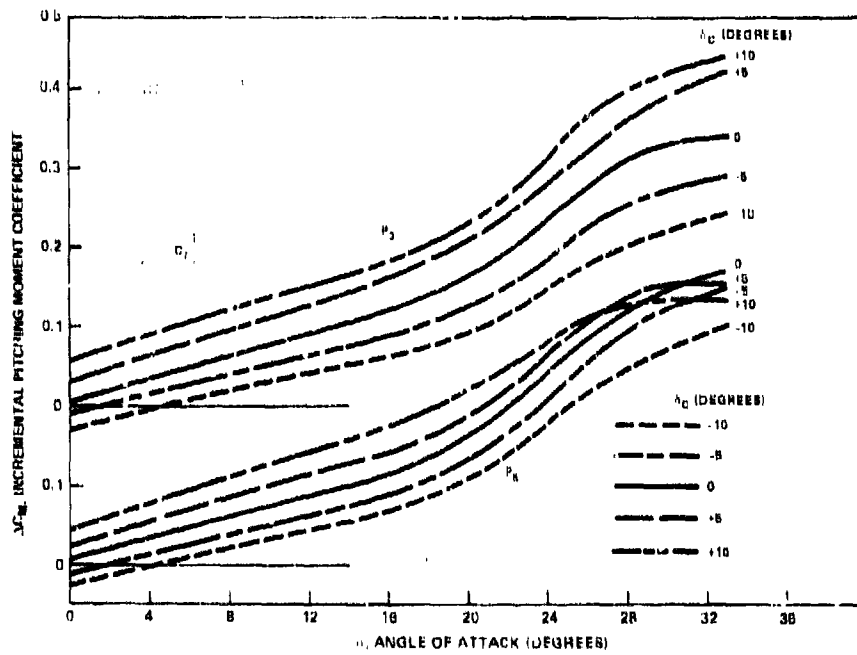


Figure 32b - Canard C_1 on 50-Degree Wing

Figure 32 (Continued)

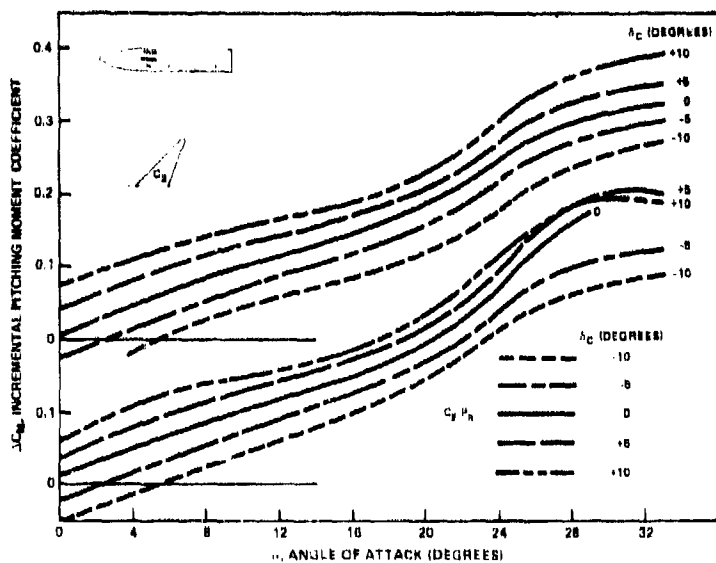


Figure 32c - Canard C_2 on 50-Degree Wing

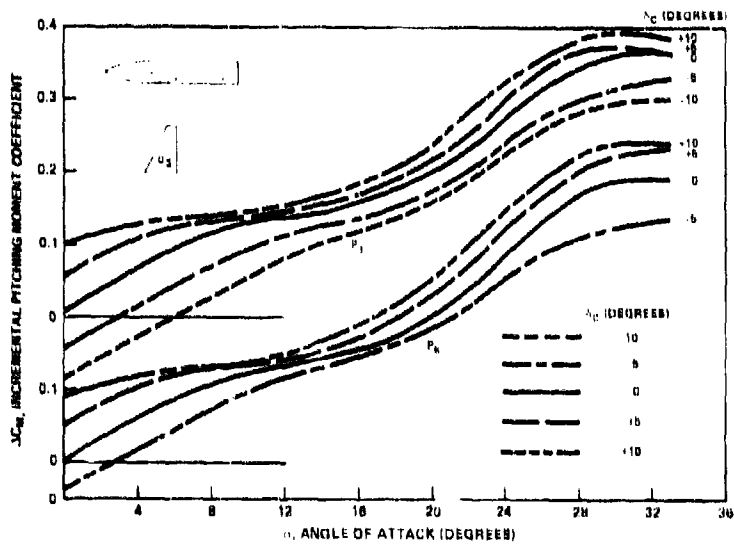


Figure 32d - Canard C_3 on 50-Degree Wing

Figure 32 (Continued)

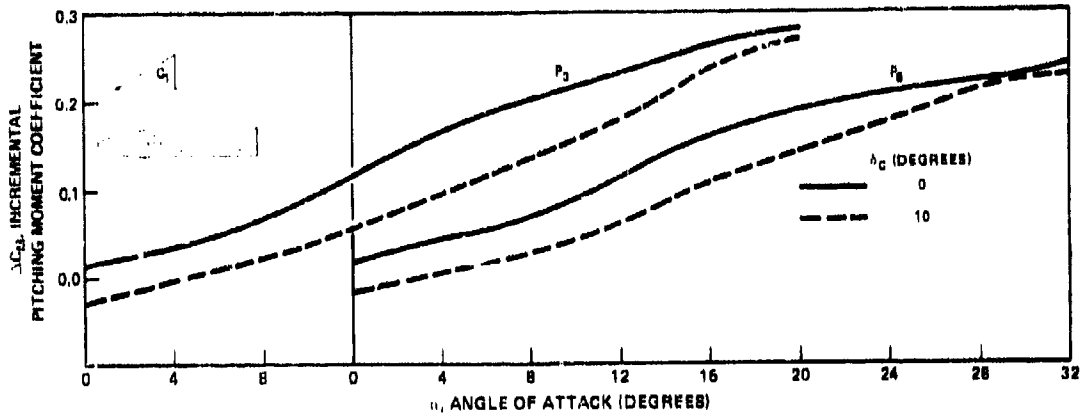


Figure 32e - Canard C_1 on 25-Degree Wing

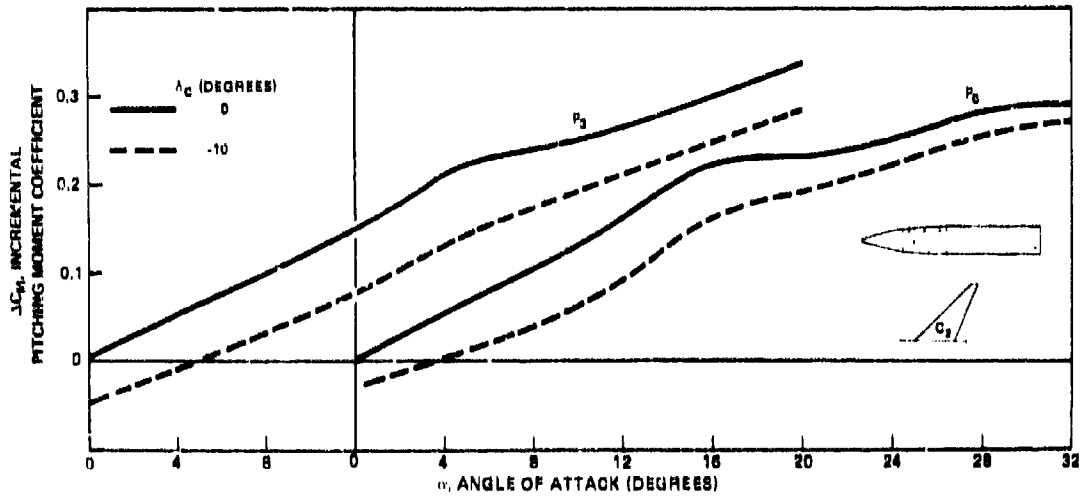


Figure 32f - Canard C_2 on 25-Degree Wing

Figure 32 (Continued)

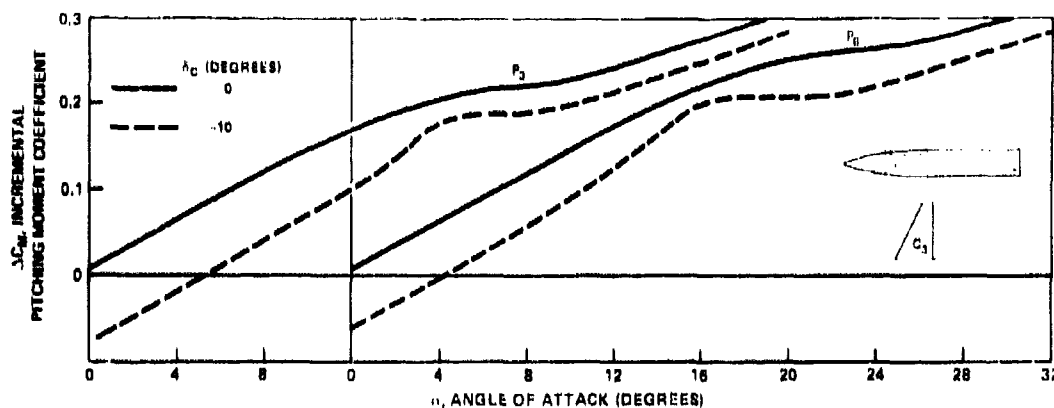


Figure 32g - Canard C_3 on 25-Degree Wing

While the data indicated little change in incremental moment slope with deflection at Position 3, this is not the case at the lower position P_6 . At this position the incremental slope is decreasing with increasing deflection angle indicating that the interference between canard and wing is no longer favorable or that the canard is stalled. This decrease in moment is seen more clearly in Figure 33 when incremental pitching moment at 32-degree angle of attack is presented versus canard deflection angle. At the high position P_3 incremental moment increases with canard deflection, however, at the low position P_6 the converse is true. This is most notable for the 60-degree canard C_1 , and for the 45-degree high aspect ratio canard C_2 . These canards have a reduction in incremental moment at positive deflection angles. Similar trends were noted for the incremental lift at 32 degrees due to deflection presented in the previous section.

The incremental lift presented in Figure 14 showed a reduction in lift of approximately 0.28 due to a positive 10-degree deflection for the 60-degree canard at P_6 . The incremental moment, however, does not indicate a change of this magnitude, for, if all the incremental lift were due to the canard stalling, the expected change in moment would be $\Delta C_l \cdot \frac{l_c}{\bar{c}}$

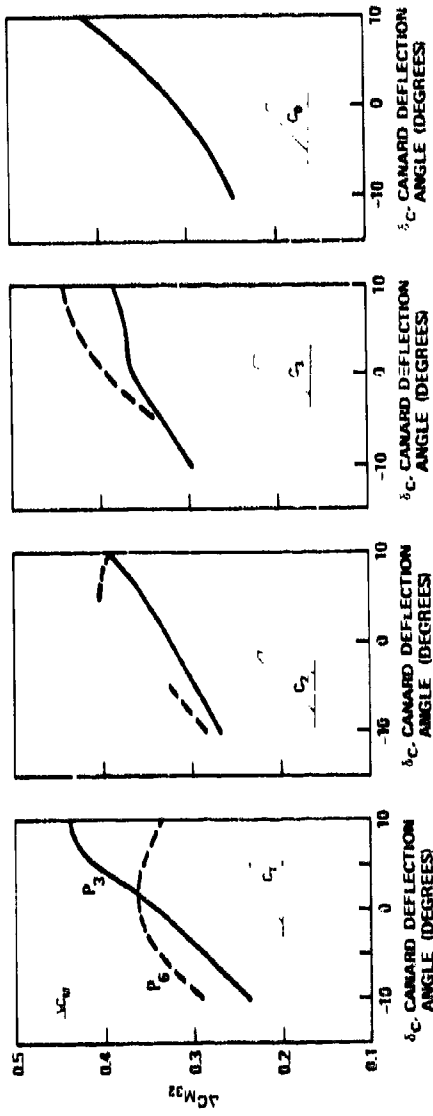


Figure 33a - Moment on 50-Degree Wing

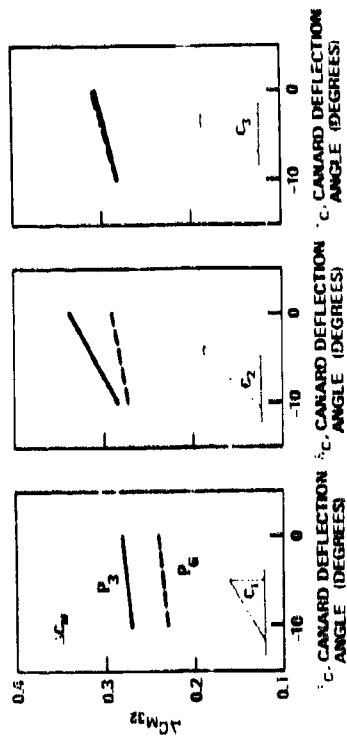


Figure 33b - Moment on 25-Degree Wing

Figure 33 - Variation of $C_{M_{32}}$ with Canard Deflection

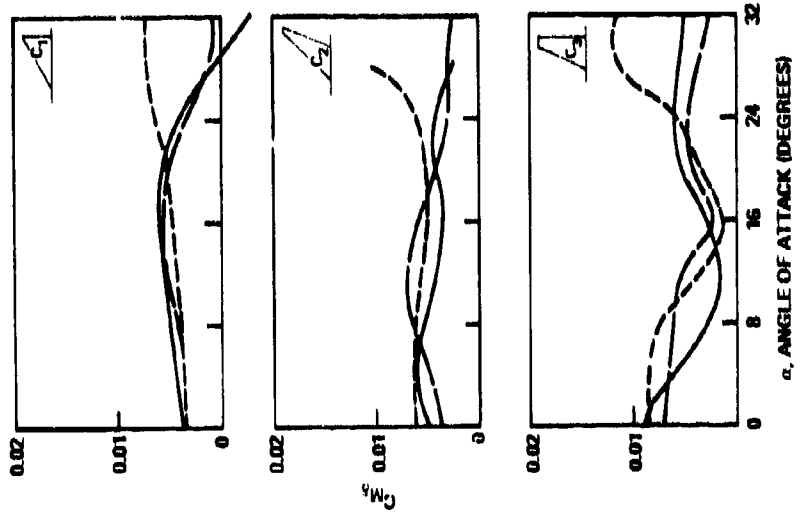


Figure 34b - Position 6

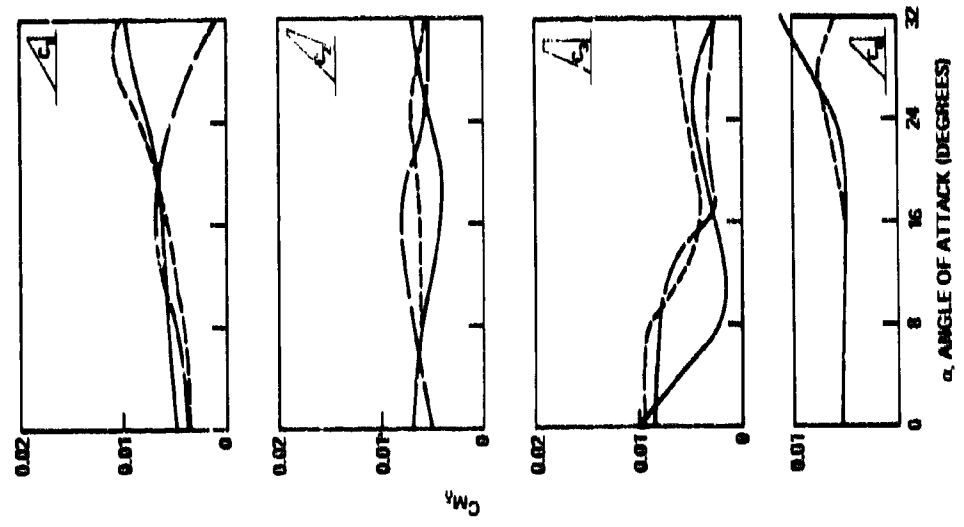


Figure 34a - Position 3

Figure 34 - Canard Control Power

or approximately 0.28. Thus it appears that while the canard may have suffered a slight reduction in lift (hence a reduction in moment) the major loss of lift is on the wing.

The variation of control power $C_{M\delta}$, with angle of attack is shown in Figure 34 for both 25- and 50-degree wing models. The data are evaluated from 0 to +10 degrees and from 0 to -10 degrees.

At P_3 no significant differences in $C_{M\delta}$ occur if the value of $C_{M\delta}$ is computed from either positive or negative deflections, although differences do occur at low angles of attack for the 25-degree sweep canard C_3 which, as noted is due to canard stall. More significant differences occur at P_6 . At P_6 , $C_{M\delta}$ is higher when computed with the negative deflection than with positive, thus indicating a possible canard stall. In general, there are only slight differences in control power between the 25- and 50-degree sweep models over most of the angle of attack range.

Control power was not as sensitive to canard position for the 25-degree wing model as was the 50-degree sweep model. Control power for the 25-degree sweep model was based only on negative deflection and thus the influence of positive deflection is not known.

WING LEADING EDGE CHANGES

The effect of a -9-degree leading edge droop on the 25-degree wing model is presented in Figure 35. As for the previously discussed lift, the -9-degree droop delays stall of the basic wing by approximately 4-degree angle of attack. The incremental moments due to the canard, presented in Figure 36, reflect this change in stall because in the region between 8 to 20-degree angle of attack the canard, located on the normal wing, has a slight increase in incremental moment when compared with the drooped leading edge configuration. This increase in moment is not as large as that which would be expected from the incremental lift data, i.e., $\Delta C_M = \Delta C_L \ell_c / \bar{c}$,

thus indicating that the primary moment change is due to delay of separation on the wing rather than a lift increase on the canard.

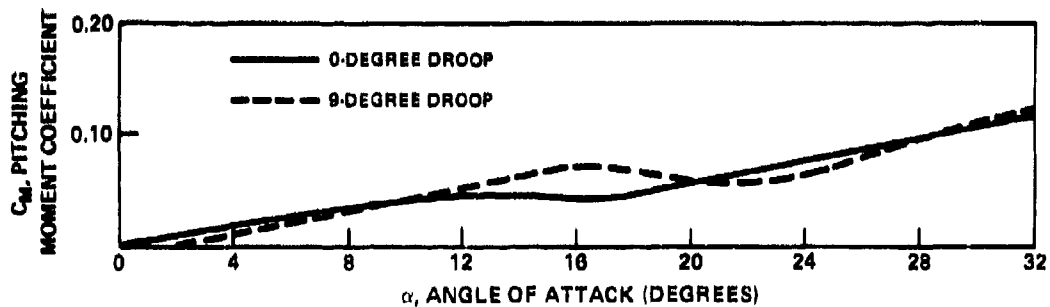


Figure 35 - Moment Characteristics of Basic 25-Degree Wing and 25-Degree Wing with -9-Degree Droop

DRAG

The primary aerodynamic influence of the close-coupled canard is to delay separation on the wing. This delay in separation results in a sizeable reduction in induced drag at moderate to high angles of attack. This reduction in induced drag is seen quite dramatically in Figures 37 and 38.

Figure 37 presents the variation of drag with lift coefficient for the 60-degree delta canard C_1 , the 45-degree high aspect ratio canard C_2 ,

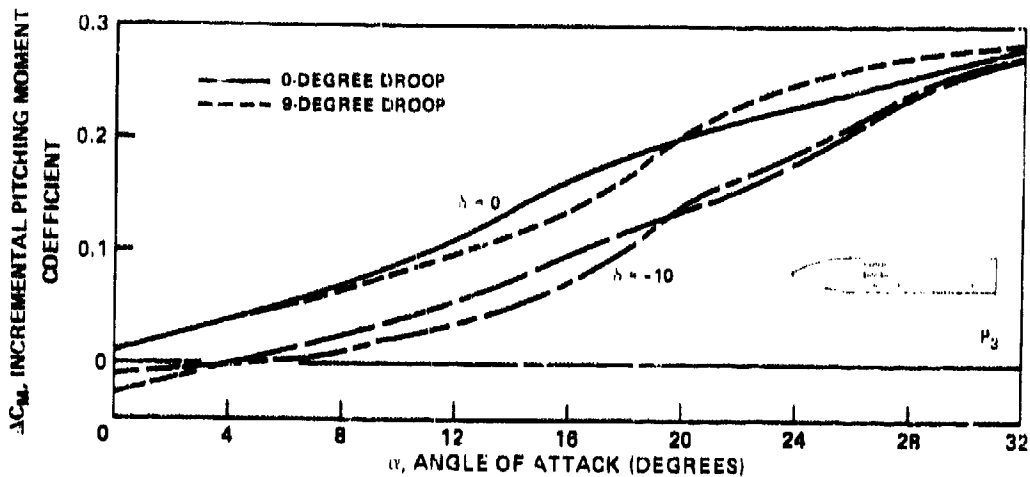


Figure 36a - Position 3

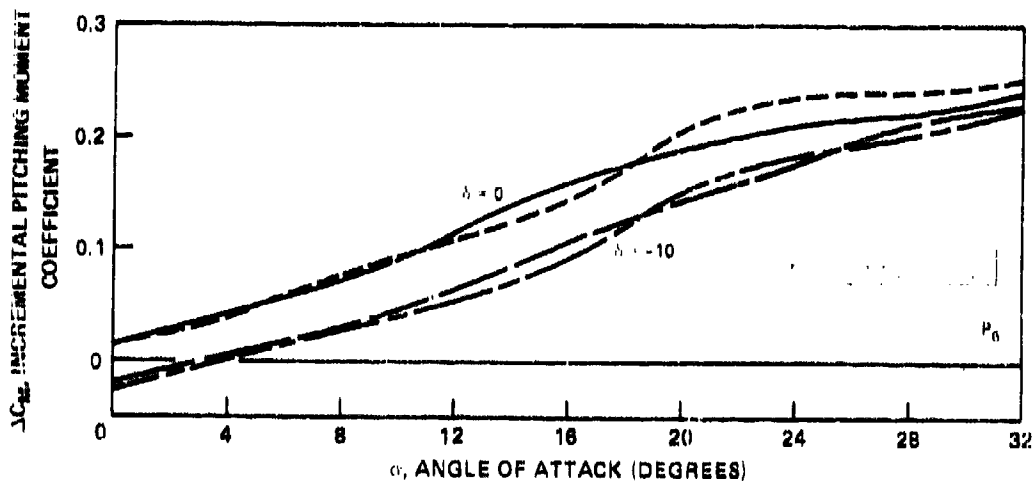


Figure 36b - Position 6

Figure 36 - Incremental Moments due to Canard on Basic and Modified 25-Degree Wing

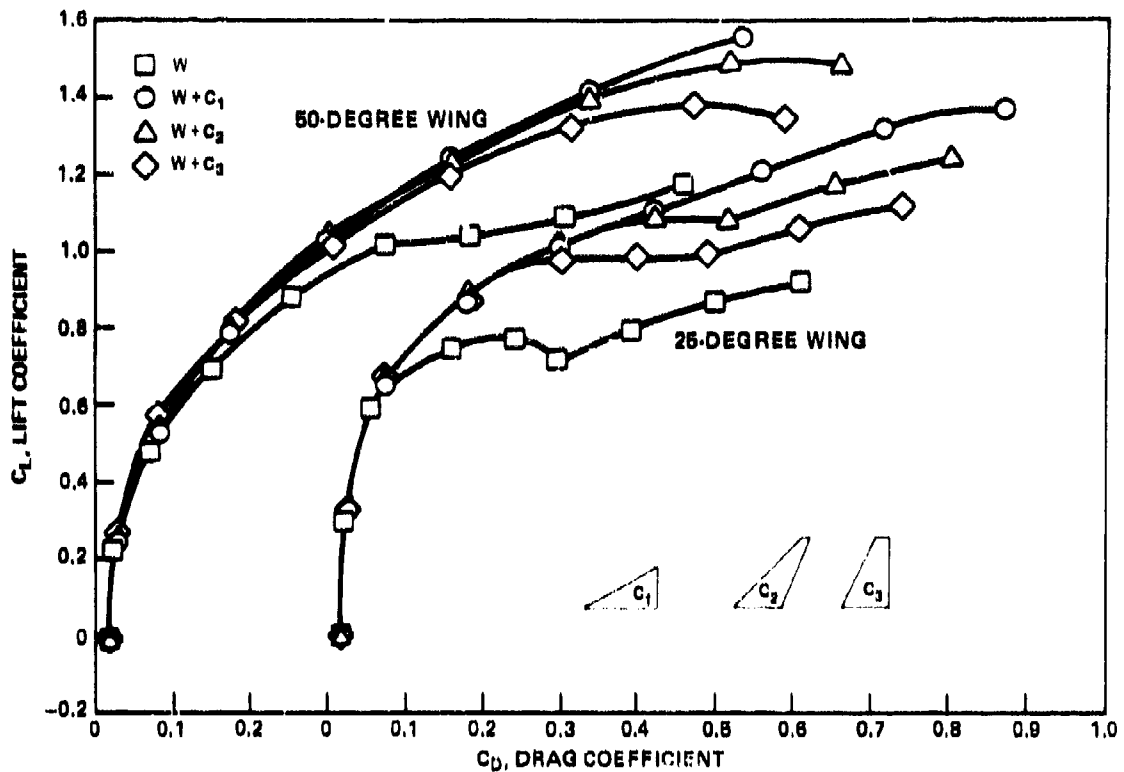


Figure 37 - Typical Drag Characteristics

and the 25-degree high aspect ratio canard C_3 . Data are presented for both 25- and 50-degree sweep models and the canard is located at P_2 . As seen in the figure the canard configured vehicles have less drag at lift coefficients of approximately 0.3 and 0.6 for the 50- and 25-degree sweep models, respectively. Figure 38 presents the corresponding variation of lift-to-drag ratio versus lift coefficient for the data presented in Figure 37. As noted in the figures, there is a decrease in maximum lift-to-drag ratio $(L/D)_{max}$ when the canard is installed. The magnitude of this reduction in $(L/D)_{max}$ is a function of canard planform, position, and deflection. The influence of these parameters on lift-to-drag ratio and induced drag will be discussed in the following sections.

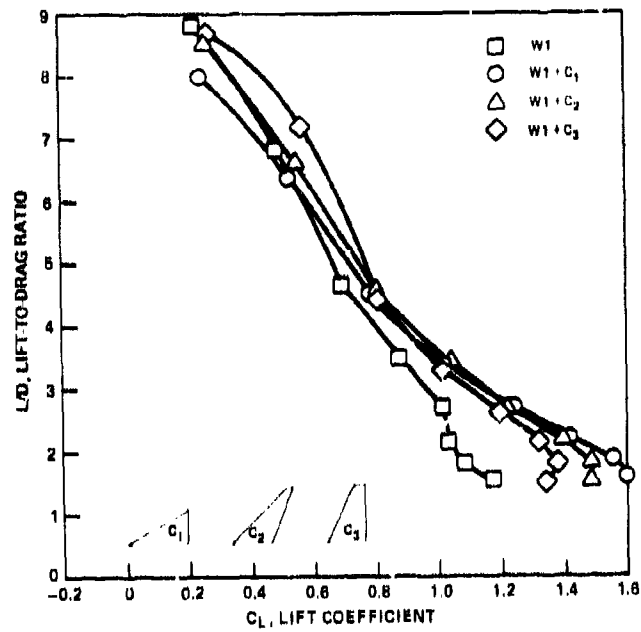


Figure 38a - Lift-to-Drag Ratio for a 50-Degree Wing

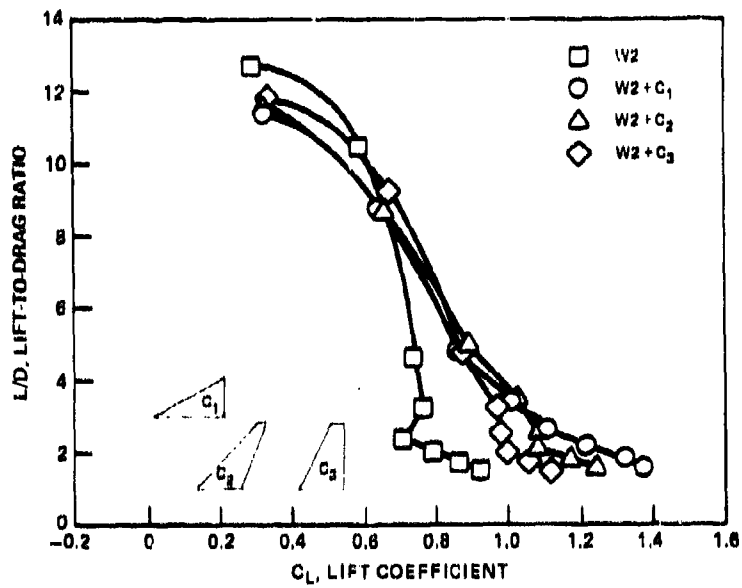


Figure 38b - Lift-to-Drag Ratio for a 25-Degree Wing

Figure 38 - Typical Lift-to-Drag Ratio Characteristics

SIZE

The data available on the effect of canard size on drag are somewhat limited. Only one wind-tunnel program at DTNSRDC evaluated canard size as a parameter and the angle of attack was limited to 20 degrees. Significant data regarding drag was obtained only with the two largest canards having projected area ratios of 0.20 and 0.25. Certain trends, however, can be obtained from these data.¹ The first trend noted is the behavior of the drag developed on the canard due to deflection at zero lift coefficient. Figure 39 presents this variation of drag versus deflection for the two canard sizes. As indicated in the figure, the shape of C_{D_0} versus deflection is approximately parabolic in shape suggesting that the data may be analyzed in the form of $C_D = C_{D_{\delta=0}} + K_1 (C_{L_\delta})^2 \delta^2$.

Utilizing the zero lift moment data due to deflection¹ and dividing by the corresponding canard distance ratio, C_{L_δ} has been obtained. The variation of C_D with $(C_{L_\delta})^2$ is presented in Figure 40. Data have been referenced to the canard exposed area. For up to approximately 15 degrees deflection, the data approximates a linear fit. At deflection angles greater than 15 degrees, the slope becomes steeper indicating canard stall. It thus appears that as with the incremental lift and moment, drag due to the canard is a function primarily of exposed area ratio rather than total area ratio. This is further verified by Figure 41, which presents the variation of aircraft lift-to-drag ratio at a lift coefficient of 1.0 versus exposed area ratio. As shown, the change is linear albeit based on only three data points. Data, however, from the F-4 aircraft where canard exposed ratios of 0.05 and 0.10 were evaluated also exhibit this increase in lift-to-drag ratio with canard exposed area ratio. Thus, for at least up to 20-degree angle of attack, a linear increase in lift-to-drag ratio with canard exposed area ratio appears to be valid.

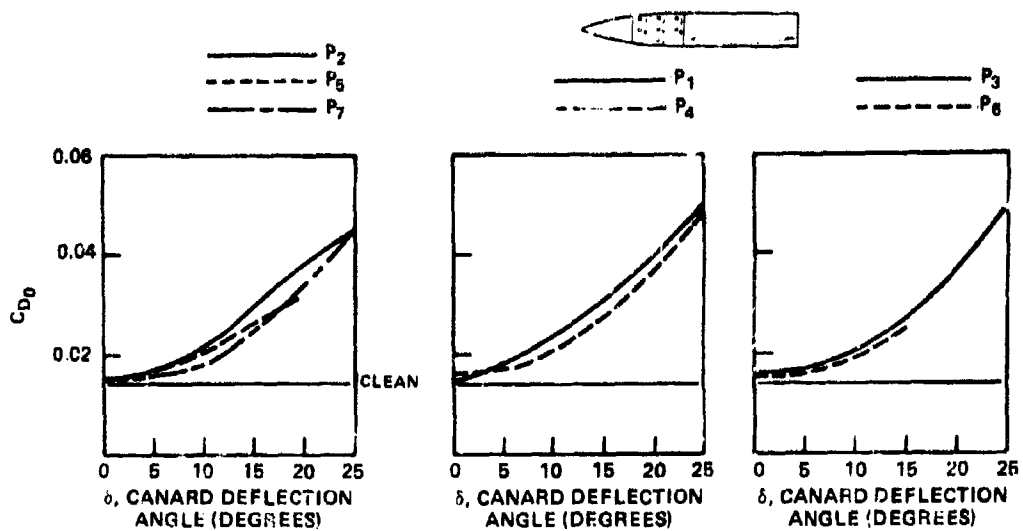


Figure 39a - Drag for a 0.20 Canard

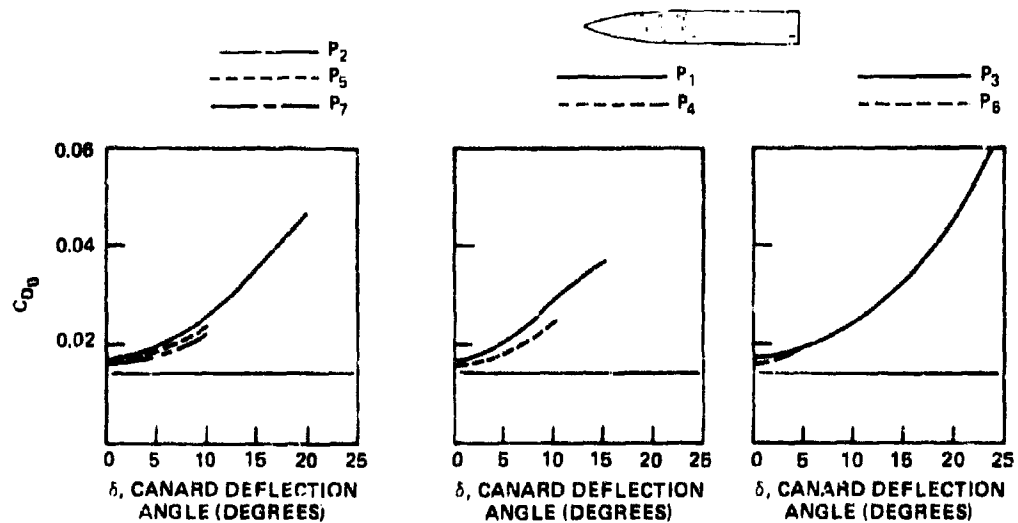


Figure 39b - Drag for a 0.25 Canard

Figure 39 - Effect of Deflection on Zero Lift Drag C_{D0}

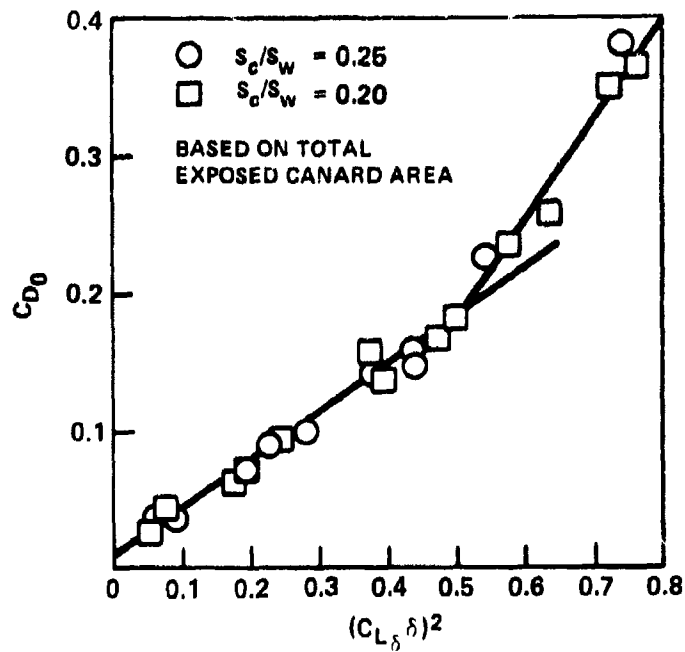


Figure 40 - Variation of Canard Drag Coefficient with Canard Lift

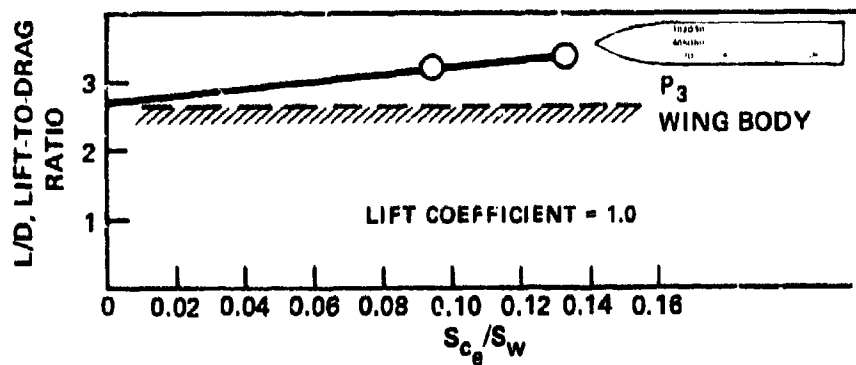


Figure 41 - Variation of (L/D) with Canard Exposed Area Ratio

SHAPE

The effects of canard shape on maximum lift-to-drag ratio $(L/D)_{\max}$ and lift-to-drag ratio at lift coefficients of 0.6, 0.8, and 1.2 are presented in Figure 42. Lift-to-drag ratio is plotted versus the quarter chord sweep angle of each canard λ_{25} . Data are presented for both 25- and 50-degree sweep models. The canards are located at P_3 at 0-degree canard deflection. Also presented in the figure are the corresponding lift-to-drag ratios of the individual wing-bodies. Maximum lift-to-drag ratio is lower for the canard configurations than for the wing-body alone for both sweep models. This is to be expected since a penalty must be paid for the zero lift drag increase due to the canard. The penalty in lift to drag varies from 9 percent to 15 percent for the 25-degree wing model and from 4 to 7 percent for the 50-degree model. These losses in $(L/D)_{\max}$ can be reduced by proper placement and deflection which will be discussed in following sections. As angle of attack and thus lift coefficient are increased, the canard configurations have better lift-to-drag ratios than the basic wing-body. The lift coefficient where this increase first occurs is approximately 0.7 for the 25-degree wing and 0.4 for the 50-degree wing model.

At low lift coefficients $C_L \leq 0.6$ the loss in lift-to-drag ratio is clearly a function of the quarter chord sweep angle as shown by the linear variation. At higher lift coefficients this is not the case because the amount of variation with canard quarter chord sweep angle is minimal for the 50-degree wing model. The canards on the 25-degree model exhibit a nonlinear behavior with canard sweep angle at a C_L of 0.8 ($\alpha \sim 10$ degrees), L/D increased with decreasing sweep angle up to λ_{25} of 40 degrees and then decreased. This behavior is due to the early stall of the 25-degree canard C_3 when located on the 25-degree wing model.

The improvement in lift-to-drag ratio is due to a reduction in induced drag. Using the definition of drag as

$$C_D = C_{D_{\min}} C_{L_0} + K_1 [C_L - C_{L_0}]^2$$

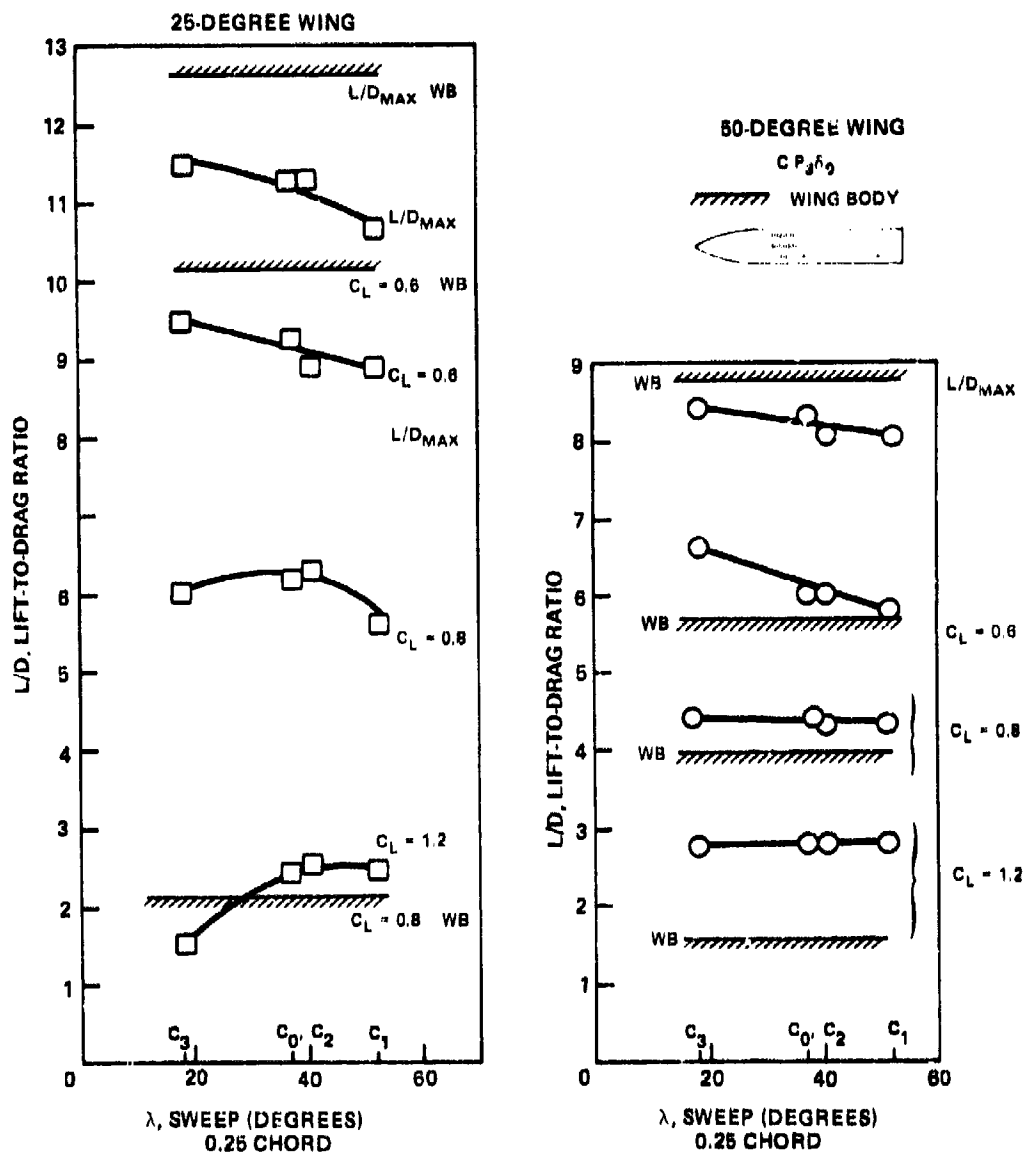


Figure 42 - Lift-to-Drag Ratio Variation with Canard Shape

Figure 43 has been developed for the four canard shapes on each model as well as each wing-body. The value of $C_{L,0}$ is approximately zero for each configuration. At the value of C_L for $(L/D)_{\max}$ ($\alpha \approx 4$ degrees), the induced drag factor is higher than the basic wing-body for all configurations. This is due to the unfavorable interference of the canard on the wing. Then the angle of attack is increased, the canards have a lower induced drag factor than the basic wing-body. This reduction occurs at an angle of attack of approximately 8 degrees. No strong influence of shape on the induced drag factor is seen for the 50-degree wing model.

Shape does influence the induced drag on the 25-degree wing. At low lift coefficients, the 25-degree canard C_3 had the lowest induced drag and the 60-degree canard C_1 the highest. As angle of attack is increased, their trends were reversed and the C_3 canard had the highest induced drag and the C_1 canard the lowest.

POSITION

The effect of canard position on maximum lift to drag ratio $(L/D)_{\max}$ and lift to drag ratios at lift coefficients of 0.6 and 1.2 are presented in Figure 44. Data are presented for both 25- and 50-degree sweep models. Shown for each canard is the position where the canard exposed root trailing edge initially overlaps the exposed wing root leading edge.

For all configurations maximum lift to drag ratio occurs at a position forward of the exposed overlap position. In general the maximum value occurred at P_2 , however, the 60-degree delta canard had a maximum value at P_6 for the 50-degree wing model. Lowering the canard reduced $(L/D)_{\max}$ except in the case of the 60-degree canard as mentioned above. A comparison with data for the basic wing-body shows only small losses in $(L/D)_{\max}$ for each canard if the canard is at the optimum position. These losses in $(L/D)_{\max}$ were on the order of 3 and 7 percent for the 50- and 25-degree sweep models, respectively. As lift coefficient is increased, canard configurations have less drag than the basic wing-body for the 50-degree wing model. Lift to drag ratio is still optimized at positions forward of the canard wing overlap. As with $(L/D)_{\max}$, lowering the canard reduced the lift to drag ratio.

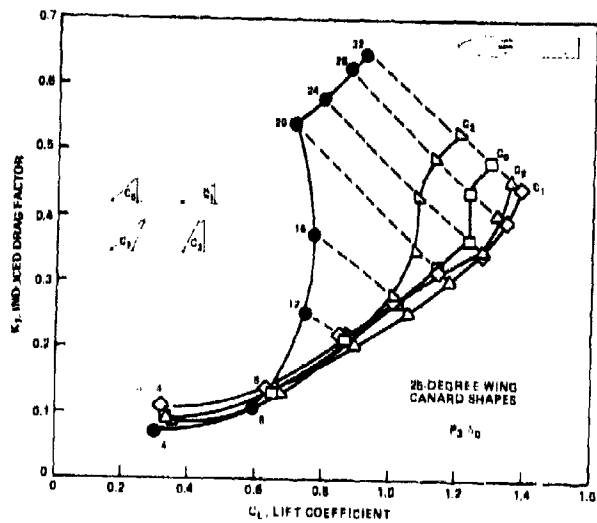


Figure 43a - Drag for a 25-Degree Wing

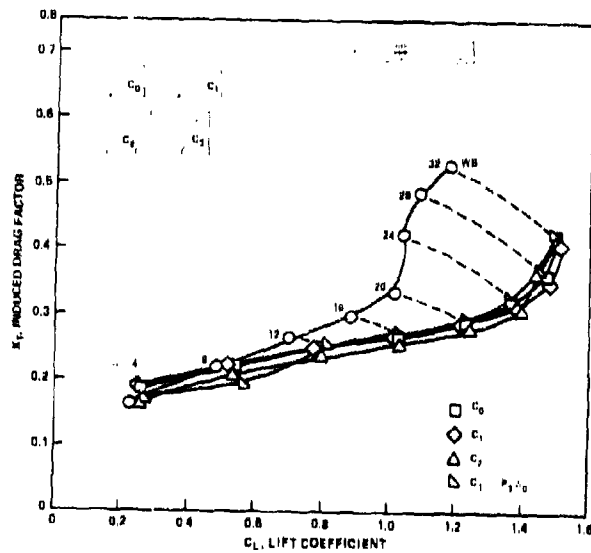


Figure 43b - Drag for a 50-Degree Wing

Figure 43 - Induced Drag Factor

Figure 44 - Lift-to-Drag Ratio Variation with Canard Position

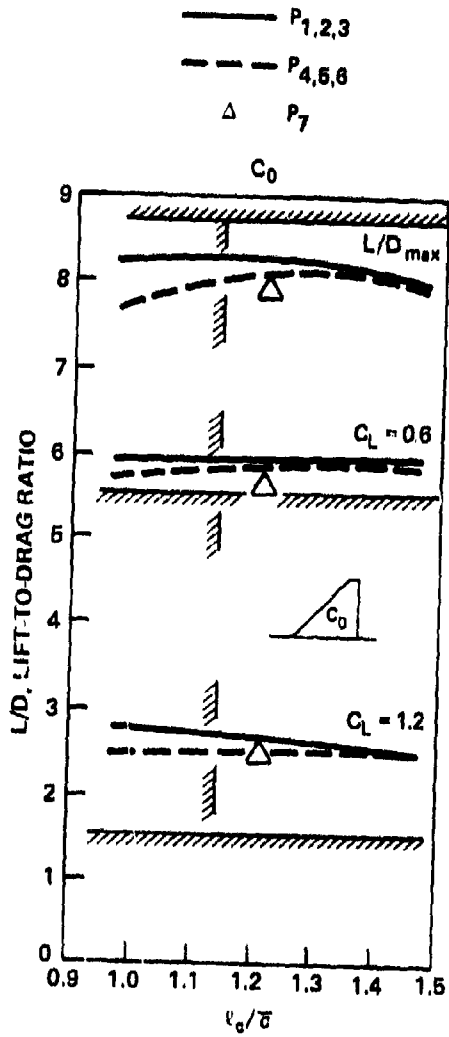


Figure 44a - Canard C_0 on 50-Degree Wing

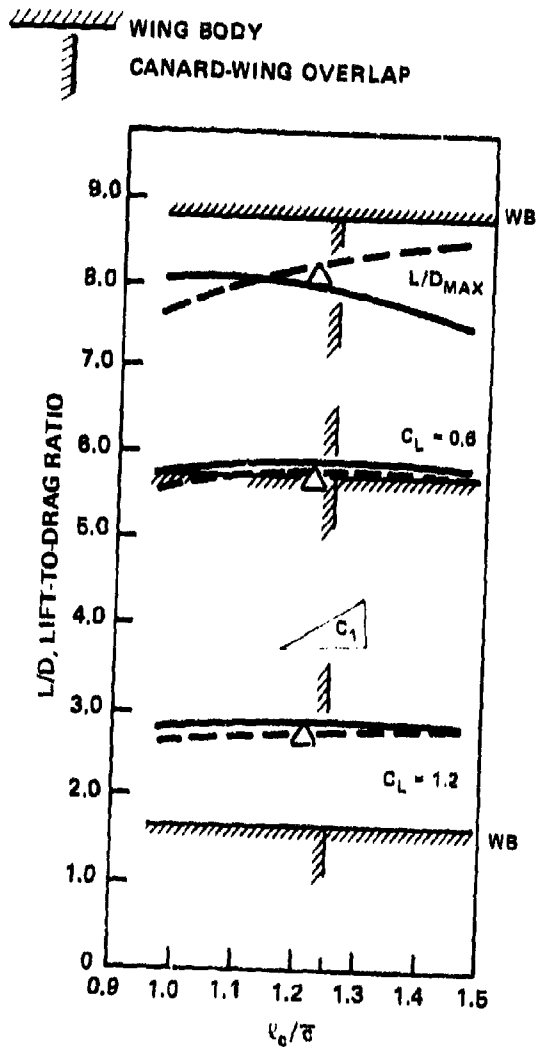


Figure 44b - Canard C_1 on 50-Degree Wing

Figure 44 (Cont'ued)

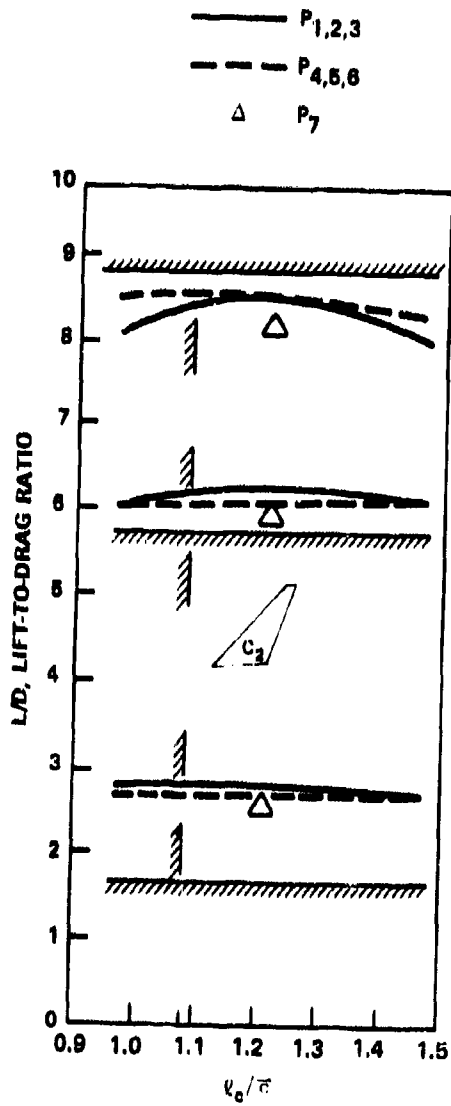


Figure 44c - Canard C_2 on 50-Degree Wing

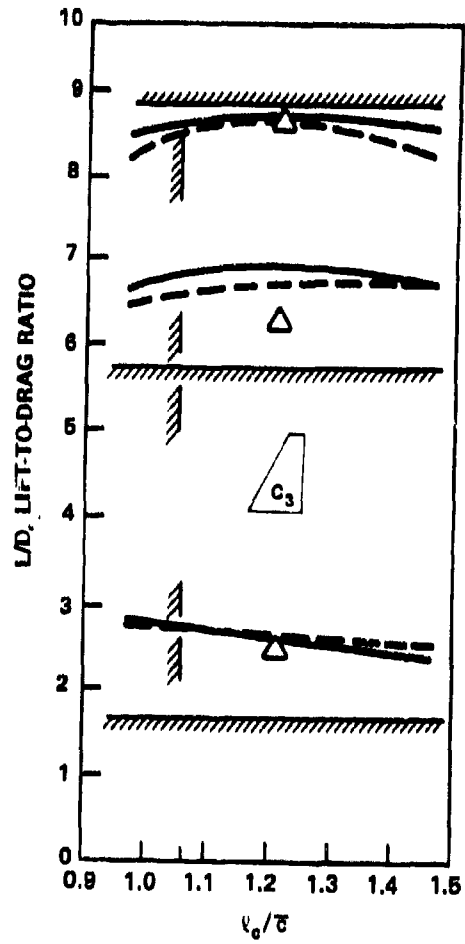
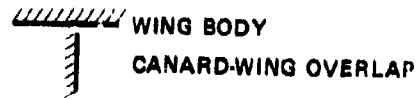


Figure 44d - Canard C_3 on 50-Degree Wing

Figure 44 (Continued)

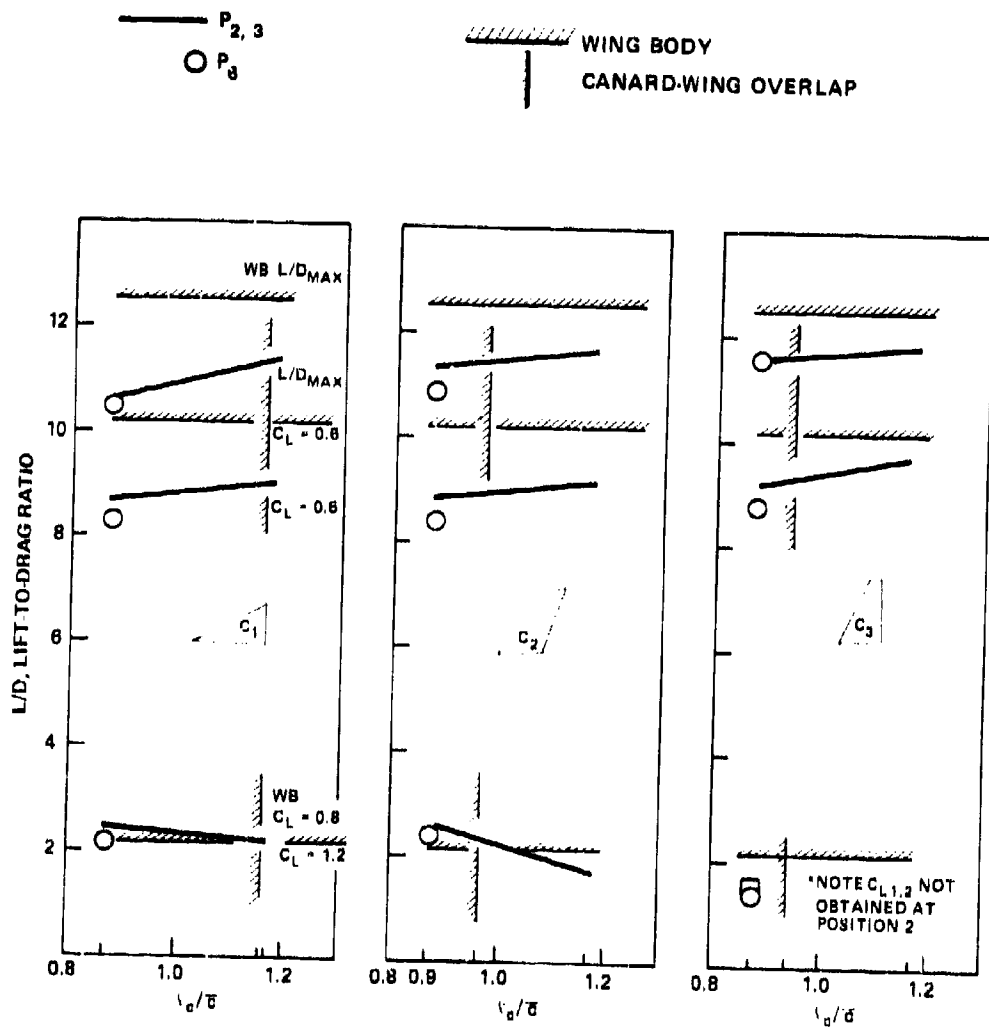


Figure 44e - Canards on 25-Degree Wing

At $C_L = 1.2$, only slight changes occur in the lift-to-drag ratio, the location for maximum value of L/D has, however, moved aft of the overlap juncture. Lift-to-drag ratio at this C_L tended to be lower at the forward and low positions.

The effect of position on the minimum drag coefficient C_{D0} is presented in Figure 45. Position has a minimal effect of C_{D0} but moving the canard and downward increased minimum drag.

As stated earlier the major effect of the canard on drag is to reduce the induced drag component of the total drag. The effect of canard position on the induced drag factor K_1 , is presented in Figure 46 for the 50-degree model. The influence of canard position on induced drag is somewhat dependent on canard geometry. The 60-degree delta canard C_1 has the smallest change in K_1 due to position. Minimum K_1 occurred at P_2 over most of the angle of attack range.

Moving the canard aft increased induced drag. The three other canards show a greater dependence on canard position. Maximum induced drag occurred at the most forward positions P_1 and P_4 . Minimum induced drag occurred at P_2 for the 45-degree sweep canards C_0 and C_2 and P_3 for the 25-degree canard C_3 . For all canards lowering the canard increased the induced drag factor.

Figure 47 presents similar data for the 25-degree wing model. More variation of K_1 with position is evident for the canards on the 25-degree wing model than for the 50-degree wing model. At low lift coefficients K_1 did not vary significantly for the 50-degree model, whereas for the 25-degree model these differences are more evident. At low C_L P_2 clearly has a lower induced drag factor for all three canards. As lift coefficient is increased the induced drag factor at P_2 increases to larger values than those obtained at Positions 3 and 6 for the 45- and 25-degree canards, C_2 and C_3 , and Position 3 for the 60-degree canard C_1 . This increase in K_1 was relatively large for both C_2 and C_3 indicating a large loss in effectiveness of the canard at P_2 . The increase in K_1 for the 60-degree canard was relatively small. Over most of the angle of attack range evaluated, lowering the canards to position P_6 increased the induced drag factor.

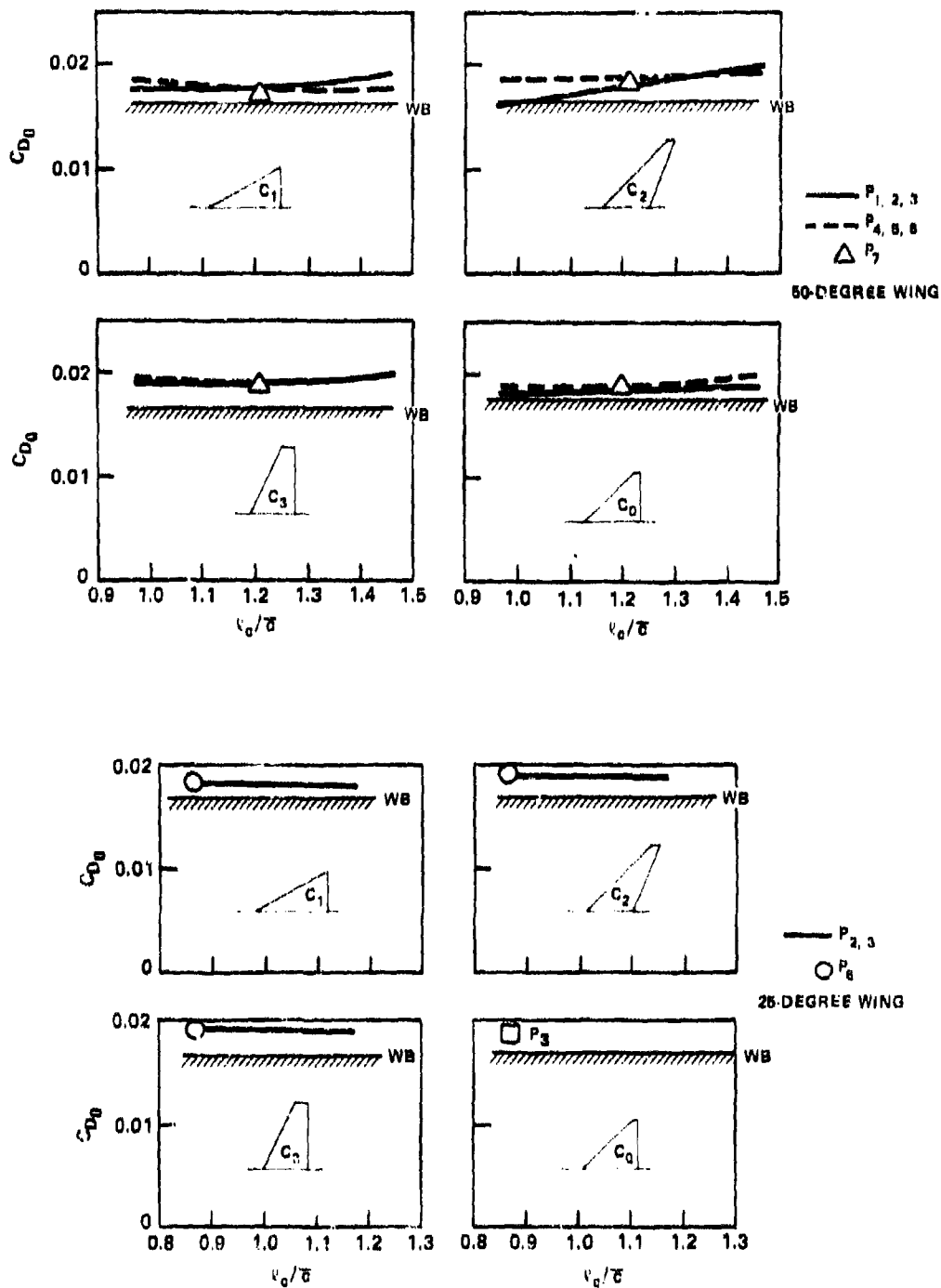


Figure 45 - Effect of Canard Position on Minimum Drag Coefficient

Figure 46 - Induced Drag Factor Variation with Canard Position for the 50-Degree Wing

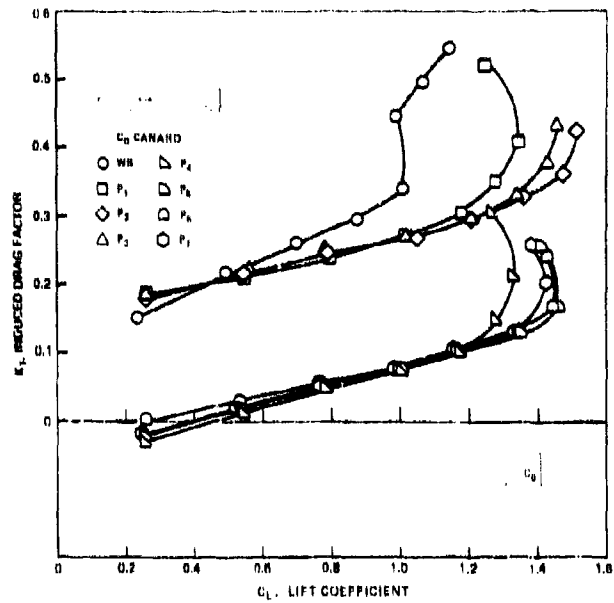


Figure 46a - Canard C_0

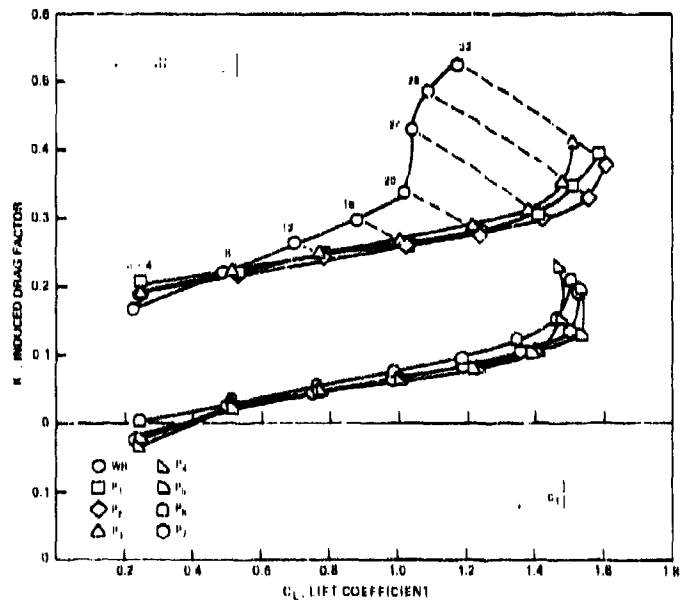


Figure 46b - Canard C_1

Figure 46 (Continued)

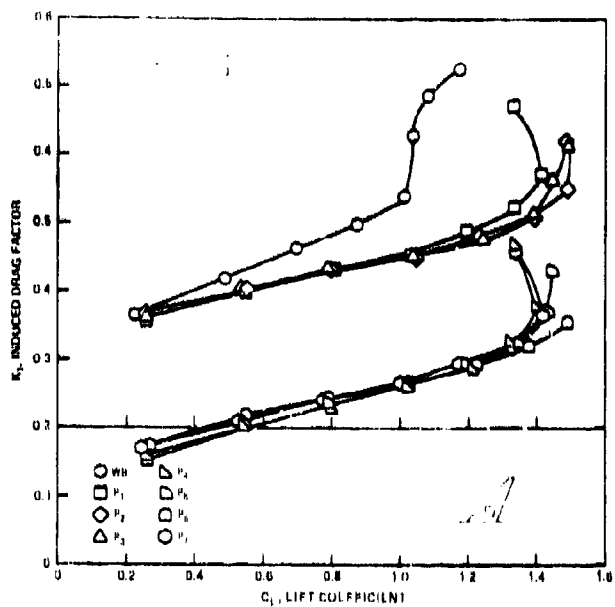


Figure 46c - Canard C_2

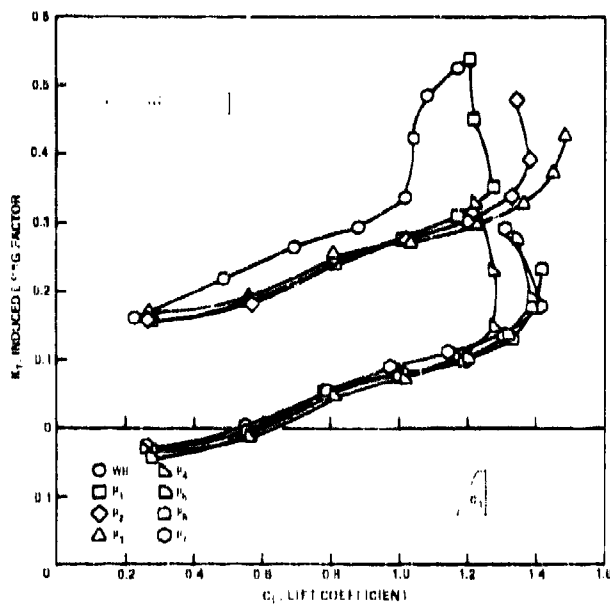


Figure 46d - Canard C_3

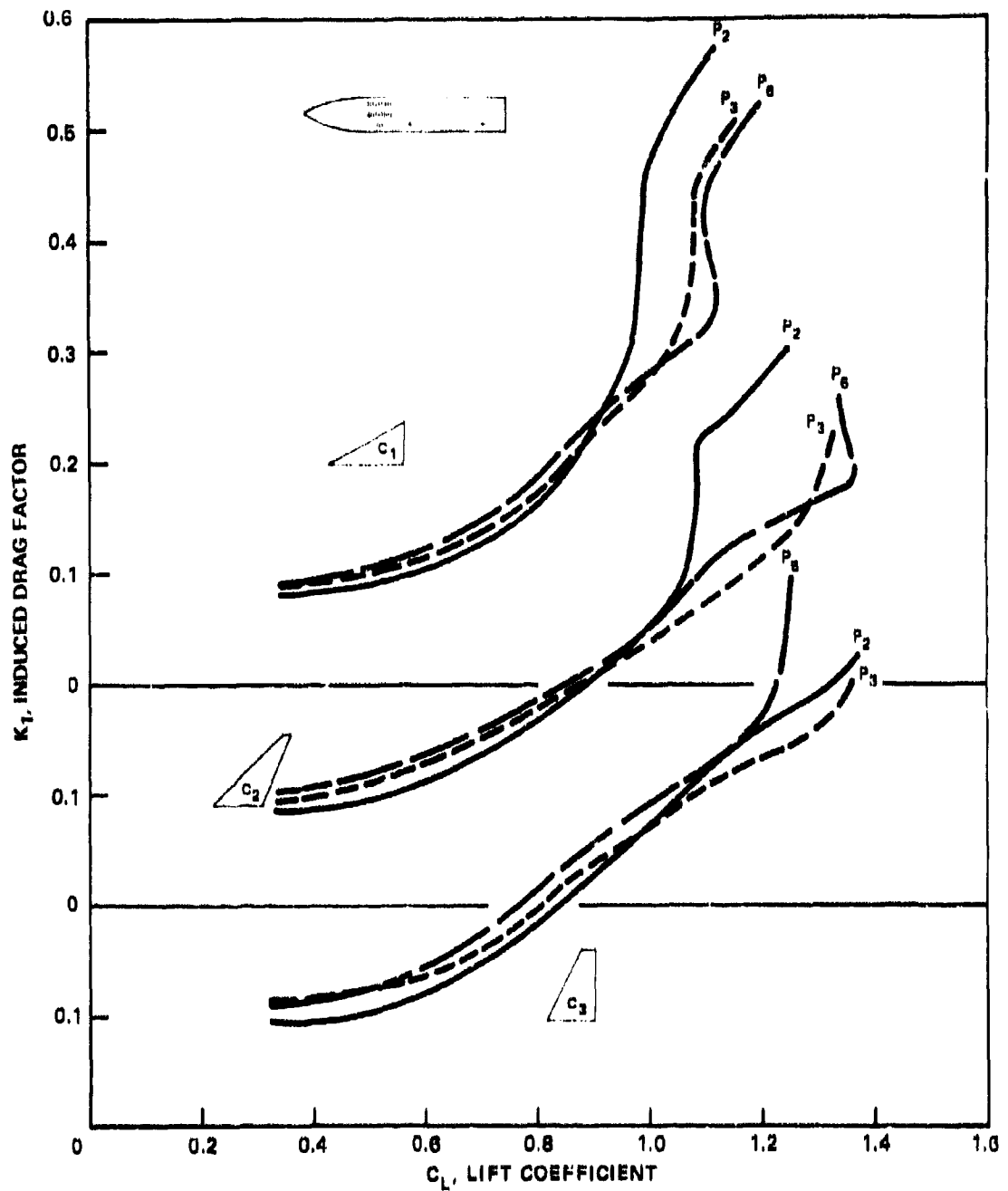


Figure 47 - Induced Drag Factor Variation with Canard Position for the 25-Degree Wing

Figure 48 indicates the minimum level of induced drag obtainable for each canard. The figure is a locus of the minimum induced drag factor based on all canard positions. Minimum induced drag is obtained for the 25-degree canard at low lift coefficients for both research models regardless of canard position.

The 60-degree canard had the highest value of induced drag at low lift coefficients and the lowest value at lift coefficients near $(C_L)_{\max}$. The intermediate canards C_0 and C_2 have values between the 25- and 60-degree canards. Thus, for good low lift performance characteristics, i.e., range and endurance, the low sweep canard is best. When maneuvering capability is the dominant design factor, the highly swept canard generates the best performance. The intermediate canards are good compromises having lower induced drag than the 60-degree delta at low lift coefficients and slightly higher values of induced drag near maximum lift. Examination of the figures indicates that while the range of induced drag between the 25- and 60-degree canards is not large for the 50-degree sweep model, large differences in induced drag plus the poor stall characteristics exhibited by the 25-degree canard preclude its use on the 25-degree swept wing model.

DEFLECTION

Positive canard deflections reduce $(L/D)_{\max}$ significantly, whereas small negative deflection improves $(L/D)_{\max}$. This behavior is illustrated in Figure 49 which presents the variation of lift-to-drag ratio versus canard deflection. Data are presented for Positions 3 and 6 for a canard deflection range from -10 to +10 degrees in 5-degree increments for the 50-degree sweep model and at -10 and 0 degrees for the 25-degree sweep model.

At both positions and for all canard shapes, a 10-degree deflection causes a loss in $(L/D)_{\max}$ of approximately 40 percent. The influence of negative canard deflection on $(L/D)_{\max}$ varied somewhat with canard position and shape. For nearly all configurations on the 50-degree wing model, a canard deflection of -5 degrees increased $(L/D)_{\max}$. The sole exception to this was a slight decrease in $(L/D)_{\max}$ when the 45-degree high aspect ratio canard C_2 was at P_3 .

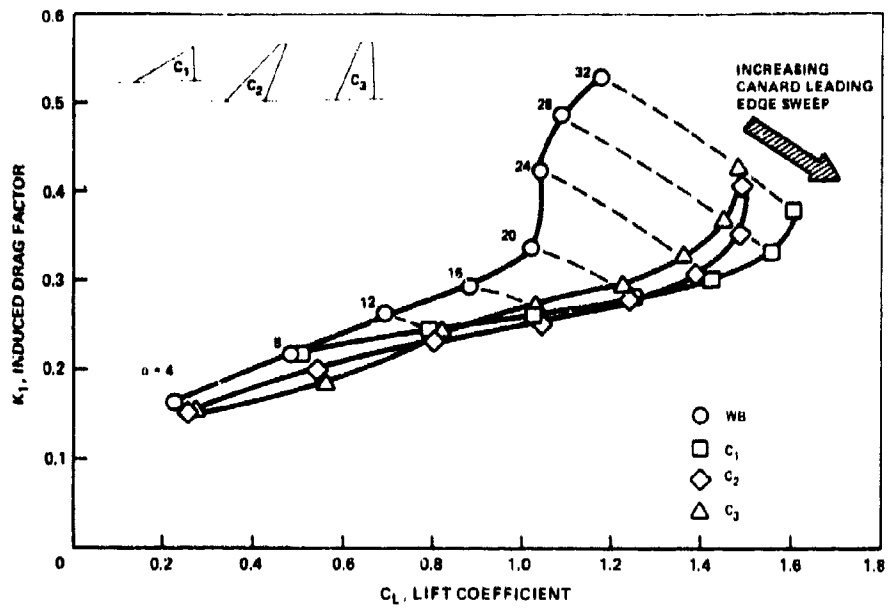


Figure 48a - Drag for a 50-Degree Wing

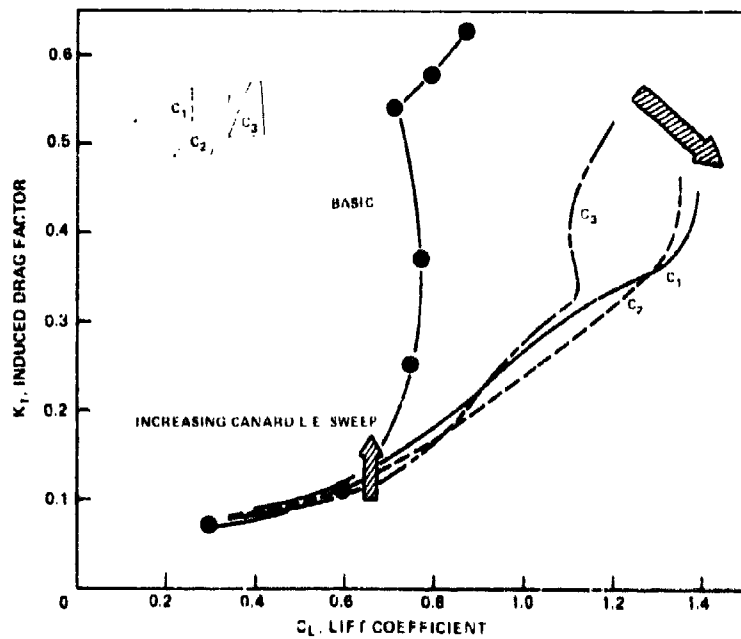


Figure 48b - Drag for a 25-Degree Wing

Figure 48 - Locus of Minimum Induced Drag Factor

Figure 49 - Lift-to-Drag Ratio Variation
with Canard Deflection

////// L/D_{MAX} WING BODY

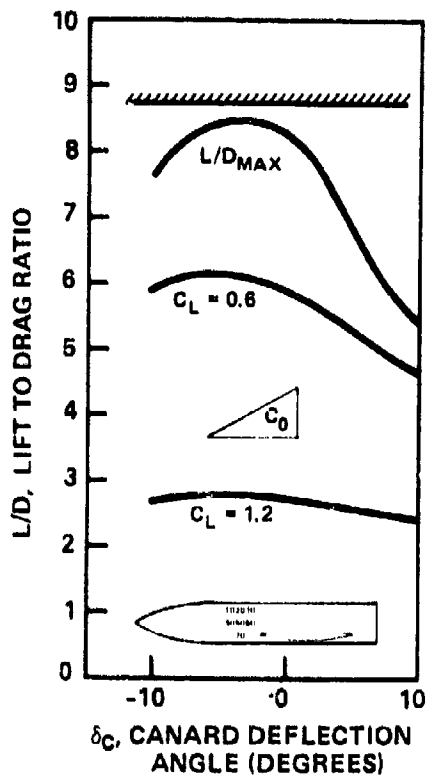


Figure 49a - Canard C_0 on
50-Degree Wing

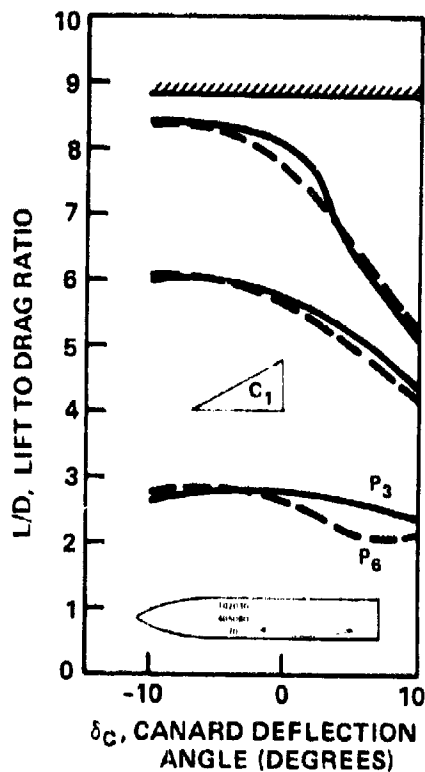


Figure 49b - Canard C_1 on
50-Degree Wing

Figure 49 (Continued)

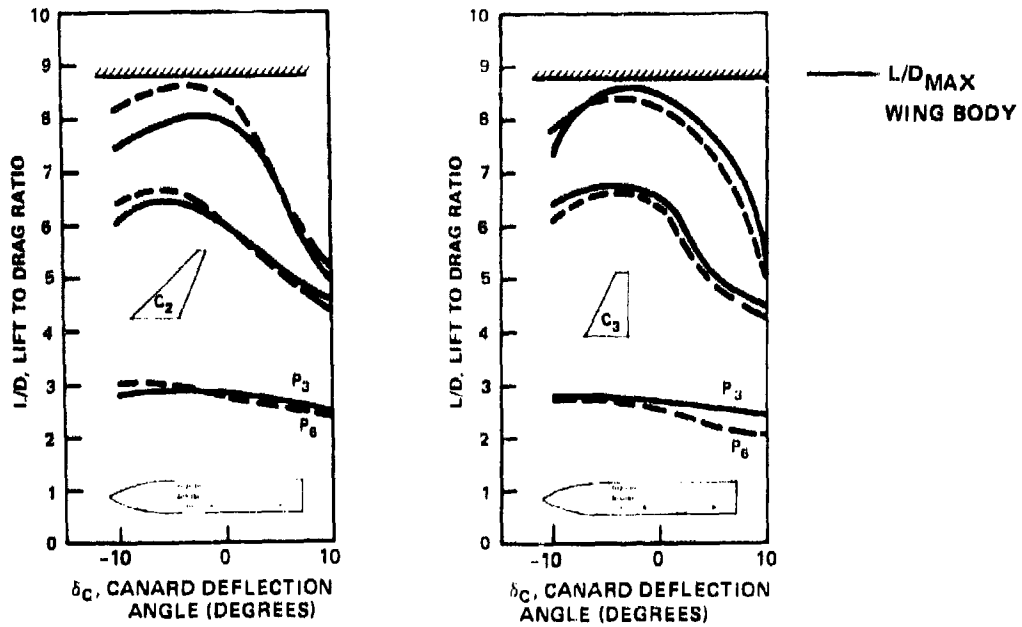


Figure 49c - Canard C_2 on 50-Degree Wing

Figure 49d - Canard C_3 on 50-Degree Wing

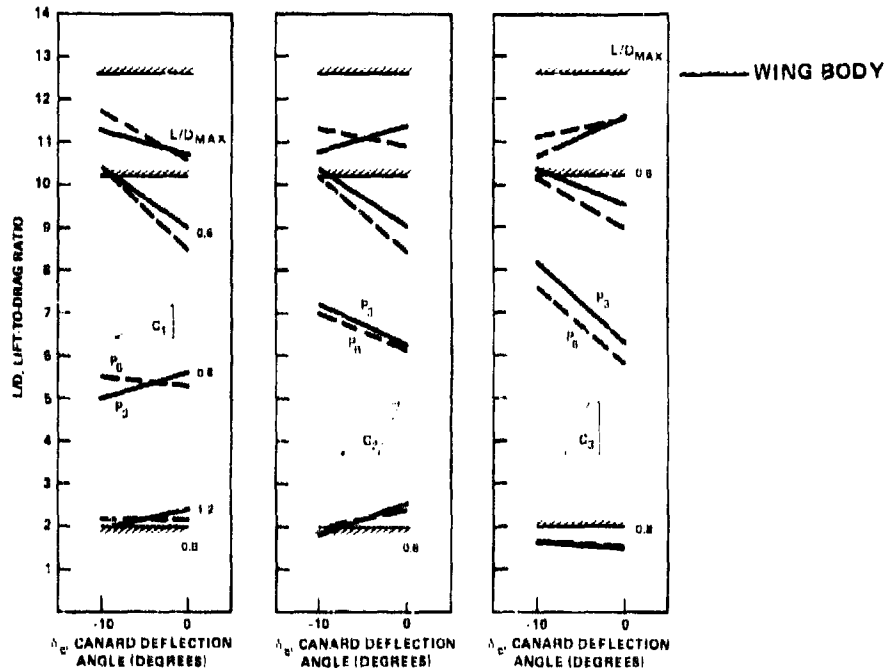


Figure 49e - Canards on 25-Degree Wing

A deflection of -10 degrees caused a reduction in $(L/D)_{\max}$ for all canards with the exception of the 60-degree delta canard C_1 . On the 25-degree model, negative 10-degree deflection caused reductions in $(L/D)_{\max}$ for the 25-degree canard at both positions. The 45-degree high aspect ratio canard C_2 and a slight increase in $(L/D)_{\max}$ at the low position P_6 and a decrease at the high position P_3 . The value of $(L/D)_{\max}$ was increased for both positions of the 60-degree canard with negative deflections.

With increasing lift coefficient the effect of canard deflections becomes less dramatic. Positive deflections still cause reduction in lift-to-drag ratio yet the magnitude of these losses is reduced. Lift-to-drag ratio was improved by a negative 5-degree canard on the 50-degree swept wing model. Canard deflection had only a small effect on lift-to-drag ratio at maneuvering lift coefficients ($C_L > 1.0$). Slight losses do occur, however, due to positive deflection. Negative deflections had little effect on L/D at $C_L = 1.2$ on the 50-degree model. Negative deflections had a detrimental effect on lift-to-drag ratio for canards C_1 and C_2 on the 25-degree model. The lift-to-drag ratio was slightly increased for the 25-degree canard C_3 on this model.

The losses in $(L/D)_{\max}$ and L/D occurring at positive deflections are due to an increase in minimum drag and an increase in the induced drag factor K_1 . The slight gain in L/D occurring at negative deflections is due to a decrease in α_1 . The variation of C_{D_0} with canard deflection is shown in Figure 50. The curves are roughly parabolic in shape and the minimum value in general occurs at 0-degree deflection. The curves, however, have a slight bias in that the drag coefficient for negative values of deflection is, in general, slightly less than that of the corresponding positive deflection. This bias may be due to the downwash of the canard when positively deflected causing an increase in drag of the wing.

The effect of canard deflection on the induced drag factor (K_1) is presented in Figure 51 for deflections of -5, 0, and 5 degrees in the 50-degree sweep model and -10 and 0 degrees for the 25-degree sweep model. As indicated in the figure a positive 5-degree deflection increases induced drag significantly over that of the basic wing-body at low lift coefficients.

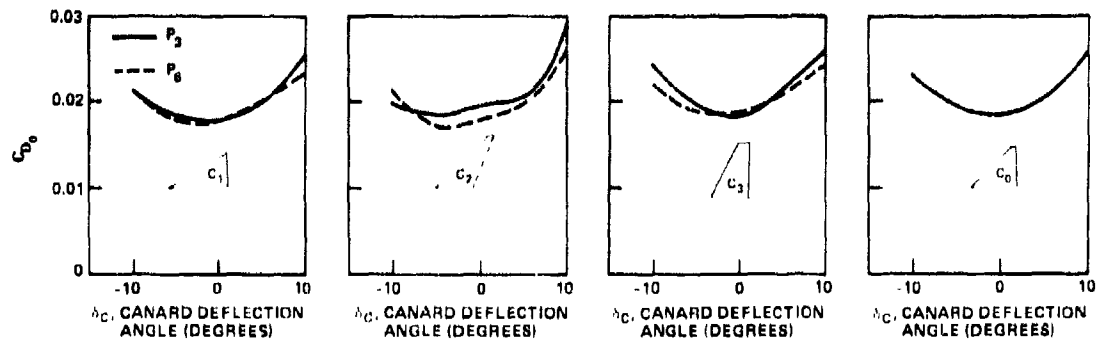


Figure 50a - Drag for a 50-Degree Wing

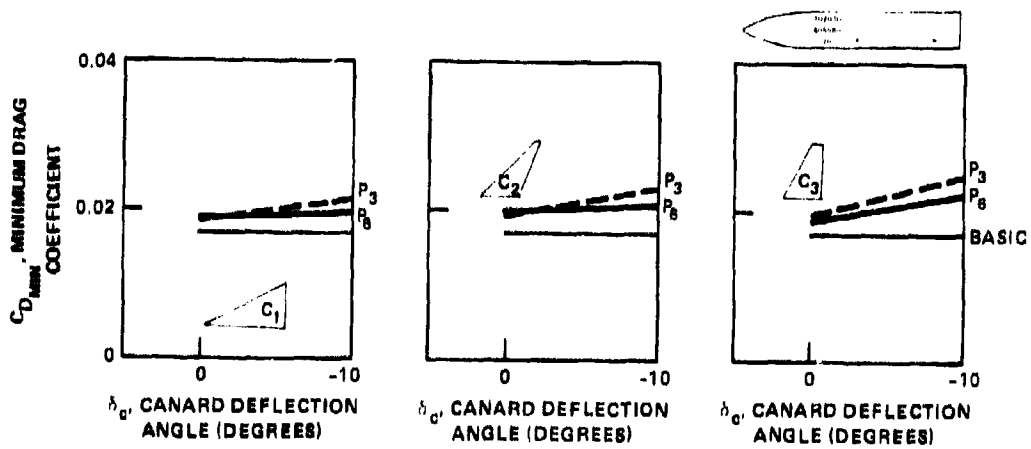


Figure 50b - Drag for a 25-Degree Wing

Figure 50 - Minimum Drag Variation with Canard Deflection

Figure 51 - Effect of Canard Deflection on Induced Drag Factor

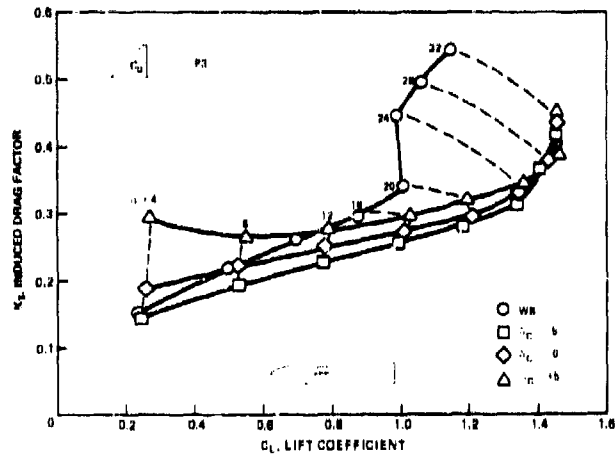


Figure 51a - Canard C_0 on 50-Degree Wing

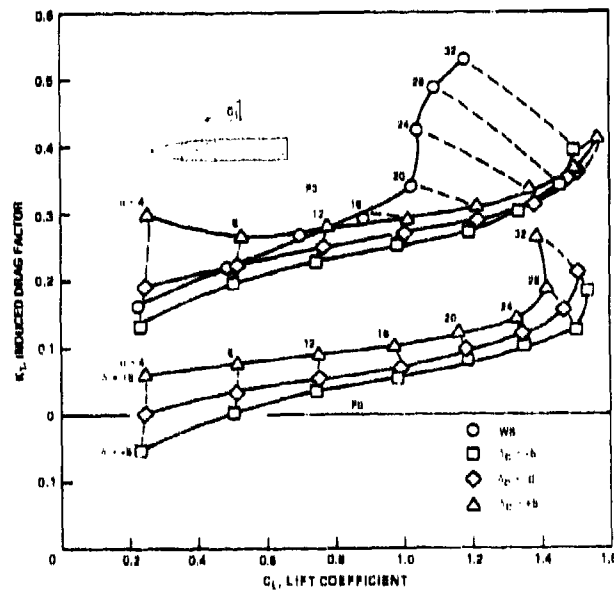


Figure 51b - Canard C_1 on 50-Degree Wing

Figure 51 (Continued)

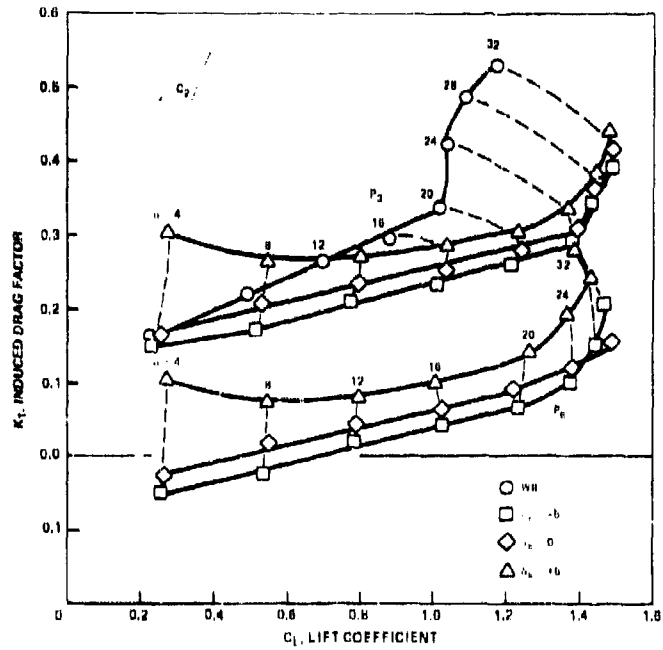


Figure 51c - Canard C_2 on 50-Degree Wing

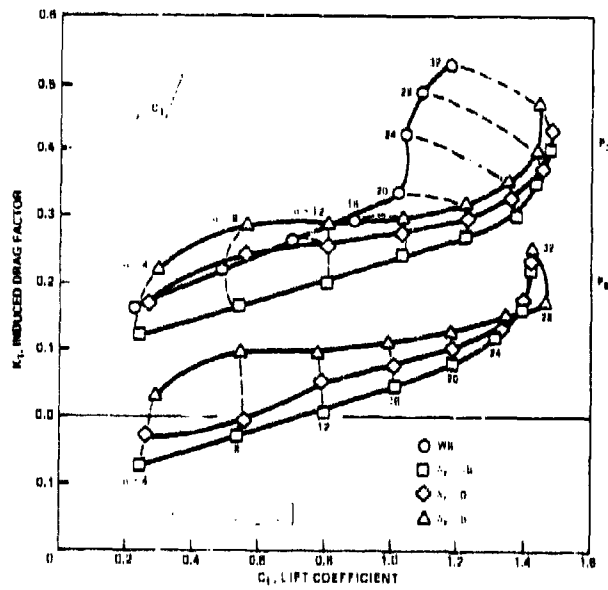


Figure 51d - Canard C_3 on 50-Degree Wing

Figure 51 (Continued)

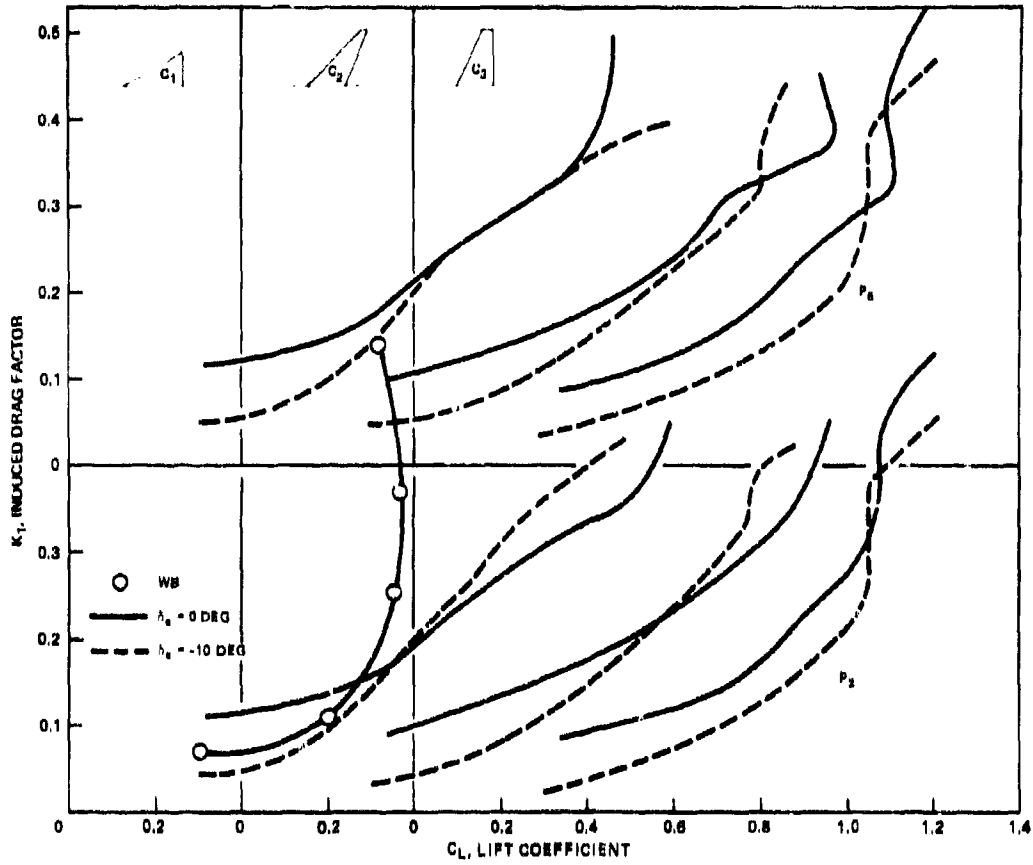


Figure 51e - Canards on 25-Degree Wing

The canard is carrying much of the load at these lift coefficients and thus has significant induced drag of its own. In addition, the downwash from this high loading is modifying the load distribution of the wing in an unfavorable manner. Lift is being suppressed on the inboard position of the wing causing a nonelliptical distribution. With increasing angle of attack the favorable effects of the canard become evident and the induced drag factor is less than that of the basic wing-body.

A negative 5-degree deflection of the canards reduced the induced drag factor to values below the basic wing-body and 0-degree deflection canard configurations throughout most of the angle of attack range. Positive deflection configurations had higher values of induced drag than the 0-degree canard configurations. At high lift coefficients only small differences in K_1 occur for either positive or negative deflections when compared to the 0-degree deflection canard configuration.

Negative 10-degree deflections on the 25-degree sweep model reduced K_1 at low lift coefficients. Negative deflection caused an increase in K_1 at high lift coefficients when the canards were located at P_3 . The increase in K_1 did not occur to any extent when the canards were located at the lower position nor did it occur to the 25-degree sweep canard C_3 . A possible explanation of this behavior is that the canard trailing edge gap may be too large and thus the favorable interference effect from the wing may be diminished somewhat.

WING LEADING EDGE CHANGES

In the earlier section on lift, it was stated that wing leading edge modifications can have a beneficial effect on aircraft performance. The increases in performance, in general, take the form of an increase in lift-to-drag ratio and increases in lift and stall angle of attack. Increases in lift and stall angle of attack did occur for the 25-degree wing model, however, leading edge droop and radius changes had little effect on the 50-degree wing. Leading edge droop increased lift-to-drag ratio for both the 25- and 50-degree swept wing models. The variation in L/D with C_L is presented in Figure 52. Data are presented for a -9-degree droop with and

Figure 52 - Effect of -9-Degree Droop on Lift-to-Drag Ratio

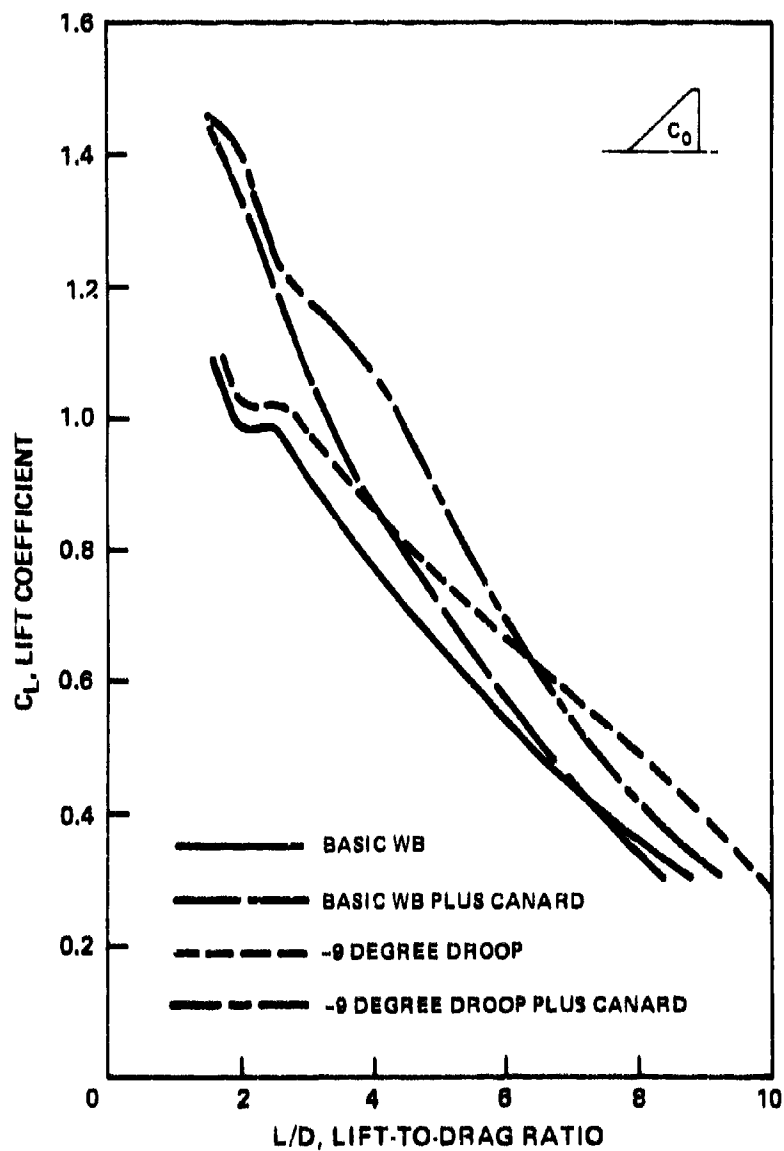


Figure 52a - Drag of 50-Degree Wing

Figure 52 (Continued)

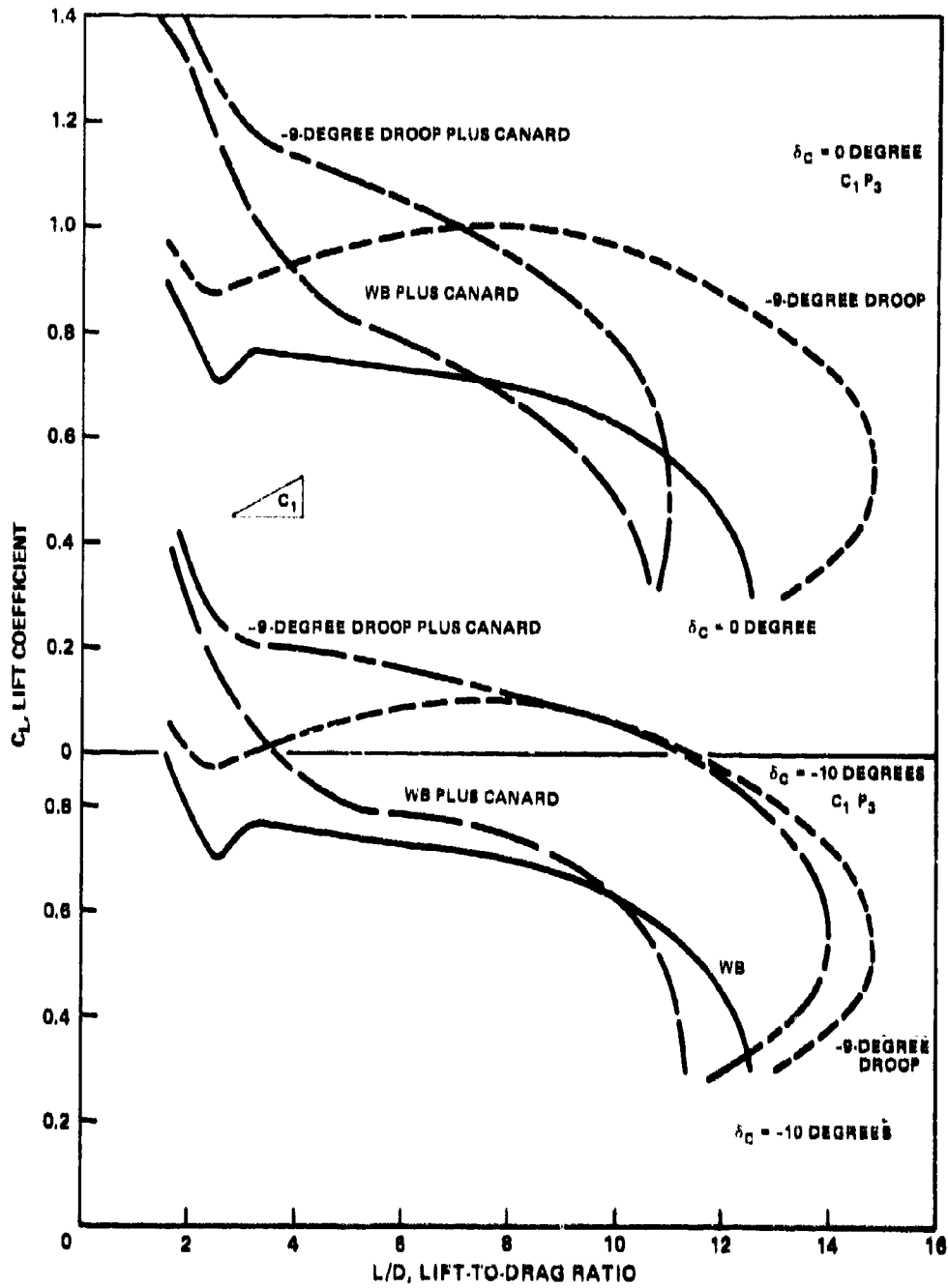


Figure 52b - Drag of 25-Degree Wing

without the close-coupled canard installed. The data for the 50-degree wing are based on the 45-degree truncated delta canard C_0 at 0-degree deflection located at P_3 .

The 60-degree delta canard C_1 , located at P_3 , was used for the 25-degree wing. The data are for deflection angles of -10 and 0 degrees.

Adding the droop to the 50-degree wing increased lift-to-drag ratio for both canard on and off configurations throughout the angle of attack range evaluated $4 < \alpha \leq 33$ degrees. The incremental change in L/D due to the addition of the -9-degree droop is shown in Figure 53. At low lift coefficients the droop improved the lift-to-drag characteristics of the basic configuration by $\Delta L/D \sim 1.5$ or approximately 14 percent. The gain in L/D for the canard configuration with droop was approximately 10 percent. These improvements in lift-to-drag ratio remained fairly constant with increasing C_L for the canard configuration but were reduced for the wing-body.

The gains in lift-to-drag ratio due to the droop are far more impressive on the 25-degree wing model than those increases noted for the 50-degree model. Maximum lift-to-drag ratio was increased from 12.5 to 14.8 when the droop was installed. The value of lift coefficient where $(L/D)_{max}$ occurred was increased for C_L from 0.3 to 0.54.

The amount of increase in L/D due to the droop of the canard configuration was dependent on the canard deflection angle as can be seen in Figure 53 which presents the change in L/D due to the droop for the three configurations. As shown, the gains in L/D exhibited by the -10-degree canard configuration are similar in shape and magnitude to those of the basic wing-body. The zero degree canard configuration data has the same general shape as that of the -10-degree canard configuration but the magnitude of the increase is significantly smaller. A possible explanation for these differences is that the combination of the droop and downwash from the canard are having a detrimental effect on the improved flow created by the droop. Similar results were seen on the F-4 when the inboard slat and canard were both installed. Deflecting the canard negatively,

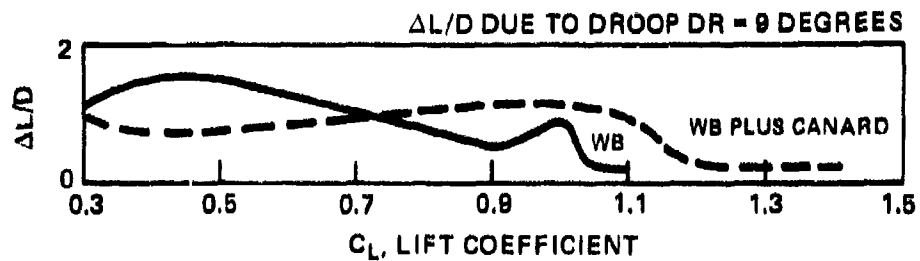


Figure 53a - Lift to Drag for 50-Degree Wing

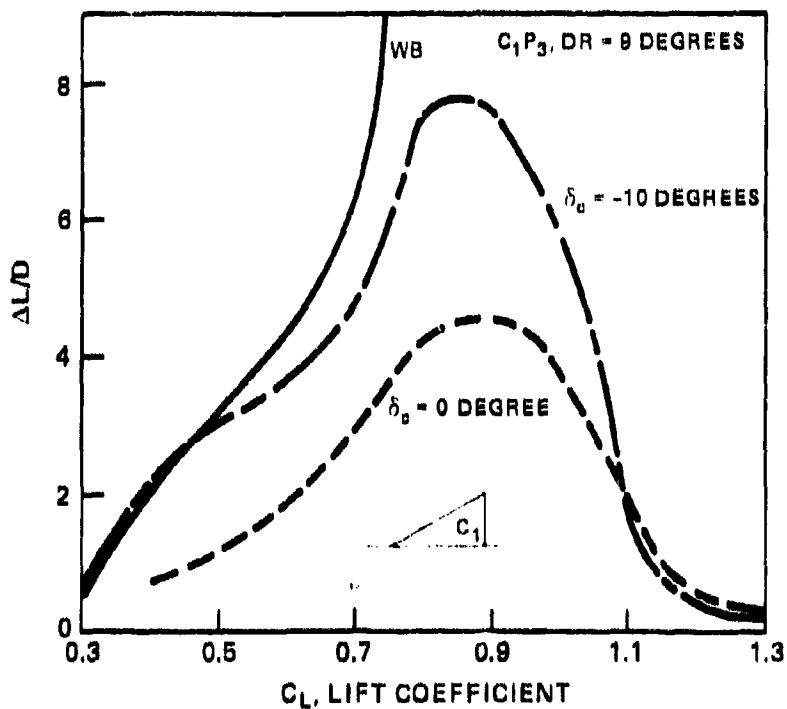


Figure 53b - Lift to Drag for 25-Degree Wing

Figure 53 - Incremental Change in Lift-to-Drag Ratio due to -9-Degree Droop

however, will not change the wing flow significantly at low angles of attack--hence, the similarity of improvements in lift-to-drag ratio for the basic wing-body and the -10-degree canard configuration.

Thus it appears that it is possible to overdo the canard interference at low angles of attack and the full performance potential of the canard wing interaction will not be attained.

FLOW VISUALIZATION

The previous discussion presented in this volume has been based primarily on force and moment data. A limited amount of flow visualization data has also been obtained on the 50-degree sweep model in the angle of attack range between 0 and 20 degrees. Tufts were installed on canards and wing and photographed with a motion picture camera. Results from these motion pictures, at angles of attack of 10, 15, and 20 degrees, are shown in the accompanying figures. The canards were, in general, located at P_6 .

Sketches of the tuft directions for the basic 50-degree wing with canard off are shown in Figure 54 for $\alpha = 10, 15, \text{ and } 20$ degrees. At 10 degrees the basic wing has a region of flow near the body where the tufts are in the streamwise direction (unseparated) and a leading edge vortex which starts off the body. Increasing the angle of attack to 15 degrees reduces the streamwise flow area and causes the wing leading edge vortex to break down at approximately half the semispan. The outboard portion of the wing is stalled. At 20-degree angle of attack the region of streamwise flow is very small and most of the surface of the wing is in reverse flow.

The primary influence of the canard is to increase the area of streamwise flow (unseparated) and move the point where the wing leading edge vortex begins outward. This increase in unseparated flow is seen in Figure 55. Figure 55a shows the boundaries of unseparated flow for the 60-degree canard located at P_6 . Data are shown for canard deflection angles of -10, 0, and 10 degrees. Also shown on the figure are the corresponding boundaries for the basic wing-body. As indicated, the area of unseparated flow is greatly increased when the canard is installed; in addition, the vortex initiation point is moved outward. The line of flow is approximately at the location

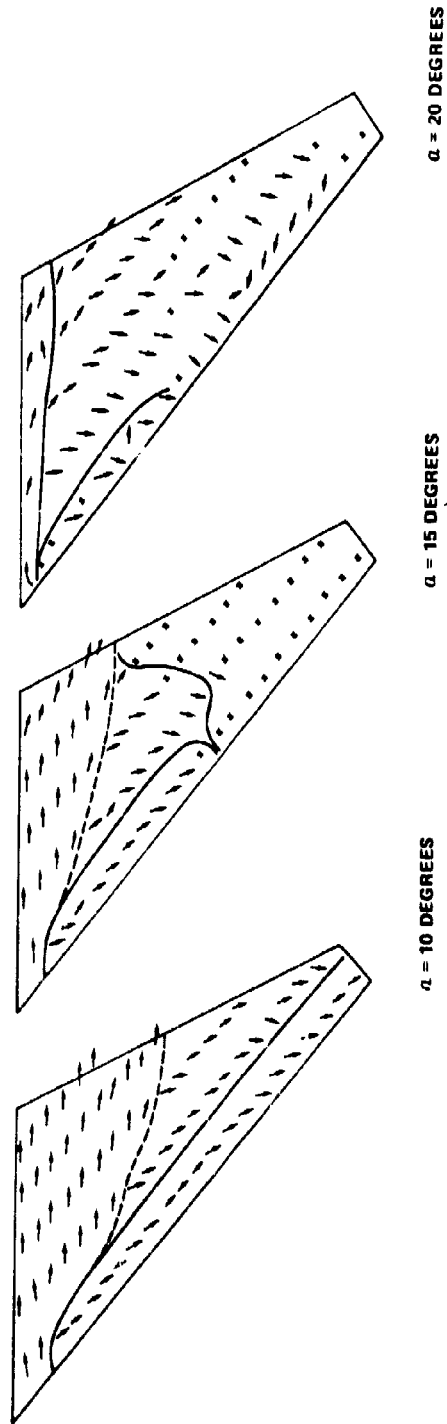


Figure 54 - Tuft Patterns of the 50-Degree Wing

Figure 55 - Effect of Canard on Unseparated Flow Region

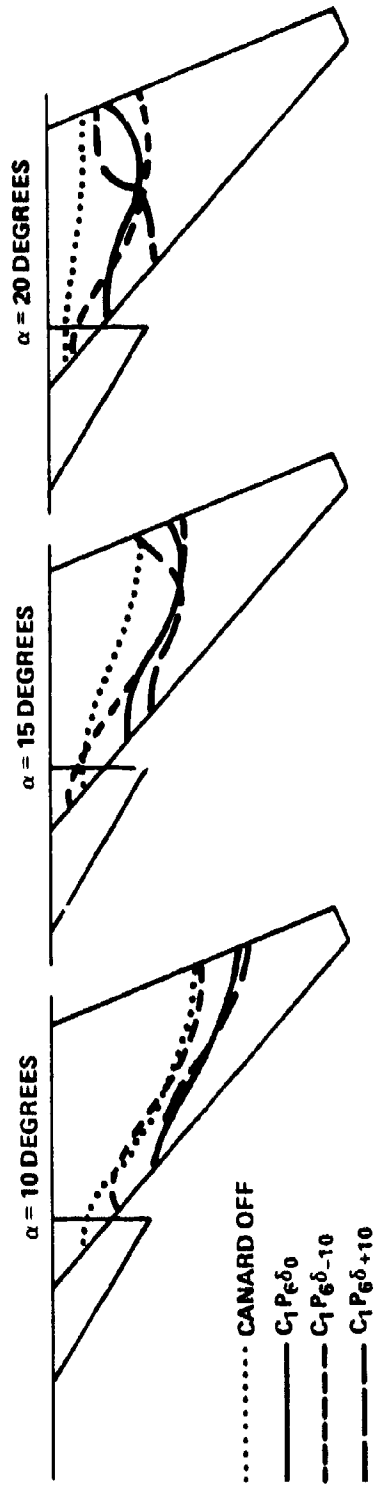


Figure 55a - Canard C_1 at Position 6

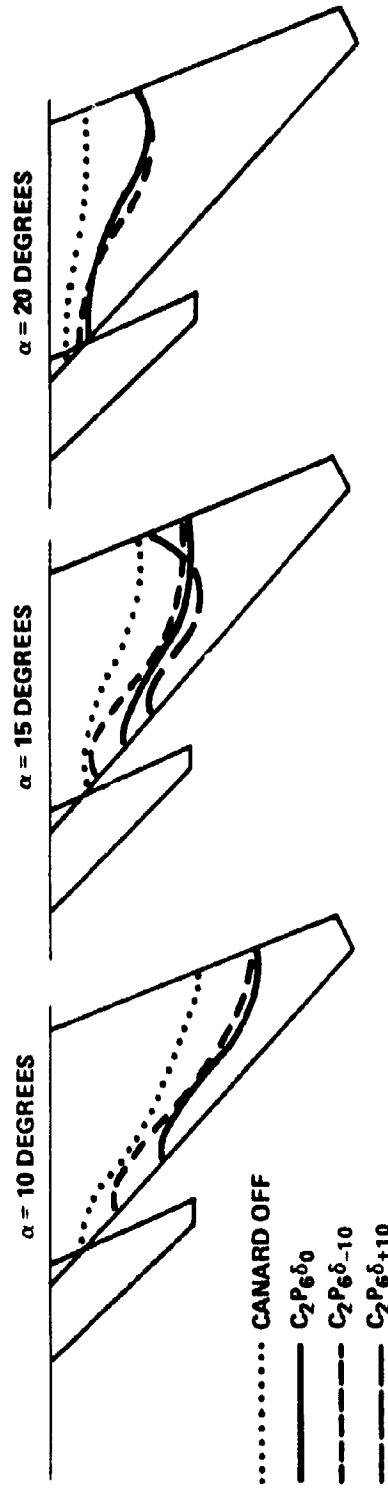


Figure 55b - Canard C_2 at Position 6

Figure 55 (Continued)

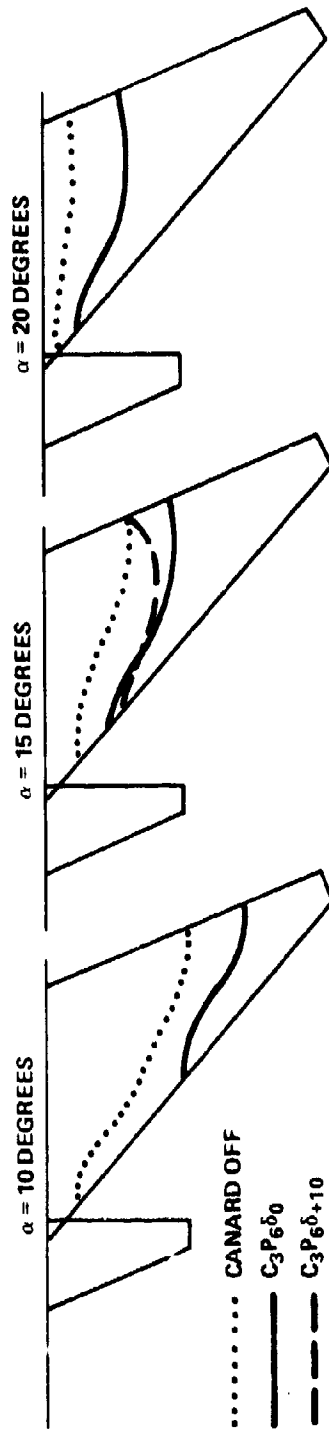


Figure 55c - Canard C_3 at Position 6

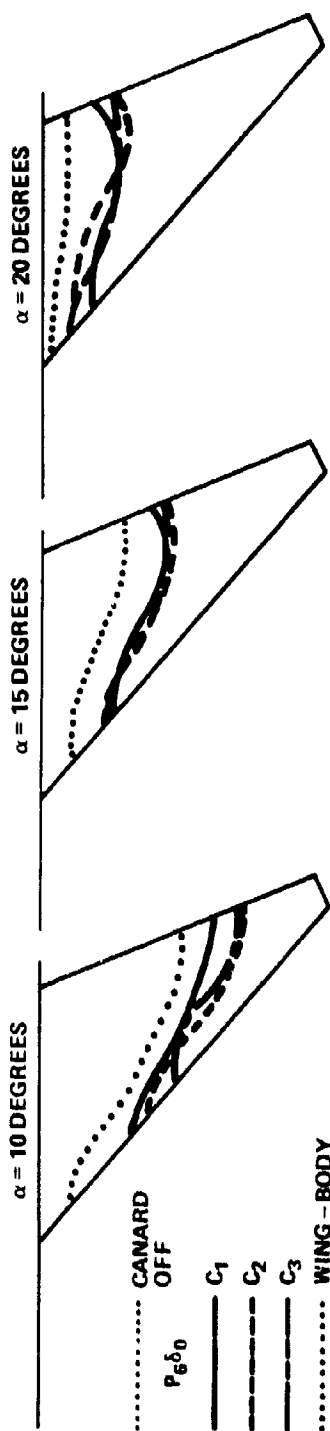


Figure 56 - Effect of Canard Shape

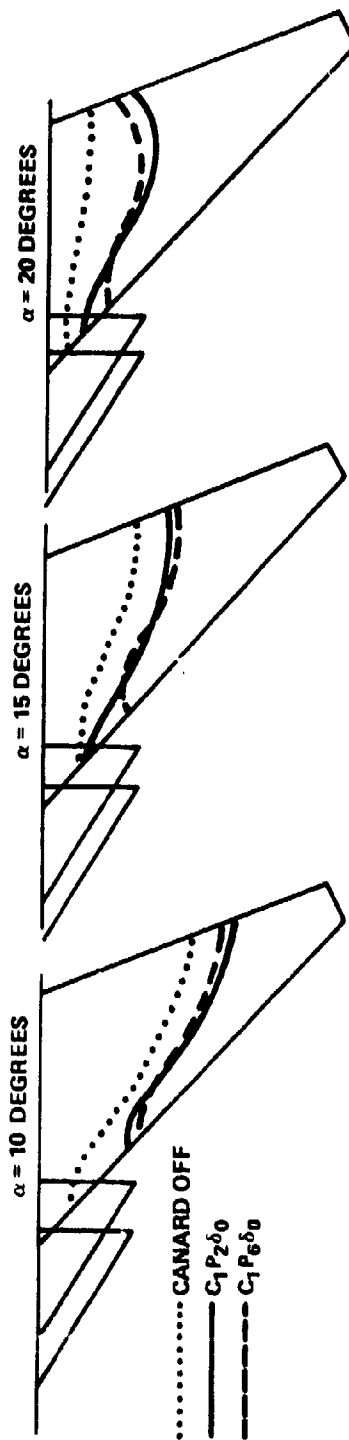


Figure 57 - Effect of Position

of the canard tip for deflections of 0 and 10 degrees. Negative deflections moved this location inboard, whereas a positive deflection moved the line outboard. The region of unseparated flow is relatively constant with angle of attack for the 60-degree canard.

The same trend with deflection occurred for the 45-degree high aspect ratio canard C_2 and the 25-degree canard C_3 as seen in Figures 55b and 55c. The separation point is, again, at approximately the canard tip but moves rapidly inboard with angle of attack. Both of these canards exhibited early stall on the upper surface and the region of unseparated flow tended to move inboard as the canard stall progressed towards the root. The 60-degree delta canard did not exhibit any pronounced stall and the region of unseparated flow did not change to any great extent.

A comparison of the three canards at zero-degree deflection is shown in Figure 56. At 10-degree angle of attack the largest region of unseparated flow is due to the 25-degree canard with the 60-degree canard having the smallest region. At 15 degrees there is little difference between the 3 canards. At 20 degrees the 60-degree canard had the greatest influence on increasing the area of unseparated flow.

The 60-degree canard was also evaluated at P_2 . Data from P_2 are compared with data at P_6 in Figure 57. Moving the canard upward and forward to P_2 moved the vortex initiation point inwards, however, the surface area of unseparated flow is relatively unchanged.

The limited flow data are in agreement with the results obtained from the force data in that the effectiveness of the higher aspect ratio canards declines with increasing angle of attack, and that the 60-degree canard has only minimal loss in effectiveness with increasing angle of attack.

SUMMARY

In the preceding analysis it will be noted that the presence of a close-coupled canard modifies the aerodynamic characteristics of the basic wing-body on which it is mounted. These changes, which are due to favorable interference, occur regardless of canard shape, size, position, or wing planform. The aerodynamic changes consist primarily of an increase in

stall angle of attack and maximum lift coefficient, and a decrease in drag at angles of attack greater than approximately 8 degrees. The extent to which these aerodynamic improvements occur is a function of canard size, shape, position, and deflection. A summary of the effects of the above parameters is given below:

SIZE

1. Changes in lift and pitching moment at low-to-moderate angles of attack ($\alpha \leq 20$) are proportional to canard exposed area ratio S_{c_e}/S_w and exposed volume coefficient $S_{c_e}/S_w * l_c/\bar{c}$, respectively, for canards of geometrically similar planform.

2. Neutral point shift at low angles of attack is proportional to exposed volume coefficient.

3. Incremental changes in lift-to-drag ratio are proportional to canard exposed area ratio.

SHAPE

1. Lift is maximized by high sweep canards $\lambda \sim 60$ degrees.

2. The incremental moment characteristics of each canard shape were similar in shape and magnitude to the isolated characteristics of each canard.

3. At low lift coefficients, incremental changes in lift-to-drag ratio are proportional to the quarter chord sweep angle of the canard for canards of equal exposed area.

4. Induced drag factor is reduced by the canard.

5. Induced drag factor was lowest for low sweep canards at low lift coefficients and highest at high lift coefficients. High sweep canards exhibit opposite trends.

POSITION

1. Moving the canard longitudinally forward and downward reduces maximum lift increments.

2. Maximum lift increments occur when the canard exposed root trailing edge is slightly forward of the exposed wing root leading edge.

3. At low lift coefficients, moving the canard forward increases incremental moment. Maximum incremental moments, in general, occur at the same position where maximum lift occurs.

4. At low angles of attack, incremental pitching slope $\frac{\partial(\Delta C_M)}{\partial\alpha}$ is a linear function of isolated canard lift curve slope multiplied by the canard exposed volume coefficient.

5. Lift-to-drag ratio was maximized at the same location where lift was maximized.

6. Moving the canard forward and downward increased minimum drag.

DEFLECTION

1. Neither positive nor negative deflections of the canard have any significant effect on lift if the gap between canard trailing edge and wing surface divided by canard span is greater than 0.1. Reducing this gap ratio by positive canard deflection caused large reductions in maximum lift.

2. Similar reductions in incremental moment occurred if the gap was reduced. The reductions in incremental moment were not as correspondingly large as the reductions in lift. These characteristics indicate a loss of effectiveness of the canard on delaying wing stall.

3. Positive deflections cause a large increase in drag and a reduction in maximum lift-to-drag ratio.

4. The increase in drag with positive deflection is due to an increase in minimum drag and in the induced drag factor.

5. Small negative deflections ($\delta_c \approx -5$) can increase maximum lift-to-drag ratio and reduce the induced drag factor when compared with zero-degree deflection configurations.

6. The gains or penalties in lift-to-drag ratio at large lift coefficients $C_L \geq 1.0$ are small for either positive or negative deflections.

WING LEADING EDGE CHANGES

1. Increasing the canard-off stall characteristics of the 25-degree wing by 4 degrees, delayed the favorable influence of the canard by a similar amount. Maximum incremental lift due to the canard was the same for both basic and improved configurations.

2. Incremental improvements in lift-to-drag ratio due to installation of a -9-degree droop were approximately the same for both canard on and off configurations of the 50-degree wing.

3. A similar -9-degree droop on the 25-degree wing model required a -10-degree canard setting to obtain the incremental improvement due to the droop.

4. Neither droops nor wing leading radii change significantly modified the benefits in lift, drag, or pitching moments due to the canard.

ACKNOWLEDGMENTS

The author wishes to thank Stephen J. Chorney, John R. Krouse, and Jonah Ottensoser for their help in obtaining and evaluating the data presented in this report. Additional acknowledgment is given to James H. Nichols and Dr. Roger J. Furey for their guidance and support.

APPENDIX
MODEL GEOMETRY

The data presented in this report are based on two research models. The models consist of steel wings and a steel central core. Fuselages are wooden fairings surrounding the central core. The canards and horizontal tail are wood and fiberglass fairings built up around a steel spar. Attachment of the canards and horizontal tail is provided by steel plates flush with the fuselage. Seven canard and three horizontal tail mounting positions are provided. Each canard can be rotated through a deflection range from -10 to +25 degrees in 5-degree increments. Horizontal tail deflection range is from -25 to +10 degrees. Rotation point for both canards and horizontal tail is 40 percent of the exposed surface root chord. Moment reference point for both research models is $0.27 \bar{c}$.

Detailed dimensions of the wings are given in Table 1. Table 2 presents dimensions of the four canards. Figure 58 shows the common fuselage shape for both models. Wing planform geometries are given in Figure 59. Canard geometry is given in Figure 60. Canard locations are presented in Figure 61. A photograph of the various model components is shown in Figure 62.

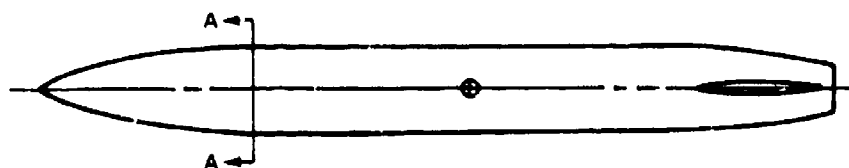
TABLE 1 - GEOMETRIC CHARACTERISTICS OF THE WINGS

	W1($\Lambda = 50$ Degrees)	W2($\Lambda = 25$ Degrees)
Airfoil Section (NACA)	+	64A008
Projected Area, square inches	304	295
Span, inches	35.50	42.00
Chord, inches		
Root (centerline)	15.38	12.20
Tip	1.90	1.90
Mean Aerodynamic Chord, inches		
Length	10.30	8.30
Spanwise Location from Body Centerline	6.70	7.90
Aspect Ratio	4.15	6.00
Taper Ratio	0.12	0.16
Sweepback Angle, degrees		
Leading Edge	50.0	25.0
Quarter Chord	45.5	20.0
Trailing Edge	23.5	-1.5
Incidence Angle, degrees	0	0
Dihedral Angle, degrees	0	0
Twist Angle, degrees	0	0
*64A008 Airfoil swept 25 degrees around $0.27\bar{c}$ chord line.		

TABLE 2 - GEOMETRIC CHARACTERISTICS OF THE CANARDS

	C ₀	C ₁	C ₂	C ₃
Airfoil Section (NACA)	64A008	64A006	64A008	64A008
Exposed Area, square inches	39.8	39.8	47.2	49.3
Projected Area, square inches	76.0	89.5	76.0	76.0
Exposed Semi-Span, inches	5.74	4.79	7.60	7.60
Total Span, inches	16.28	14.38	20.00	20.00
Chord, inches				
Root (centerline)	8.73	12.45	6.70	6.12
Root (exposed)	6.33	8.30	5.31	5.00
Tip	0.59	0	0.90	1.48
Aspect Ratio	3.50	2.31	5.26	5.26
Taper Ratio	0.07	0	0.13	0.24
Sweepback Angle, degrees				
Leading Edge	45	60	45	25
Trailing Edge	0	0	22.8	0
Dihedral Angle, degrees	0	0	0	0

NOTE: VERTICAL TAIL WAS NOT TESTED WITH THE
25-DEGREE LEADING-EDGE SWEEP-WING (W2)



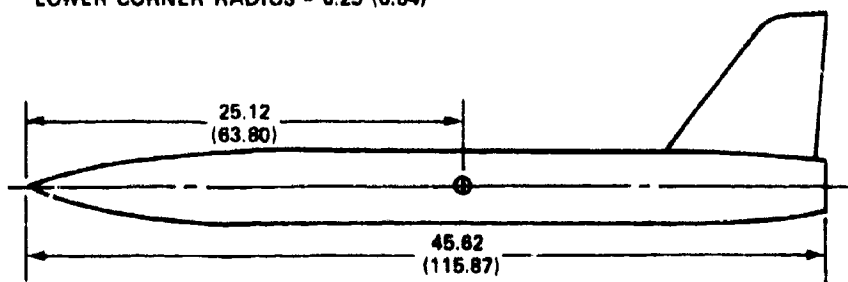
(a) Top View

SECTION A-A



ALL DIMENSIONS ARE IN INCHES (CENTIMETERS)

WIDTH = 4.75 (12.06); HEIGHT = 4.15 (10.54)
UPPER CORNER RADIUS = 1.00 (2.54)
LOWER CORNER RADIUS = 0.25 (0.64)



(b) Side View

Figure 58 - Research Aircraft Fuselage

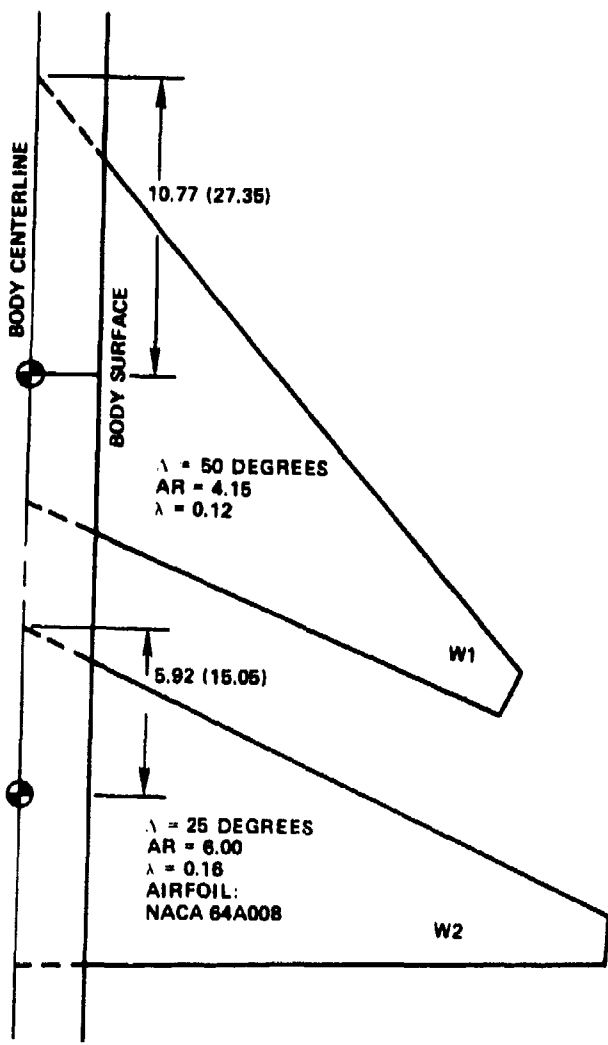


Figure 59 - Planform View of the Wings

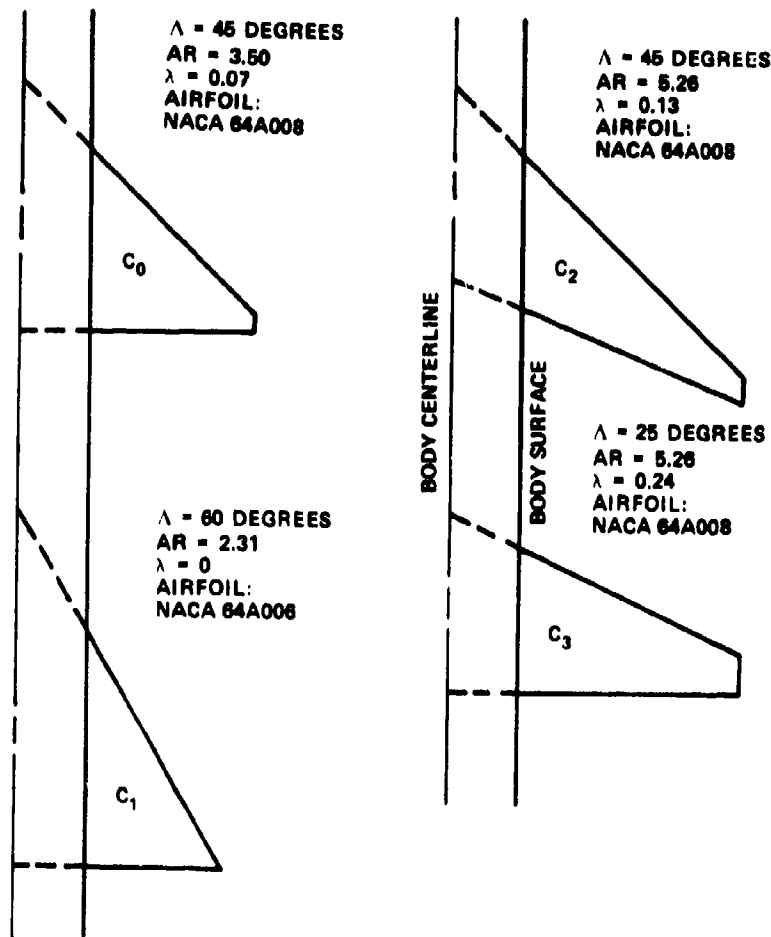
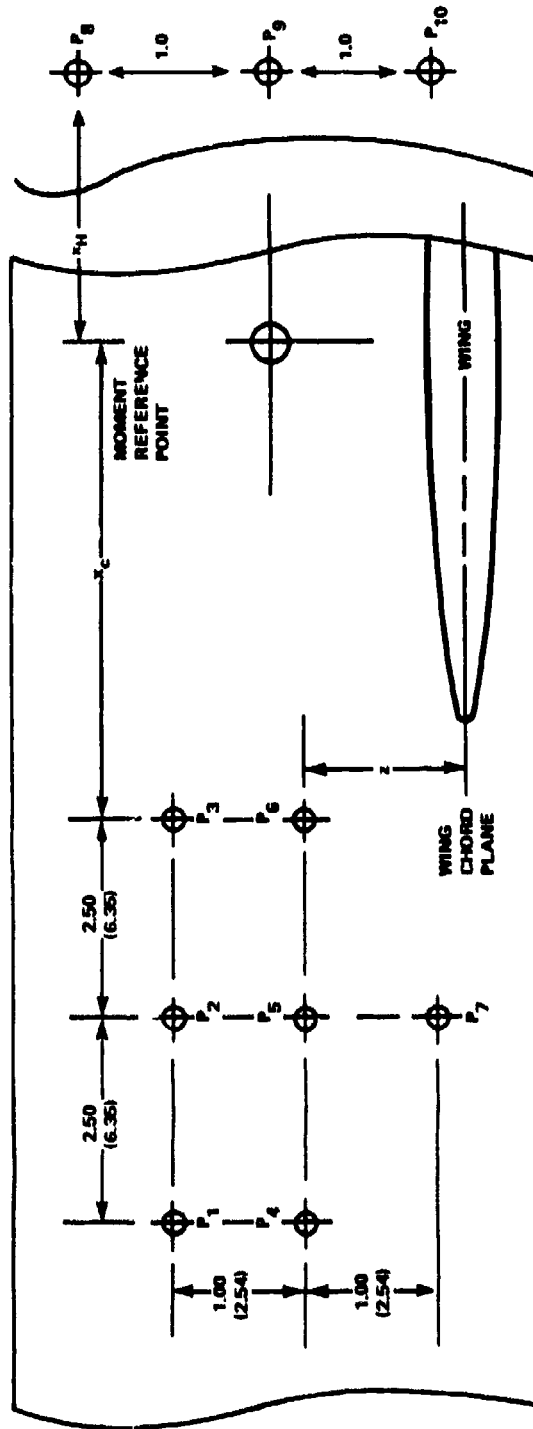


Figure 60 - Planform View of the Canards

NOTE: ALL DIMENSIONS ARE IN INCHES (CENTIMETERS)



W1 ($\Lambda = 50$ DEGREES): $x_c = 10.00$ (25.40); $z = 1.40$ (3.56), $x_H = 15.00$ (38.10)

W2 ($\Lambda = 25$ DEGREES): $x_c = 7.18$ (18.24); $z = 1.14$ (2.90)

Figure 61 - Canard Pivot Locations



Figure 62 - Wind Tunnel Model Components

REFERENCES

1. Lacey, D.W. and S.J. Chorney, "Subsonic Aerodynamic Characteristics of Close-Coupled Canards with Varying Area and Position Relative to a 50-Degree Swept Wing," Naval Ship Research and Development Center, DTNSRDC ASED-199, AD 882-702 (Mar 1971).
2. Krouse J.R., "Effects of Canard Planform on the Subsonic Aerodynamic Characteristics of a 25-degree and a 50-Degree Swept-Wing Research Aircraft Model," Naval Ship Research and Development Center Evaluation Report, AL-91, AD909-459 (May 1972).

INITIAL DISTRIBUTION

Copies		Copies	
1	OUSD (R&E)/Mr. Makepeace	1	MIT/Lib
1	DARPA/COL. Krone	1	N. Carolina State U./ Raleigh Lib
1	CHONR 704/R. Whitehead	1	Stanford U./Lib
1	NAVMAT 08T23	1	Virginia Polytech Inst/Lib
3	NADC	1	Boeing Aerospace Company/ H. Yoshihara
	1 Terry Miller (V/STOL Project Office)	1	General Dynamics/Fort Worth/ C.E. Kuchar
	1 Bill Becker	1	Grumman Aerospace Corporation/ Nick Dannerhoffer
	1 Carman Mazza	1	Lockheed-California/ Andy Byrnes
1	NAVPGSCOL 1 Lou Schmidt	2	McDonnell Douglas Corp/ St. Louis 1 Jim Sinnett/MCAIR 1 Jim Hess/MCAIR
9	NAVAIRSYSCOM	1	Northrop Corp Labs/ I. Waller
	1 AIR 03E	1	Rockwell International, Columbus/Lib
	1 AIR 03PA	1	Rockwell International, Science Center
	3 AIR 320	1	Vought Corporation/H. Diggers
	4 AIR 530		
12	DDC		
2	AFFDL		
	1 CAPT Bill Sotomayer		
	1 R. Dyer		
1	NASA, HQ/Scientific Tech Info Branch		
1	NASA Ames/Preston Nelms		
3	NASA Langley		
	1 Joe Chambers		
	1 Blair Gloss		
	1 Bill Henderson		
1	Calif. Inst of Tech Grad Aero Labs		
1	U. of Cincinnati/Lib		
1	U. of Maryland/Lib		

CENTER DISTRIBUTION

Copies	Code	Name
10	5211.1	Reports Distribution
1	522.1	Library (C)
1	522.2	Library (A)
2	522.3	Aerodynamics Library

DTNSRDC ISSUES THREE TYPES OF REPORTS

1. DTNSRDC REPORTS, A FORMAL SERIES, CONTAIN INFORMATION OF PERMANENT TECHNICAL VALUE. THEY CARRY A CONSECUTIVE NUMERICAL IDENTIFICATION REGARDLESS OF THEIR CLASSIFICATION OR THE ORIGINATING DEPARTMENT.

2. DEPARTMENTAL REPORTS, A SEMIFORMAL SERIES, CONTAIN INFORMATION OF A PRELIMINARY, TEMPORARY, OR PROPRIETARY NATURE OR OF LIMITED INTEREST OR SIGNIFICANCE. THEY CARRY A DEPARTMENTAL ALPHANUMERICAL IDENTIFICATION.

3. TECHNICAL MEMORANDA, AN INFORMAL SERIES, CONTAIN TECHNICAL DOCUMENTATION OF LIMITED USE AND INTEREST. THEY ARE PRIMARILY WORKING PAPERS INTENDED FOR INTERNAL USE. THEY CARRY AN IDENTIFYING NUMBER WHICH INDICATES THEIR TYPE AND THE NUMERICAL CODE OF THE ORIGINATING DEPARTMENT. ANY DISTRIBUTION OUTSIDE DTNSRDC MUST BE APPROVED BY THE HEAD OF THE ORIGINATING DEPARTMENT ON A CASE-BY-CASE BASIS.